SYSTEM IDENTIFICATION AND OPTIMIZATION METHODOLOGIES FOR ACTIVE STRUCTURAL ACOUSTIC CONTROL OF AIRCRAFT CABIN NOISE

by

Scott Paxton

Thesis submitted to the Faculty of the

Virginia Polytechnic Institute and State University

in partial fulfillment of the requirements for the degree of

MASTER OF SCIENCE

in

Mechanical Engineering

APPROVED:

C.R. Fuller, Chairman

R.A. Burdisso

H.H. Cudney

July 23, 1997

Blacksburg, Virginia

SYSTEM IDENTIFICATION AND OPTIMIZATION METHODOLOGIES FOR ACTIVE STRUCTURAL ACOUSTIC CONTROL OF AIRCRAFT CABIN NOISE

by

Scott Paxton

Committee Chairman: Chris R. Fuller, Mechanical Engineering

(ABSTRACT)

There has been much recent research on the control of complex sound fields in enclosed vibrating structures via active control techniques. Active Structural Acoustic Control (ASAC) has shown much promise for reducing interior cabin noise in aircraft by applying control forces directly to the fuselage structure. Optimal positioning of force actuators for ASAC presents a challenging problem however, because a detailed knowledge of the structural-acoustic coupling in the fuselage is required.

This work is concerned with the development of a novel experimental technique for examining the forced harmonic vibrations of an aircraft fuselage and isolating the acoustically well-coupled motions that cause significant interior noise. The developed system identification technique is itself based upon an active control system, which is used to approximate the disturbance noise field in the cabin and apply an inverse excitation to the fuselage structure. The resulting shell vibrations are recorded and used to optimally locate piezoelectric (PZT) actuators on the fuselage for ASAC testing.

Experiments for this project made use of a Cessna Citation III aircraft fuselage test rig. Tests were performed at three harmonic disturbance frequencies, including an acoustic resonance, an off-resonance, and a structural resonance case. In all cases, the new system identification technique successfully isolated a simplified, low-magnitude vibration pattern from the total structural response caused by a force disturbance applied at the fuselage's

rear engine mount. These measured well-coupled vibration components were used for positioning candidate piezoelectric actuators on the fuselage shell. A genetic algorithm search provided an optimal subset of actuators for use in an ASAC system. ASAC tests confirmed the importance of actuator location, as the optimal sets outperformed alternate groupings in all test cases. In addition, significant global control was achieved, with sound level reductions observed throughout the passenger cabin with virtually no control spillover.

Acknowledgments

I would like to thank my thesis advisor, Dr. C. R. Fuller, for introducing me to active control and providing a position and challenging project in his research group. I would also like to Dr. R. A. Burdisso and Dr. H. H. Cudney for serving as members of my thesis committee.

I am indebted to the NASA Langley Research Center for their support of this work under grant NAG-1-1681.

Thanks also to the research associates and fellow graduate students in Vibrations and Acoustics Laboratory for valuable advice and discussions throughout the course of my research.

Finally, I'd like to thank my friends and most especially my family for much support and encouragement during the past several years.

Contents

List of Figures

List of Tables

Chapter 1

Introduction

1.1 Motivation

Interior cabin noise presents a challenging problem in most aircraft. The level of passenger comfort must be balanced with the cost, complexity, and physical constraints of potential noise reduction technologies. The situation presents numerous engineering tradeoffs, and continues to evolve as new higher-powered engine designs are introduced. While demand for improved passenger conditions persists, the development and improvement of noise reduction technologies for aircraft will likely remain an important area of practical research.

Active noise control provides a promising solution to the cabin noise problem. High sound levels in aircraft, especially those due to engine vibration and propeller blade noise, are often most severe at low frequencies. Traditional passive noise reduction techniques are not highly effective in this low-frequency range. However, it is exactly this range where active control technology demonstrates its best results. Therefore, an attractive

solution would add the benefits of active control to a previously existing noise abatement system to decrease sound levels with little added penalty in terms of weight or space requirements.

The implementation of such a method is far from straightforward since the combined structural-acoustic system comprising a fuselage's interior space is typically very complex. A clear understanding of the mechanisms of sound transmission and radiation in this coupled system is essential for the design of efficient noise reduction techniques, either active or passive in nature. Recent research has demonstrated successful control of aircraft cabin noise using forces applied directly to the fuselage structure. To best position the force actuators in these systems, the fuselage motions which are well-coupled to the interior acoustic space must be separated from the total structural response. Thus there exists a need for an effective system identification procedure that can quickly bring focus to the acoustically important behavior of the total fuselage system and aid in control system development.

The work presented here concerns the development of such an experimental system identification methodology, which itself makes use of active control technology. Following the separation and measurement of the acoustically well-coupled structural vibrations, this thesis continues tracing the development of an active controller design from the gathering of diagnostic information through control system testing in the cabin of an actual fuselage. The discussion of the project begins with background information about active control techniques in general, followed by previous work addressed specifically towards aircraft interior noise.

1.2 Active Control

The general principles of active control have been understood for some time, but only with the relatively recent development of fast inexpensive digital signal processors has the development of practical systems become feasible. Good overviews of the history of the active control field have been presented by Warnaka [1] and Elliot and Nelson [2]. In addition, recent textbooks by Nelson and Elliot [3] and Fuller, et al. [4] have presented in detail the current state of the art of the active control field.

Active control techniques rely on the well-known principle of superposition, which allows cancellation of an offending noise with "anti-noise." The combination of two or more coherent acoustic waves leads to destructive or constructive interference of the pressure waves, resulting in either reductions or increases in sound levels. The concept of active control is to produce a sound field identical in amplitude and opposite in phase (180^o difference) to the offending noise, so that the combination of the two fields yields a constant pressure field, resulting in silence. The control, or secondary, sound field is produced by one or more secondary sources, which are typically placed close to the sources of disturbance to best produce an appropriate anti-sound field. Any discrepancies in amplitude or phase of the secondary sound field reduces the potential sound reductions. In fact "spillover", or inadvertent localized increases in sound levels due to constructive interference between disturbance and control fields, is a very common problem. Though the secondary source is usually treated as causing simple destructive interference with the noise field as just described, a more useful interpretation when considering active control of vibrations is that the secondary source causes a change in system input impedance as seen by the primary disturbance source. Creation of an impedance discontinuity acts to

reflect a portion of the input energy, thus causing attenuation in the system downstream of the secondary source as expected.

The German physicist Paul Lueg first described active noise control in a 1936 U.S. patent [5] and gave examples of a one-dimensional duct problem and a free field propagation situation. The fundamental concept of the proposed noise reduction method was to use a feedforward control approach in which a signal correlated with the disturbance is detected, shifted 180^{o} in phase, and used to cancel the offending noise via a secondary acoustic source as described above. This feedforward method, still prevalent in modern active control work, exploits the fact that the speed of sound in air is very much less than the speed of electrical propagation and signal processing needed to produce an appropriate control field via the secondary source. Despite demonstrating a good understanding of the principles of active control, Lueg's proposed concept was not pursued further because practical systems were well beyond the capabilities of the electronics technology of the time.

In the 1950's, several researchers again began investigating active techniques for noise reduction. Olson [6] proposed an electronic sound absorber, which used a closely-spaced microphone and speaker system to produce a "zone of silence" around the microphone sensor. This is achieved by adjusting the phase of the speaker diaphragm's motion to produce a null in pressure at the microphone location. Olson's work also introduced concepts of noise-reducing headsets and helmets, as well as some vibration control applications.

Also in the mid-1950's, Conover [7] investigated the problem of active control of transformer noise, which has become a classic problem in the active control field. His system involved placing loudspeakers near the surface of a large transformer to cancel

sound radiating from the structure. However, Conover's feedforward controller scheme required manual adjustment of a sinusoidal reference signal in both magnitude and phase as automatic control systems were still technologically unfeasible. He therefore abandoned active control as a viable alternative at that time and returned to a more conventional passive approach.

Interest in active control was again revived in the mid and late 1960's and has continued to grow steadily as advances in digital electronic technology allow research on increasingly complicated systems. Initially, the effectiveness of active techniques was demonstrated on spectrally simple problems like transformer hum noise and spatially simple systems such as ducts. More recently, researchers have been exploring a wider range of applications with more complicated systems, among them the control of complex sound fields in passenger vehicles. Commercial products making use of active control technology have also begun appearing recently, especially in the areas of noise-reducing headphones, HVAC sound reduction systems, and aircraft applications such as aviation headsets and integrated systems for cabin noise reduction.

1.3 Aircraft Interior Noise Applications of Active Control

In addressing the aircraft interior noise problem, particularly that of low frequency noise, active control techniques have shown much potential. Active systems, inherently most effective at low frequencies, can greatly reduce the large weight and space requirements of additional passive materials for handling these frequencies, an issue of critical importance in aerospace applications. As a result, aircraft interior noise has been an important area of focus for active control researchers.

Much analytical work has investigated the transmission of sound in aircraft fuselages and provided theoretical studies of active control of interior cabin noise. Fuller [8] greatly aided the understanding of transmission phenomena in propeller aircraft with the development of a simplified cylinder model to simulate fuselage behavior. The work showed that the fuselage structural response due to two external dipole sources (representing turbo-prop excitation) is dominated by relatively few low-order circumferential vibration modes. Later, Fuller [9] added to the analytical work addressing fuselage behavior by studying the influence of a cabin floor on sound transmission.

1.3.1 Active Noise Control

Lester and Fuller [10] provided a simulation of an active control system in a propeller aircraft, using an idealized cylinder model as in [8]. The control sources used were multiple acoustic monopoles arranged in the cabin interior. Sound level reductions of up to 20 dB were predicted using judicious placement of control actuators in the model. It was found that a circumferential ring arrangement of multiple sources in the propeller plane resulted in the best control performance. The Nyquist criterion shows the required number of actuators for effective control, which corresponds to twice the order of the highest-order offending circumferential mode. Abler and Silcox [11] performed early experimental demonstrations of active noise control with loudspeakers in a cylinder section and confirmed these source placement predictions while showing that significant sound reductions of 25 dB or more are achievable in practice.

Using a cylindrical model of similar nature to the above work, though finite in length, Bullmore, et al. [12] investigated the feasibility of active control in a B.Ae. 748 aircraft

cabin. The model was an extension of previous work addressed at active control of enclosed harmonic sound fields, particularly those in aircraft [13-16]. The control system consisted of 16 secondary acoustic sources and 32 error sensors, acting to reduce simulated propeller-induced noise at the fundamental and second harmonic of the blade passage frequency. The possibility of producing global sound level reductions with a control system of this scale was rejected, and research was instead directed at producing an extended region of decreased sound at passenger head level throughout the length of the cabin. This arrangement provided a 14 dB predicted average reduction at the fundamental excitation frequency, and a 4 dB reduction for the second harmonic frequency.

Several researchers have performed in-flight control experiments in a B.Ae. 748 aircraft. Using a commercially-developed control system with 24 control outputs and 32 error sensors, Dorling, et al. [17] demonstrated sound level reductions on the order of 8 to 13 dB at the first three harmonics of the blade passage frequency. These results were largely similar to predicted reductions presented in the same work. Elliott, et al. [18] used a number of different configurations of 16 sources and 32 error sensors, as modeled in the previously-cited work [12], with a multichannel generalization of the LMS adaptive control algorithm. The researchers achieved sound reductions of approximately 13 dB at the fundamental blade passage frequency in most configurations. The second and third harmonics were generally reduced from 6 to 9 dB, and when using a circumferential array of loudspeakers near the propeller plane, up to 12 dB reductions were achieved at these frequencies. These results are generally comparable to the predictions from previous modeling work, as well as being close to the optimum achievable levels as determined by transfer function measurements. In addition to focusing on an extended area of global

sound reduction, a 2 channel "local" control system was also investigated in-flight, resulting in measurable noise reduction within 200 mm of each secondary source with no far-field spillover effects.

Other recent research has focused on similar localized active control methods. These systems use control loudspeakers to create a limited zone of reduced pressure fluctuation in a volume around a seated passenger's typical head position. Salikuddin and Ahuja [19] proposed a system using acoustic sources mounted on the exterior cabin walls. Warner and Bernhard [20] tested a similar arrangement in an 18 passenger aircraft and achieved reductions of 10-20 dB over a substantial frequency range at a single seat location. More recently, Carme, et al. [21] demonstrated a localized active cancellation system with control sources and sensors integrated into seat headrests. The system acted to create a three-dimensional sphere of decreased sound levels for each seat, providing reductions of 10 dB or more for the first three harmonic frequencies at a passenger's ear locations.

The control method used in all of the above research, using conventional voice-coil loudspeakers or other acoustic drivers as secondary control sources, is often termed active noise control (ANC). As described, such systems have proven successful in reducing cabin noise. However, the approach often requires a large number of control sources, and the requirement that sensors and actuators be positioned unobtrusively in the cabin causes further practical difficulties.

1.3.2 Active Structural Acoustic Control

Fuller and Jones [22-25] have proposed an alternative control method for enclosed noise fields, known as active structural acoustic control (ASAC). The ASAC approach

uses structurally-based actuators to exert control forces on the structure itself in order to minimize radiated sound. The initial work referenced above used electromagnetic shakers to provide point force control inputs to simplified cylindrical test sections. The controller made use of error sensor microphones placed in the cylinder interior, such that interior sound levels were minimized by the control of structural vibration. This work demonstrated that in general, fewer control actuators are required by the ASAC approach as compared to ANC techniques. Also, control spillover in the interior acoustic space was reduced in the ASAC experiments. This effect was due to energy of control spillover entering poorly-coupled modes of cylinder vibration, thereby limiting the energy radiated into the interior sound field. However, despite reducing unwanted spillover effects on the controlled interior noise field, the structural control spillover often had the undesirable effect of increasing vibration levels on the cylinder shell. In aerospace applications, this result could have serious implications to structural fatigue issues, and has not yet been closely investigated. Other recent comparative work at NASA Langley Research Center [26] and Thomas Lord Research Center [27] have confirmed these general comparisons between the ANC and ASAC approaches via experiments in fuselage structures.

There are two primary mechanisms of control in ASAC systems [4]. For harmonic disturbance cases near a system resonance, the structural response is dominated by one or a small number of modes, depending on modal density. In such cases, "modal suppression" is usually observed, where only the few dominant radiating modes are reduced in amplitude. Other structural modes that are poorly coupled with the noise field are left unchanged by the control system. Applying ASAC in off-resonance situations may result in "modal restructuring", in which the total modal response distribution of the structure is changed in both amplitude and phase. Modal restructuring acts to decrease

the radiation efficiency of the structure, but often results in increased vibration levels due to structural control spillover as described above.

Simpson, et al. [28] performed control experiments in a test section comprising the aft portion of a furnished DC-9 aircraft, demonstrating the potential of ASAC to reduce cabin noise in realistic aircraft structures. The fuselage was excited structurally by two external electromagnetic shakers, intended to simulate an engine vibration disturbance. Control forces were exerted by two additional shakers placed inside the fuselage as near as possible to the disturbance source locations. Using a typical feedforward controller arrangement, the researchers achieved global sound level reductions of up to 9 dB using various configurations of 7 error microphones. Additionally, several tests were performed using accelerometers mounted on the fuselage as error sensors, resulting in markedly decreased vibration levels but significantly less attenuation of cabin noise.

Houston, et al. [29] proposed an alternate actuation scheme whereby control forces are applied axially to a fuselage structure. Using a numerical model of a cylinder section, the authors discussed the possibility of placing force actuators in an equally-spaced circumferential arrangement at both cylinder ends. The analytical results showed potential sound level reductions of 13 dB using these axial control forces. However, implementation of this system in an actual fuselage would likely be difficult.

Because point forces are spectrally white in a spatial sense, their use as controlling forces in ASAC work can lead to undesired spillover into many structural vibration modes, even while interior sound levels are reduced. In seeking a control actuator with more distributed forcing properties, many researchers have recently investigated the use of piezoceramic materials for applying bending moments or in-plane strains to structures [30, 31]. In particular, lead zirconium titanate (PZT) materials have been widely used in

ASAC work, providing sufficient forcing capabilities with the benefit of greatly reduced mass and space requirements as compared to electromagnetic shaker devices.

Much of the recent research into interior noise control with piezoceramic actuators has been performed at NASA Langley Research Center. Fuller, et al. [32] used an aluminum cylindrical test section with a removable floor structure to simulate an aircraft fuselage environment. The cylinder structure was 0.508 m in diameter, 1.245 m long, and 1.63 mm thick. Piezoelectric patches were bonded directly to the cylinder surface and the system was excited acoustically with an exterior loudspeaker noise source. The chosen testing frequencies were 260 Hz and 666 Hz, which correspond to structural and acoustic resonances respectively. Using two microphones as error sensors, the ASAC system provided global attenuations on the order of 10 dB in the cylinder interior. These results were achievable for both acoustic and structural resonances, though for the case of an acoustic resonance, shell vibration response was increased by the control system.

Further work at NASA by Lefebvre and others [33, 34] made use of a graphite epoxy composite cylinder structure with plywood floor section to model an aircraft fuselage. This fuselage was 1.68 m in diameter and 3.66 m in length. Single frequency excitation tests were performed at 136 Hz (a structural resonance), 172 Hz (an acoustic resonance), and 280 Hz (an off-resonance case). Using configurations of up to four PZT control actuators mounted on the structure, global interior sound level reductions of 12 dB were demonstrated in an acoustic resonance case. The interior noise field in a structural resonance case was attenuated by 9 dB. Positioning of the actuators on skin panels versus structural frames was shown to have little impact on control performance.

Recently, ASAC tests were performed at VPI&SU [35] in the cabin of a Cessna Citation III fuselage, a typical mid-sized business jet. PZT actuators bonded to the

fuselage skin were used as control actuators, to reduce interior noise due to a harmonic structural disturbance applied at an engine mount. Using four actuator arrays, each consisting of four patches wired in series, and four error microphones, control was applied to acoustic resonance and off-resonance cases. In the acoustic resonance case, noise reductions of 20 dB or more were achieved at the error sensors, but an average global increase of several dB was measured at 7 additional microphones. Control performance in the off-resonance case was significantly reduced, with reductions of 2-10 dB at the error sensors and large global sound level increases measured at every global reference microphone. The spillover effects observed in both test cases are a direct result of non-optimal control actuator placement. This initial work was performed using actuator positions chosen largely "ad-hoc" or based loosely on the physics of the control problem, leading to the focus of this current work towards optimally locating the control sources and thus improving global control performance.

Some past work has addressed actuator position optimization via analytical approaches [36-38]. Additionally, work with a finite element model of the Cessna fuselage used in this work has shown the importance of position optimization to global ASAC performance [39]. Spatially averaged reductions of acoustic potential energy of up to 14 dB have been predicted using 16 optimally-located point forces, while poor control force placement may result in overall global sound increases. Cabell [40, 41] has explored another aspect of the optimization problem, developing grouping methods for assembling conceptually distributed actuators from individual piezoelectric patches. Thus, the required dimensionality of an active controller is reduced by wiring several actuators together. This grouping can result in decreased control spillover, resulting in potentially greater global noise attenuations.

1.4 Thesis Objectives and Organization

While ASAC has been demonstrated to achieve significant global sound reductions in simplified cylinder structures, its application to more complicated aircraft fuselages has proven more difficult. In order to achieve global sound reductions, control source placement is critical. Likewise, optimal actuator placement depends on a clear understanding of the specifics of structural-acoustic interactions in the fuselage system.

Therefore, the primary goals of this investigation are:

- To develop an effective system identification procedure that can isolate the fuselage structural motions that are strongly coupled to the interior cabin sound field.
- To develop an optimization methodology, based on the measured system identification data, for positioning piezoelectric actuators on an aircraft fuselage for ASAC experiments.
- To demonstrate the effectiveness of the resulting ASAC system in achieving global sound level reductions in a real aircraft fuselage.
- To use integrated curved piezoelectric distributed transducers as control actuators

Since the scope of the project is highly experimental in nature, a Cessna Citation III fuselage resident at V.P.I. is used to explore active control of aircraft cabin noise in a realistic environment. Chapter 2 addresses some theoretical background needed for the

work. A simplified model of structural-acoustic coupling in an aircraft is presented, allowing for the development of a novel system identification technique. Also provided is a discussion of numerical and computational tools for optimization of control system components. Chapter 3 presents the various experimental procedures developed for this project, and provides an overview of the mechanical and electrical equipment used with the fuselage test rig to perform control tests and acquire measurement data. Experimental data for each of three testing frequencies are presented in Chapter 4, along with a discussion and comparison of these results. Finally, Chapter 5 presents the overall conclusions drawn from this project and suggestions for future directions of research.

Chapter 2

Theory

2.1 Structural-Acoustic Interactions in an Aircraft Fuselage

The coupled behavior of an elastic aircraft fuselage and its interior air cavity can be explored generally with a simplified infinite cylinder model, as shown in Figure 2.1. The infinitely long model is sufficiently accurate to explore basic fuselage behavior because the interior noise fields and the fuselage response of mid to large size aircraft have been found to have significant damping in the axial direction. Therefore, the pressure field is typically dominated by low order circumferential modes, while the axial response is dominated by wave instead of modal behavior [4]. The cylinder carries a series of waves of circumferential order *n* and branch numbers *s*. The shell radial displacement, *w*, for a single frequency ω can be written as

$$w(x,\theta,t) = \sum_{n=0}^{\infty} \sum_{s=1}^{\infty} W_{ns} \cos(n\theta)\, e^{i\omega t \pm i k_{ns} x} \qquad \textbf{(1)}$$

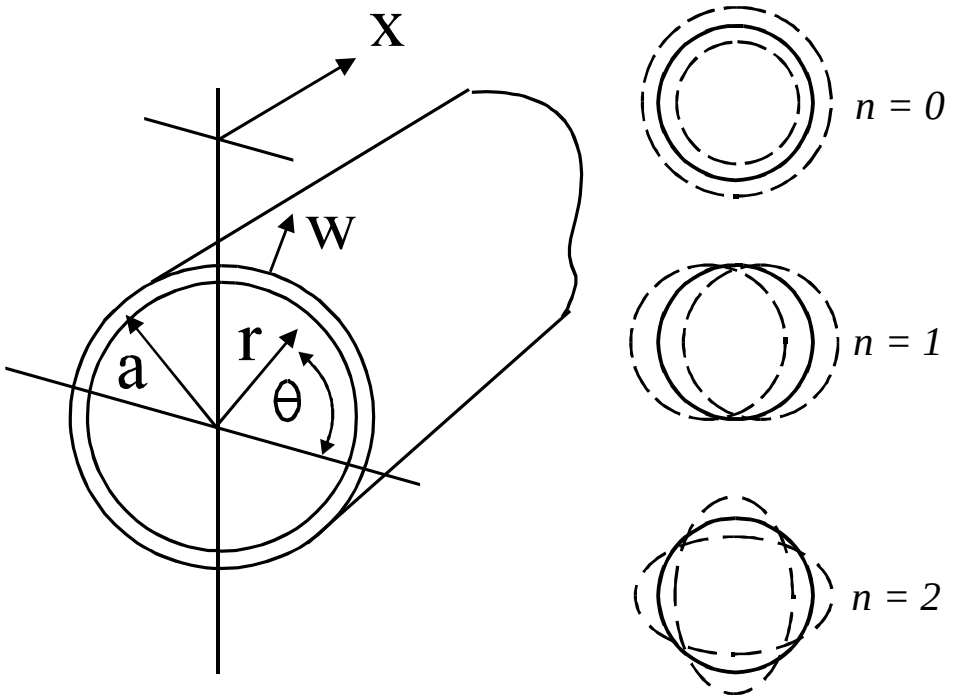

Figure 2.1 - Infinite cylinder coordinate system and modal shapes

---

where W_{ns} is the complex modal amplitude and k_{ns} is the axial wavenumber obtained from the system dispersion equation [4]. The corresponding interior pressure caused by this shell motion is given by

$$p(x,r,\theta,t) = \sum_{n=0}^{\infty} \sum_{s=1}^{\infty} P_{ns} \cos(n\theta)\, J_n(k_s{}^r{}^i r)\, e^{i\omega t - ik_{ns}x} \quad \textbf{(2)}$$

where the radial wavenumber $k_s{}^r a$ is given by

$$k_s{}^r a = \sqrt{k_o a^2 - k_{ns} a^2} \quad \textbf{(3)}$$

and $k_o=\omega/c_o$ [4]. Equation (2) shows that there is a direct one to one coupling between the circumferential modes in the shell and the fluid so the problem can be examined at individual circumferential modes, n. Evaluating equation (2) at x=0 and dropping the $e^{i\omega t}$ term results in

$$p_n = \sum_{s=1}^{\infty} P_{ns} J_n(k_s{}^r r) \qquad \textbf{(4)}$$

Fuller, et al. [4] demonstrated that the shell modal amplitude W_{ns} and the pressure modal amplitude P_{ns} are related by

$$P_{ns} = \left[\frac{\omega^2 \rho_f}{k_s{}^r J_n^{/}(k_n{}^r a)} \right] W_{ns} \qquad \textbf{(5)}$$

where ρ_f is the density of the acoustic fluid. This equation can be rewritten as

$$P_{ns} = \gamma_{ns} W_{ns} \qquad \textbf{(6)}$$

where γ_{ns} represents the coupling factor between the shell and fluid amplitudes for a wave or mode (n,s).

Restricting the evaluation of the shell modal amplitudes to a finite number M and evaluating the internal pressure at an equal number of points allows the vector of pressures to be expressed in matrix form as

$$\begin{bmatrix} p_n^{\,1} \\ p_n^{\,2} \\ \vdots \\ p_n^{\,M} \end{bmatrix} = \begin{bmatrix} \gamma_{n1}\psi_{n1}^{1} & \gamma_{n2}\psi_{n2}^{1} & \cdots & \gamma_{nM}\psi_{nM}^{1} \\ \vdots & \ddots & & \vdots \\ \gamma_{n1}\psi_{n1}^{M} & \gamma_{n2}\psi_{n2}^{M} & \cdots & \gamma_{nM}\psi_{nM}^{M} \end{bmatrix} \begin{bmatrix} W_{n1} \\ W_{n2} \\ \vdots \\ W_{nM} \end{bmatrix} \qquad \textbf{(7)}$$

where $\psi_{ns}=J_n(k_s^r r)$ is the radial mode shape of the pressure field and the superscript $j=1,2...M$ refers to each discrete pressure evaluation point.

Equation (7) reveals the essential low frequency structural acoustic behavior of an aircraft fuselage. To illustrate the effects of different coupling factors between shell displacement and acoustic response, an example with a changing γ_{ns} is considered. It is possible for instance that W_{ns} is very small, while the associated γ_{ns} is very large due to $J_n'(k_s^r a) \cong 0$ near an interior cavity resonance frequency. In this case, the coupled interior pressure due to the relatively small wall motion will be large. Alternatively, W_{ns} may be large while the modal component of pressure is small, perhaps due to $J_n(k_s^r a) \cong 0$. This behavior leads to the difficulty in identifying some fuselage motions which are important in terms of interior sound levels when their structural modal amplitudes are small compared to other motions that are weakly coupled to the interior space.

A possible solution to this problem is to use an alternate means to drive the interior pressure distribution so that it closely matches the total response due to the original structural disturbance. The resulting fuselage vibration due to this interior pressure disturbance can then be examined to determine the important small-scale motions likely to be missed in a direct analysis of the original vibration field. Inverting equation (7) gives

$$\begin{bmatrix} W_{n1} \\ W_{n2} \\ \vdots \\ W_{nM} \end{bmatrix} = [\beta] \begin{bmatrix} p_n^1 \\ p_n^2 \\ \vdots \\ p_n^M \end{bmatrix} \quad \textbf{(8)}$$

where β is the inverse of the square matrix $[\gamma^n \psi^n]$. The total pressure at $(0,r,\theta)$ is made up of a sum of circumferential modes, as

$$p(r,\theta) = p_0 + p_1\cos(\theta) + p_2\cos(2\theta) + p_3\cos(3\theta) + \ldots \quad \textbf{(9)}$$

where $e^{i\omega t}$ has been omitted for clarity.

It is clear from linear systems theory that exactly reproducing the disturbance pressure field should also cause exact reproduction of the original fuselage vibrations. However, if a gross approximation of the pressure field is constructed, consisting of only the dominant cavity modes, the many poorly-coupled structural modes should not be driven by the simplified acoustic excitation. As an example, if the disturbance interior pressure field is dominated by the n=2 mode and this n=2 pressure field component can be reproduced accurately, then the corresponding shell vibration will be given by equations (9) and (4) with p_n set to $p_2 cos(2\theta)$, where p_2 is the n=2 disturbance pressure amplitude. The resulting vibration may be small since β_{n2} may be small. Another mode ($n \neq 2$) may have a larger structural motion but with little corresponding acoustic response, and therefore will be filtered out as acoustically unimportant by the inverse excitation of the structure.

The simple analysis above illustrates the mathematical basis of a potential system identification technique for determining the fuselage vibrations that are well coupled to the cabin noise field. A more realistic fuselage model would extend this work to a finite length odd-shaped cavity. Adding cylinder end caps and a cabin floor introduces two dimensional spatial coupling and suppresses the periodicity in θ, eliminating the simple one to one coupling of the circumferential modes. However, the important modal coupling behavior between structural motion and interior pressure remains, presenting the possibility of an experimental process to explore the coupled system behavior of an actual fuselage.

2.2 Singular Value Decomposition

The singular value decomposition (SVD) [42] is a mathematical tool for separating any matrix populated with real or complex values into orthogonal components. Similar in function to the eigenvalue analysis, the SVD can operate on non-square matrices, and is very powerful and highly robust in situations with singular or nearly-singular matrices that typically cause problems with many computational techniques. The linear transformation is described by

$$U \Sigma V^{*} = A \qquad \textbf{(10)}$$

where **A** is the matrix to be decomposed and **U**, **V**, and Σ are the decomposition products. The orthonormal vectors found in the columns of **U** and **V** are termed the left and right singular vectors of **A** respectively. The matrix Σ is a diagonal matrix containing the

singular values of **A**, which are found in descending value progressing along the diagonal, and represent the weight or relative contribution of each orthogonal component to **A**.

The SVD transformation process can be used as a reconstruction tool, to focus only on certain orthogonal components of a set of data described by **A**. For example, **A** might contain an evenly-spaced grid of structural velocity measurements, and the SVD would allow examination of each individual orthogonal vibration component. The separation of principal components can be achieved by constructing a new matrix Σ'. This matrix leaves one or more of the original singular values in Σ unchanged, with the remainder of the diagonal members replaced with zeros. Σ' is substituted into equation (10) to compute a new data set **A'**, which is a reconstruction containing only the orthogonal components specified.

Because of its robust performance with numerically ill-conditioned situations, SVD is also a method of choice for solving linear least-squares problems. To find a vector **x** that minimizes the expression $|\mathbf{Ax} - \mathbf{b}|^2$, the results of the SVD of **A** can be substituted into

$$x = \sum_{i=1}^{M} \frac{u_i b}{\sigma_i} v_i \qquad \textbf{(11)}$$

where σ_i is the *i*th singular value and $\mathbf{u}_i$ and $\mathbf{v}_i$ are its associated singular vectors. In some cases, especially when dealing with an **A** matrix composed of experimentally-measured values, several of the σ_i values may be very close to zero. To avoid large errors in the least-squares fit, the corresponding $1/\sigma_i$ factors in the above summation are set to zero to remove the impact of these insignificant terms. In this way, the SVD can be used to

guarantee meaningful results for a least-squares fit in circumstances where other methods suffer severely from numerical ill-conditioning.

2.3 Genetic Algorithms for Optimization

An important consideration in the design of an ASAC system is the optimal positioning of the secondary source actuators such that they efficiently couple to the structural-acoustic system. Existing optimization techniques used throughout the engineering disciplines fall into three broad areas: enumerative, calculus-based, and random searches [43]. Enumerative searches deal with a finite, discrete search space and compare objective function values at every point in the space. While effective in finding the global maximum in any search, the inherent inefficiency of enumerative techniques makes them ill-suited for problems with high dimensionality. Calculus-based searches typically either directly solve for zero-gradient points in an analytical objective function or employ a gradient search method (the common "hill-climbing" approach) to take steps towards the nearest local maximum. While effective for many classes of problems, particularly analytical work, such methods are of limited usefulness for the noisy and often discontinuous objective functions common in some real-world problems. The third class of optimization methods, random searches, include simple random walks as well as directed searches with randomized or probabilistic decision-making, such as genetic algorithms and simulated annealing. Because they can usually locate an effective solution with far less computation than that required for an enumerative search, these randomized methods are currently very popular optimization techniques for many experimental applications, including the complex multi-modal search spaces found in the actuator positioning problem.

Genetic algorithms (GAs) [43], first developed by Holland [44], are an important branch of the more general field of evolutionary algorithms [45, 46]. GAs share with other evolutionary computing techniques the use of several idealized operators to mimic the process of Darwinian natural selection on a population of candidate solutions. In GAs, each of the potential solutions is a fixed-length string representation of the problem's parameter set. The basic operators acting on these strings are reproduction, crossover, and mutation.

Figure 2.2 shows a flowchart of a simple GA implementation. The process begins by randomly generating a starting population of solutions. Each member of the population is evaluated for "fitness" according to an analytical objective function. Solutions are selected by the reproduction operator for inclusion in the next generation with a probability proportional to the member's fitness. After a new generation is populated in this manner, the crossover operator simulates a mating process by randomly exchanging "genetic" information between an arbitrary pair of members, via partial string exchanges, with probability P_c. The mutation operator alters a random element in a string with probability P_m, adding robustness to the process by preventing focused concentration on a small area of the search space. The entire process then repeats on successive generations until acceptable convergence to an area of maximum fitness occurs.

It is important to note that GAs operate on a coding of the problem's parameter set, not the parameter variables themselves, and different coding schemes can result insignificantly different algorithm behavior. For example, a problem coded as a string of integers could be recast into a binary string representation, which although containing identical information would likely result in very different search pattern through the solution space. Changing the population size or the probabilities used by the GA

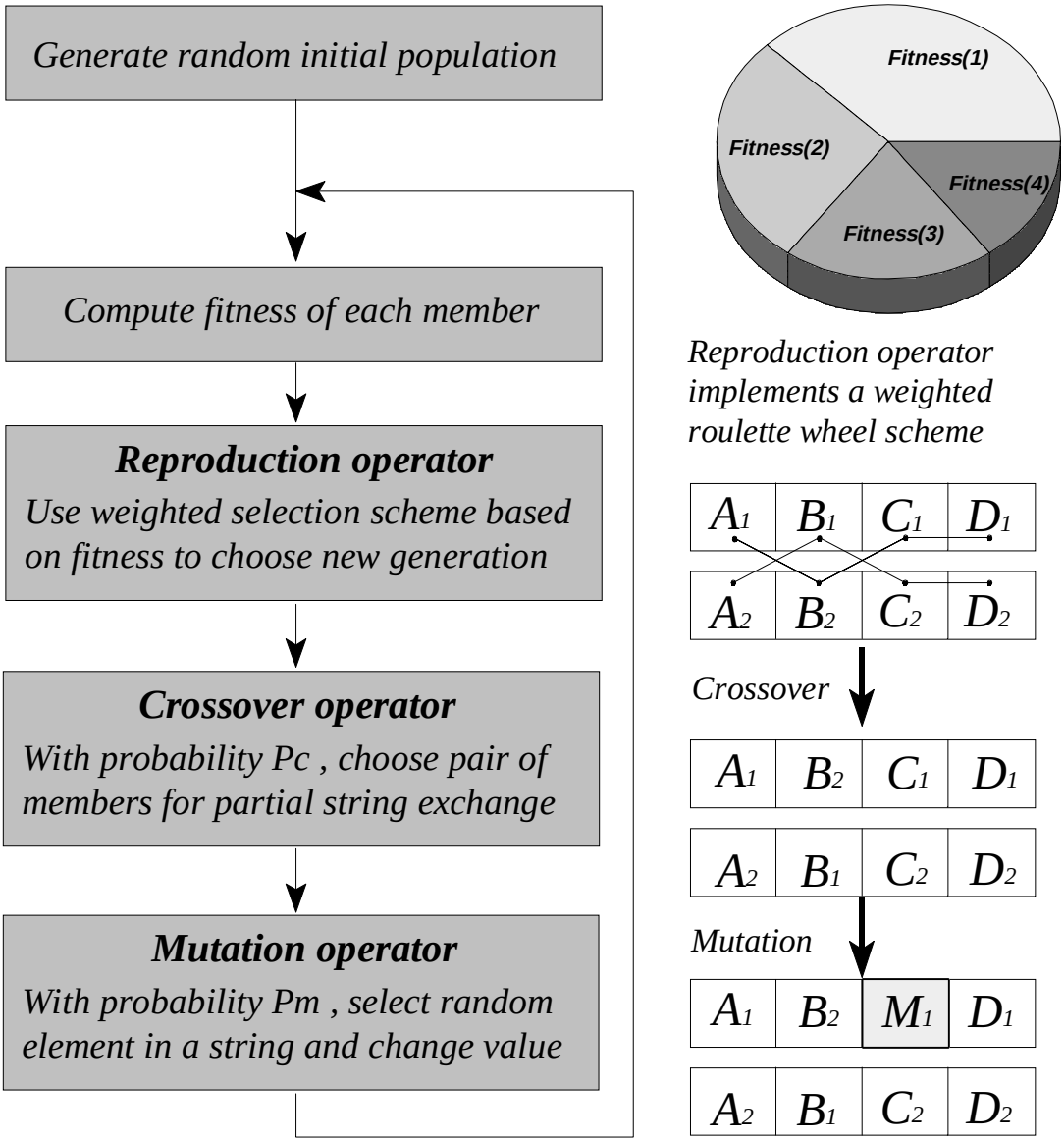

Figure 2.2 - Schematic of simple genetic algorithm

operators, as well as the implementation details of these simple operators, can also have a large impact on performance. Therefore the GA can be carefully tuned to an individual problem, allowing a search that explores large areas of the solution space and yet converges to a solution of global maximum fitness very rapidly.

GAs have recently been successfully applied to position optimization of actuators and sensors in various applications [47-49], including work specifically addressing active control in aircraft fuselages [50, 51]. The latter references in particular provide excellent discussions of issues affecting GA performance for the actuator positioning problem, such as differences in parameter coding and operator probabilities as well as fitness scaling methods and other more advanced techniques of ensuring population diversity and therefore search robustness.

Chapter 3

Experimental Procedures

3.1 Overview of Experimental Rig and Equipment

Before discussion of the experimental procedures developed for this work, an overview of the testing facilities and equipment will be given. The Cessna Citation III fuselage (M560 airframe) resident at VPI&SU provides a realistic testing platform for aircraft interior noise work. Figure 3.1 shows the fuselage in its lab environment, with an electromagnetic shaker attached to provide a radially-directed disturbance force at an engine mount at the rear of the plane. For the numerous diagnostic and control experiments required by this work, comprehensive measurements of the cabin interior pressure field and fuselage shell velocity are essential. An automated system for collecting acoustic pressure data was previously designed and built at V.P.I. for Cessna Aircraft Corp. [52], and was borrowed and adapted for this project.

The fuselage scanning system consists of a platform which traverses approximately 85% of the passenger cabin area in 27 axial steps, evenly spaced every 17 cm (6.5 in). A set of phase-matched Metravib microphone probes is arranged across the fuselage cross-

Figure 3.1 - Exterior view of fuselage test rig

section at several radial distances. For this project, 60 pressure measurements are recorded at each axial location. Also attached to the measurement platform is a Polytec OFV-501 laser vibrometer on a rotating mount, aligned radially in order to measure normal velocity of the fuselage at 22 points per axial step. The vibrometer measurement locations are separated by 12^{o}, or 19 cm (7.5 in) at the wall surface, and cover approximately 75% of the fuselage circumference, which is the area of the shell located above the cabin floor. A Macintosh-based 16-channel Zonic signal analyzer is used for data collection and signal processing, while a standard PC controls the system's axial and rotational stepper motors and stores the measurement data. Figure 3.2 shows a schematic of the measurement system. A complete scan of the fuselage interior with this system yields approximately 1600 pressure values and 600 velocity measurements.

Figure 3.3 shows a photograph of the fuselage interior with the scanning platform in place. The vibration measurement locations can be identified by the highly-reflective paint needed for accurate laser vibrometer usage. Note that all experiments for this project were performed with the fuselage in the shown "green" configuration, without interior trim.

3.2 System Identification Procedure

As described in section 2.1, the coupling factors between different modes of fuselage vibration and the resulting acoustic response in the cabin can vary widely. In order to identify only the well-coupled structural motions that lead to significant interior noise, an experimental procedure making use of an active control system was developed. This project addressed the case of a harmonic structural excitation, applied as a point force

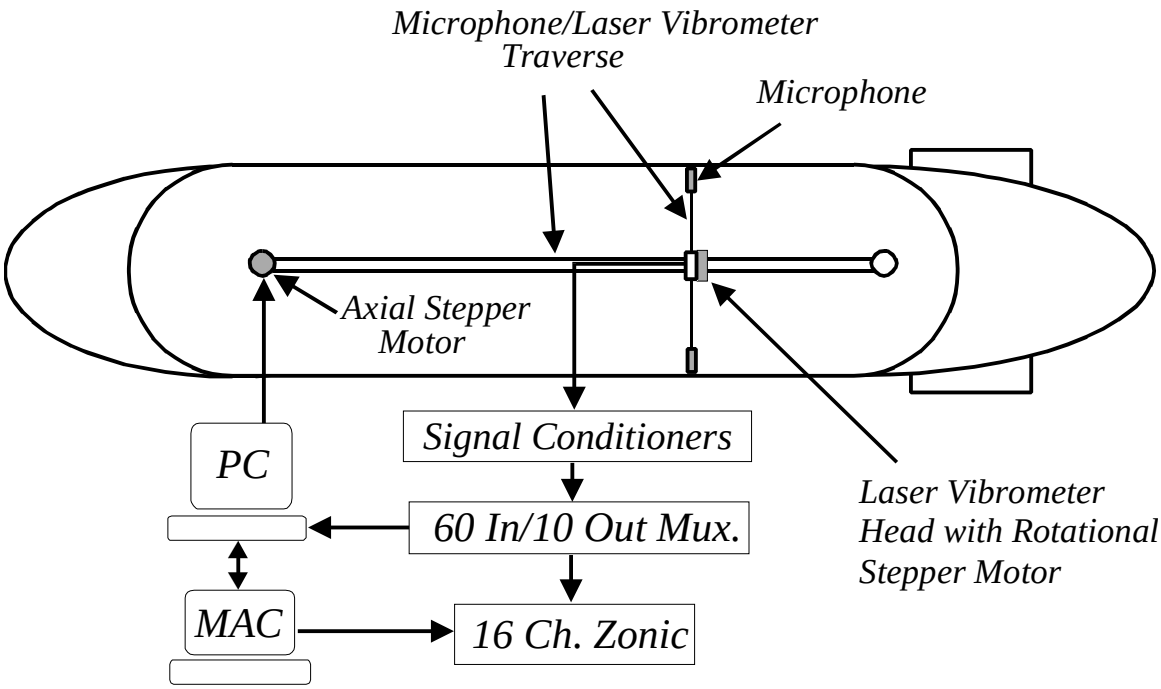

Figure 3.2 - Schematic of Fuselage Measurement System

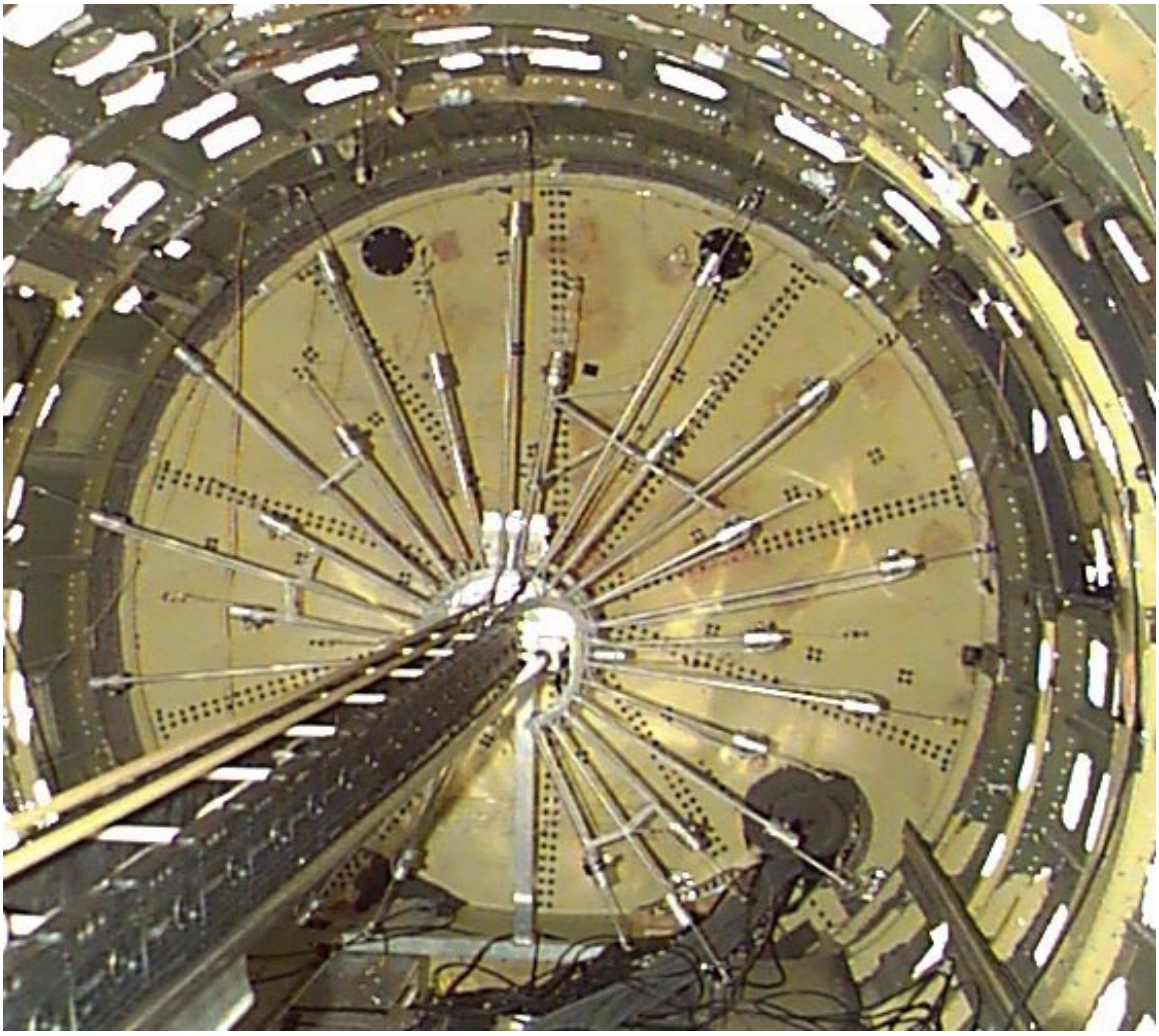

Figure 3.3 - View of fuselage interior with measurement system

input by the shaker mounted at an engine pylon. Prior to any experiments developed for this work, the fuselage scanning system is used to measure the uncontrolled cabin interior pressure field and normal velocity of the fuselage shell. Throughout this project, three frequency cases are examined: an acoustic cavity resonance, a structural resonance, and an off-resonance case.

The inverse system identification technique begins by applying active control to the interior noise field produced by the disturbance force, with a goal of maximizing the global control performance. The control system uses 12 standard 5 inch speakers as control actuators. These are arranged throughout the cabin and clamped to the fuselage walls. In most cases, the speakers are positioned in anti-nodes of the measured uncontrolled interior pressure field. Error microphones are positioned in the cabin in a similar manner, with the goal of global noise control generally dictating locations in pressure anti-node regions and some distance away from the control loudspeakers.

The active system is driven by a multi-channel time-domain feedforward filtered-X LMS control algorithm [53], implemented previously at VPI on a Texas Instruments TMS320C31 development board residing in a 486 PC host. For the system identification experiments, the controller is operated in a 12 input - 12 output configuration, requiring expansion boards for sufficient channels of A/D and D/A conversion. The 12 error microphones (PCB 513) are bandpass filtered at the excitation frequency before their input to the controller. The error sensors are arranged throughout the passenger cabin, generally near the fuselage walls and most at passenger head level. Four additional reference microphones are placed in the cabin to test for global sound reductions away from the error sensors. Lowpass filtering is applied to the controller output signals to remove the zero-order hold effect of the D/A converter.

Figure 3.4 shows a schematic of the active control system in place in the fuselage. The filtered-X LMS algorithm used widely in active control work makes use of the feedforward control paradigm. In this type of controller, a reference signal is sensed and passed through an adaptive filter to provide an appropriate control signal downstream of the system plant. The adaptive filters are automatically adjusted to minimize the resultant controller error. "Filtered-X" refers to the practice of capturing a reference signal upstream of the plant and passing it through another set of electronic filters, which model the plant dynamics. This technique provides a filtered-X signal that is insensitive to plant disturbances, and when used as part of an LMS control implementation, typically provides rapid convergence and tracking of the primary disturbance signal and robust performance in the face of plant noise.

The narrowband implementation of the filtered-X algorithm used for this work performs an off-line system identification to model the paths from actuators to error sensors with two-coefficient FIR filters. The reference signal in this work is the sinusoid used to drive the shaker disturbance, and is passed through these FIR filters to provide the filtered-X signal for the LMS algorithm.

This controller setup is used to investigate actuator and sensor arrangements that maximize the global effects of the control pressure field. As described earlier, the loudspeakers and error microphones are positioned primarily in pressure anti-nodes of the uncontrolled cabin noise field. Several geometry configurations are compared in terms of achievable global noise reductions, as measured by several auxiliary reference microphones in the cabin. Once a control configuration has been selected, the controller is allowed to converge and is then locked by setting the adaptation coefficient, μ, to zero. With the sinusoidal reference signal still supplied to the controller, the disturbance force is

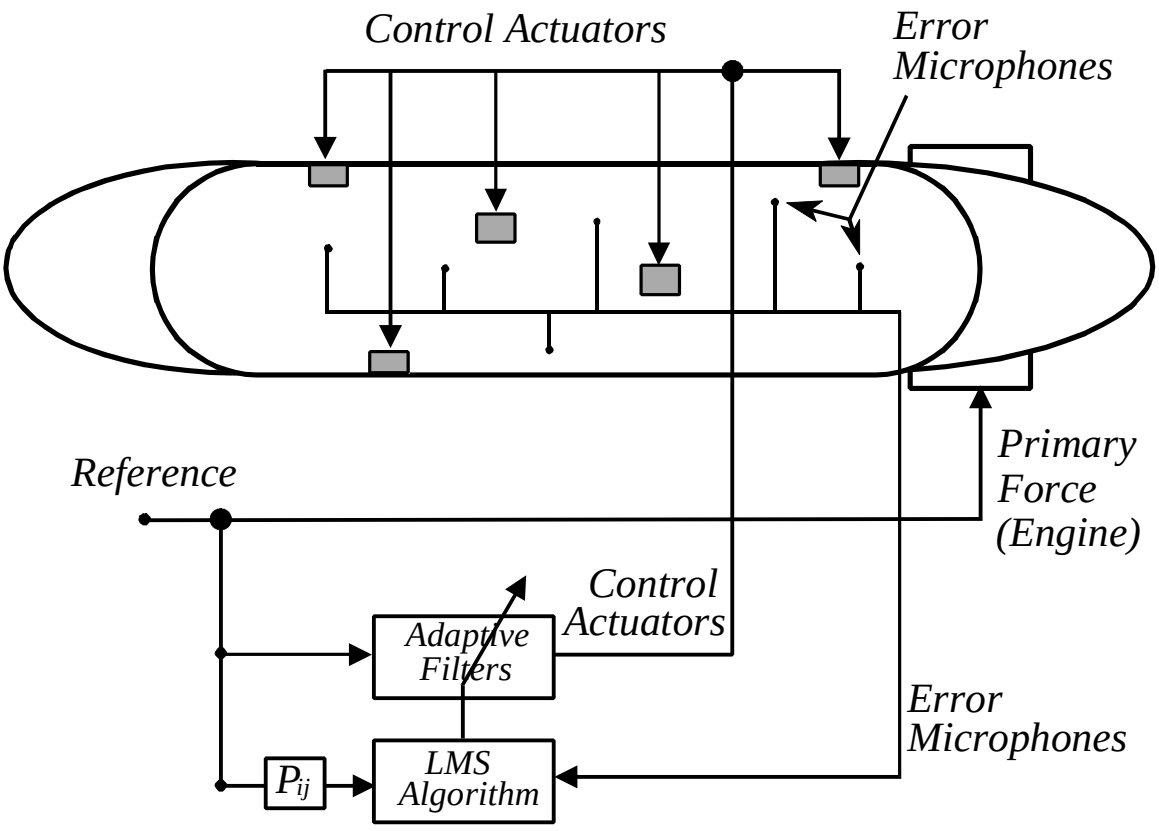

Figure 3.4 - Schematic of Active Control System

removed. This leaves an approximation of the original disturbance noise field, generated by the control speakers, which is 180^{o} out of phase with the original. This pressure field induces fuselage structural motions, which contain only the normal vibration components most strongly coupled to the interior cabin noise field. A set of fuselage scans with the laser vibrometer is performed to measure these motions, as well as to record the interior pressure field for later comparison to the uncontrolled case.

The experimental steps in system identification phase of this work can be summarized as follows:

- Measure uncontrolled fuselage interior pressure and shell normal velocity due to shaker force disturbance.
- Position control loudspeakers and error microphones to maximize global noise control performance. Several different configurations are evaluated.
- Lock LMS controller after sufficient global cabin noise reductions are achieved.
- Remove disturbance force
- Measure cabin noise field and acoustically-induced shell vibrations with measurement system. The new vibration field should contain only the well-coupled fuselage motions responsible for the cabin noise problem.

3.3 Actuator Position Optimization

After the procedures described above, candidate positions for piezoelectric (PZT) actuators are selected based on the measured system identification data. The vibration patterns recorded in that work should consist of only the acoustically important fuselage

motions. Therefore, an appropriate goal in positioning control actuators for an ASAC system is to provide for direct reproduction of the well-coupled vibration field measured during the system identification. The goal of the ASAC experiments in this work is once again to maximize the global effects of cabin interior noise control. Using a controller configuration with more error sensors than actuators is one method of improving the global performance, so therefore only six actuators will be used in the ASAC tests, as compared to the 12 active sources in the system identification work.

The following sections detail the processes for analysis of the system identification data, placing actuators on the fuselage, and selecting the optimal set of actuators from among many potential candidate groups. In keeping with the experimental approach used to this point, the final actuator groupings for ASAC work are determined via analysis of physical data from the fuselage test rig.

3.3.1 Candidate Actuator Placement

Determining appropriate candidate actuator positions on the fuselage test rig begins with analysis of the system identification data collected by following the procedure described above. Since piezoelectric patches typically cause large local structural excitations, an obvious placement scheme is to focus on regions of the largest fuselage motions, induced by the inverse excitation of the structure with the approximated interior pressure field. As an aid in examining the principle components of the response patterns, the SVD is used as a reconstruction tool as described in section 2.2. The contributions of the first three singular vectors of the decomposed fuselage motions are considered. Based on the resulting smoothed vibration fields, a number of candidate positions are chosen on

the fuselage, and are mounted near the center of wall panels between structural frames and stringers. The number of candidate positions selected in this step of the test procedure for each test frequency is much larger than the six actuators planned for use in the ASAC tests. An optimization search will be later used to select the best set of actuators from among the 16 total candidates.

The actuators used in this project are custom PZT patches, approximately 7.6 cm long by 3.8 cm wide by 0.76 mm thick. The patches were manufactured pre-curved to match the radius of curvature of the fuselage test rig used in this work, which is approximately 0.9 meters. Thin copper leads are attached to both sides of a patch to provide an input voltage. Standard 5 minute epoxy is used to bond the actuators directly to the fuselage skin. The actuators are positioned flush to the surface with a sufficient glue layer to avoid electrically grounding a patch to the aluminum shell.

The center-of-panel mounting location was determined by an analysis of simply-supported plate motion. Piezoelectric patch actuators bonded to a structure cause out-of-plane motion via plate bending by inducing strain in the structure under the patch area. Thus, the actuator should ideally be located in the area of maximum strain of the vibrating plate. For a simply-supported plate, the displacement is described by

$$w(x,y) = \sum_{m=1}^{\infty} \sum_{n=1}^{\infty} a_{mn} \sin(\frac{m\pi x}{L_x}) \sin(\frac{n\pi y}{L_y}) \qquad \textbf{(12)}$$

and the strain on the top surface of the plate is described as

$$\varepsilon_x = -\frac{t}{2}\frac{\partial^2 w}{\partial x^2}, \quad \varepsilon_y = -\frac{t}{2}\frac{\partial^2 w}{\partial y^2} \tag{13}$$

where t is the plate thickness [54]. These strain expressions are evaluated to determine the maximum magnitude for the (1,1) mode of the plate, which is the most efficient sound radiator. The optimal actuator placement is thus seen to be at $x=L_x/2$ and $y=L_y/2$, the center of the plate surface.

The use of a simply-supported plate to model an individual fuselage wall panel in this actuator position analysis is clearly a simplification from the actual conditions of both curved wall surfaces and curved actuators. However, experience shows that the actuators used in this research cause out-of-phase vibration response in the fuselage wall panels adjacent to the actuator mounting point, so approximating the frames and stringers as pinned edge conditions appears to be an acceptable modeling decision in this case.

3.3.2 ASAC Actuator Configuration Optimization

After candidate actuators are mounted in positions chosen in the above step, an optimal ASAC configuration is determined via a genetic algorithm search. In order to rate the performance of a given actuator set, information concerning the structural response due to each patch is required. This information is gathered by individually exciting each candidate actuator with a harmonic disturbance voltage. For each actuator, a full scan of the fuselage shell motion is performed, yielding transfer functions between actuator input signal and resulting shell motion for a large number of measurement points. The vibration

fields recorded this way provide a measure of the actuator-structure coupling behavior, and are used in the fitness evaluation needed by the genetic algorithm.

The GA code developed for the actuator grouping problem was written in C++, and is similar in function to the simple genetic algorithm (SGA) presented by Goldberg [43]. The parameter representation chosen for this work is a simple integer coding, where each candidate actuator is assigned a unique value and each string contains a concatenated list of the selected actuators. The three fundamental GA operators act as described in section 2.3, with additional checks occurring in each step to prevent repeated members in the string representing the chosen actuator group. Appendix A provides a complete listing of the optimization program.

The fitness evaluation for each potential grouping of six candidate actuators is performed by using a least-squares fit as described in section 2.2. The target vector, *b*, in this case consists of the normal velocities that are measured during the system identification phase of the work. Some measurement points located on windows, doors, or in the immediate vicinity of the candidate actuator positions are eliminated from *b*, resulting in a vector containing approximately 480 measured velocities. The columns of the matrix *A* are populated with the corresponding velocities that were measured when each of the candidate actuators under consideration was excited individually. Solving the resulting overdetermined system in a least-squares sense yields a complex vector *x* representing optimal actuator control voltages for the chosen grouping. Substituting this vector back into $|A \cdot x - b|^2$ provides a value of the mean squared error between the desired response, or the vibration field measured during system identification, and the calculated response potentially achievable by the six chosen control actuators. A value proportional to the reciprocal of this error value is used for a fitness measure in the GA.

The GA program is executed for a number of generations until convergence to one or more high-fitness candidate groups is exhibited. From the above least-squares formulation, the highest fitnesses correspond to the actuator sets best able to reproduce the desired structural vibration patterns. Thus, the six candidate actuators belonging to the highest-fitness group as chosen by the GA are selected for future ASAC work.

To gauge the performance of the GA in this work and also guarantee an appropriate grouping of actuators for the ASAC experiments, an enumerative search is also carried out. The fitness value described above is calculated for all combinations of six candidate actuators and stored in a list for later use.

3.4 ASAC Testing

After the optimal set of PZT actuators is determined for a particular ASAC experiment, the control system's effectiveness is tested with the same 12-channel controller used in the earlier ANC work (section 3.2), but with a configuration making use of only six of the control outputs (i.e. a 12 input - 6 output controller). As described earlier, use of an overdetermined control setup with more control inputs than outputs should result in increased global control performance. In order to provide a direct comparison of ANC and ASAC control system effectiveness, the error sensors are positioned in the same locations used for the system identification setup.

Control of the harmonic excitation is now initiated and the sound level reductions at the 12 error microphones and four additional reference microphones are recorded. After adjustment of controller convergence parameters and sensor input levels to maximize the global control performance, the fuselage measurement system is used to comprehensively

record the interior cabin pressure and fuselage shell normal velocity. Scans are performed before and after control is applied, as well as in the case described previously for the system identification experiments in which the controller is locked and the disturbance force is removed. Both interior noise reductions and structural response are used to evaluate the ASAC performance. The importance of determining an optimal actuator group is also investigated by performing ASAC tests for each test frequency on different actuator groups with an average and a worst-case fitness value.

Chapter 4

Experimental Results and Discussion

4.1 Overview of Test Cases

This chapter presents the highlights of the results obtained during this project's experimental work. To properly validate the information from the newly developed system identification technique and investigate the performance of the resulting ASAC systems, three testing frequencies are chosen. Figure 4.1 shows typical frequency response functions for the structural and acoustic components of the fuselage system in response to a broadband random noise input. Dashed marks on the figure correspond to the chosen testing cases of 125 Hz, 170 Hz, and 225 Hz. These frequencies correspond to an acoustic resonance (of the cabin space), an off-resonance, and a structural resonance (of the fuselage) respectively. Each of the resonant cases is chosen such that the opposing component of the coupled system exhibits off-resonance or anti-resonance behavior at that frequency. This allows the structural and acoustic systems to be treated somewhat separately as the dominant responding component when validating the inverse excitation technique in the system identification work.

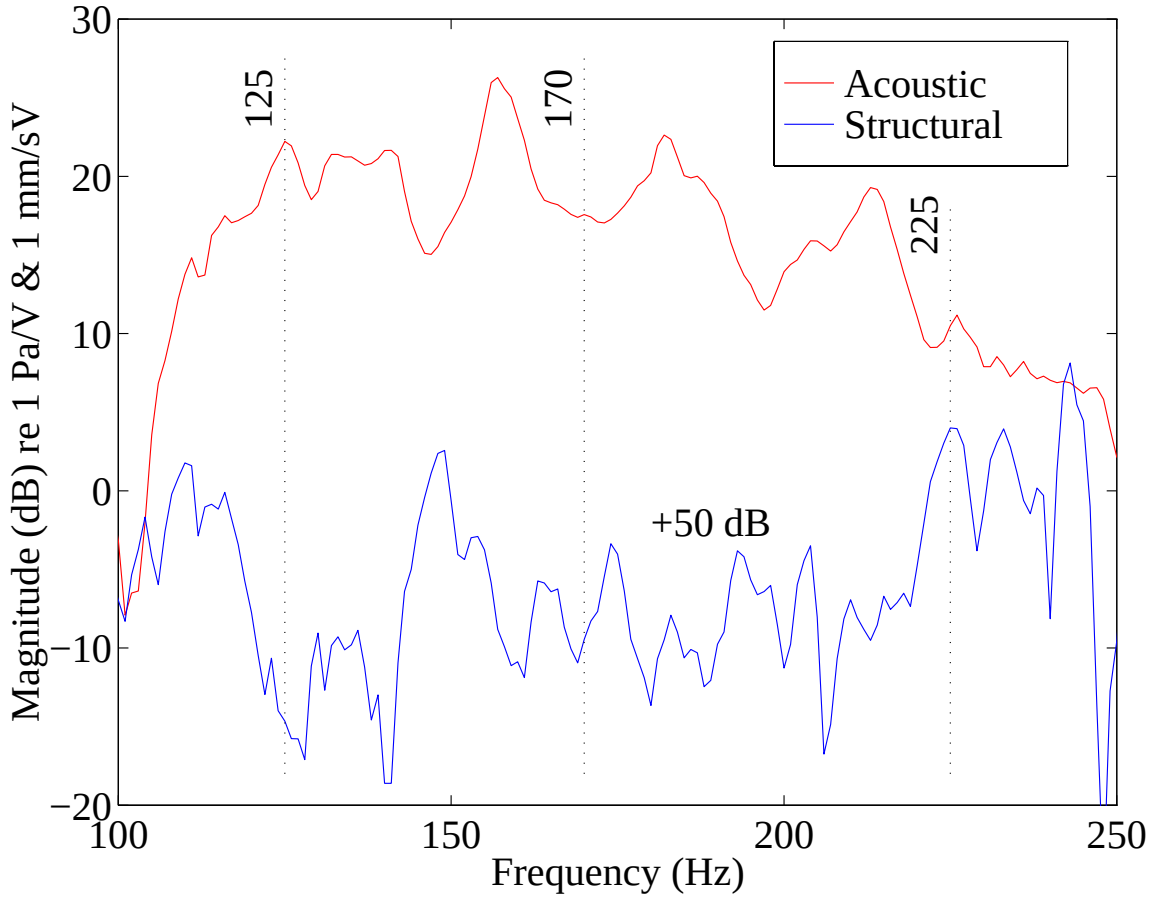

Figure 4.1 - Typical structural and acoustic frequency response functions of fuselage test rig showing chosen test frequencies

4.2. System Identification

4.2.1 System Identification Test Results: 125 Hz Case

Figure 4.2 shows the total interior acoustic response due to harmonic excitation from the attached shaker, driven at the acoustic resonance disturbance case of 125 Hz. The resulting three dimensional interior pressure field is represented by two cross-sectional slices and one axial section comprising the total scanned length of the cabin. The response plot is oriented with the rear of the fuselage towards the upper left of the figure. As a result, one pressure cross section is located at the farthest aft extent of the scanning region and the other approximately 2/3 forward from the rear, slightly aft of the main cabin door.

Figure 4.3 contains a mapping of the out-of-plane fuselage shell velocity response produced by the disturbance force. The view presented is seen "unwrapped" from above the fuselage, with the fuselage facing to the left. The locations of structural frames and stringers, as well as those of windows, the rear escape hatch, and the cabin door, are drawn overlaid on the velocity plot.

Following the procedure detailed in section 3.2, and making use the cabin pressure response information shown in Figure 4.2, a 12 channel ANC system is assembled in the fuselage. Figure 4.4 shows the approximate locations of the control speakers and error microphones on an unwrapped fuselage view. Note that the speakers are mounted directly to the fuselage shell in the positions shown, but the error sensors are located 4 to 12 inches radially inward from the cabin wall. The positions of four global reference microphones, also located up to 12 inches radially inward from the fuselage walls, are also shown on the plot. Using this physical configuration, the controller is allowed to converge

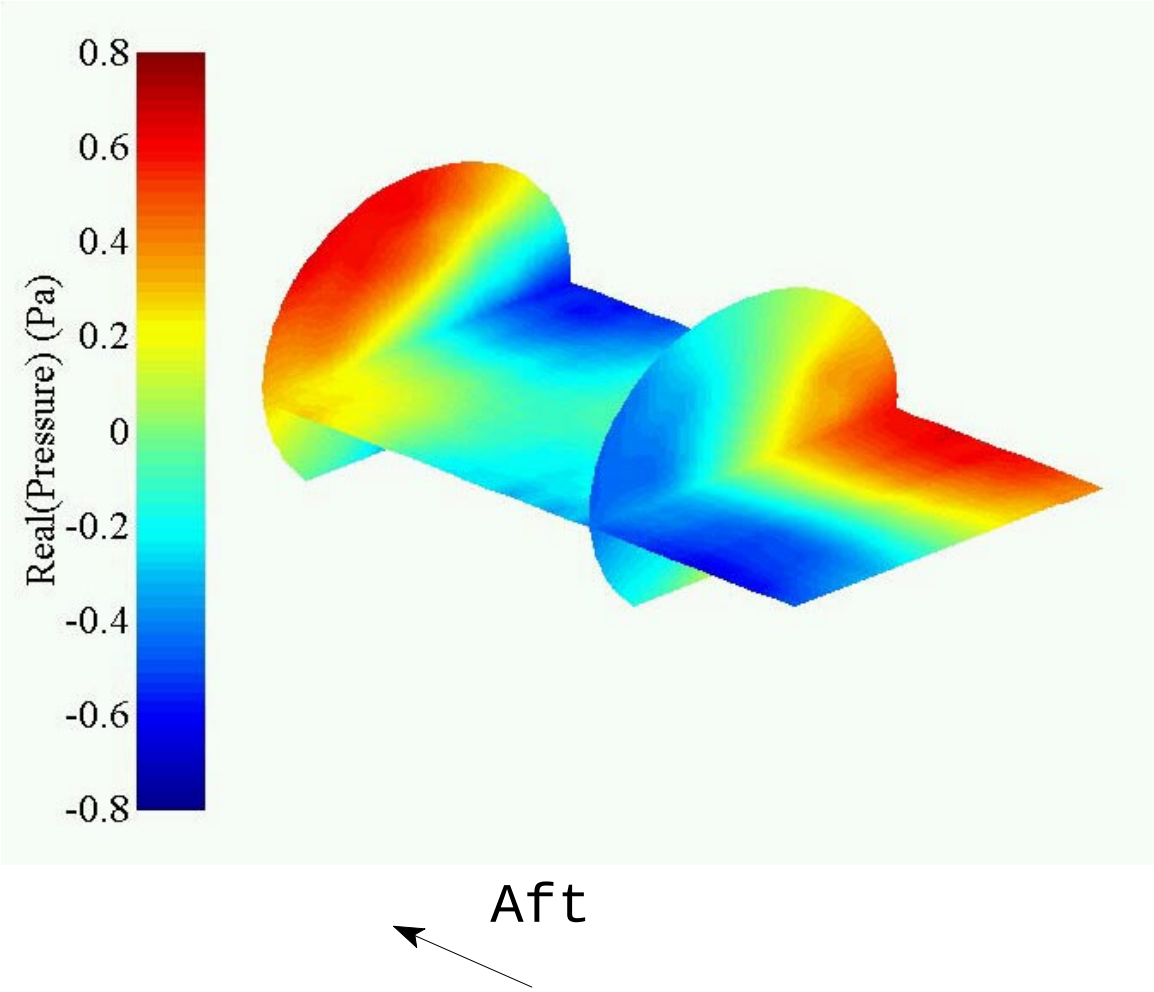

Figure 4.2 - Interior pressure field due to disturbance force at 125 Hz

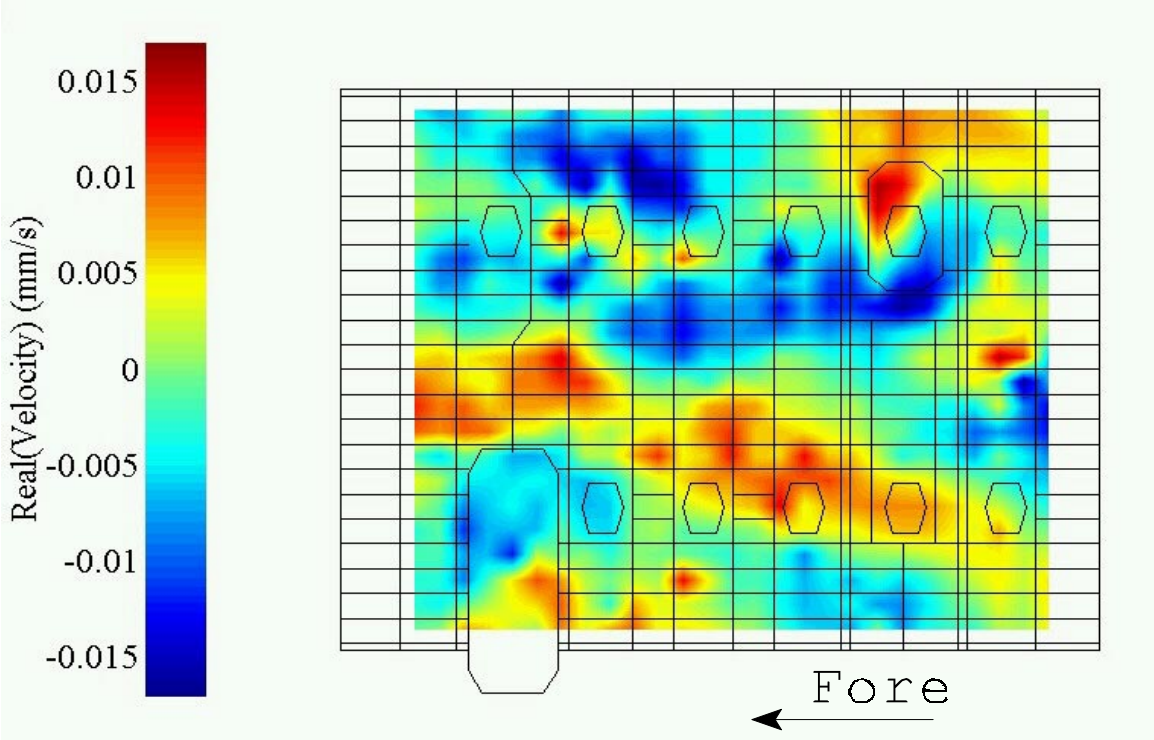

Figure 4.3 - Fuselage vibration field due to disturbance force at 125 Hz

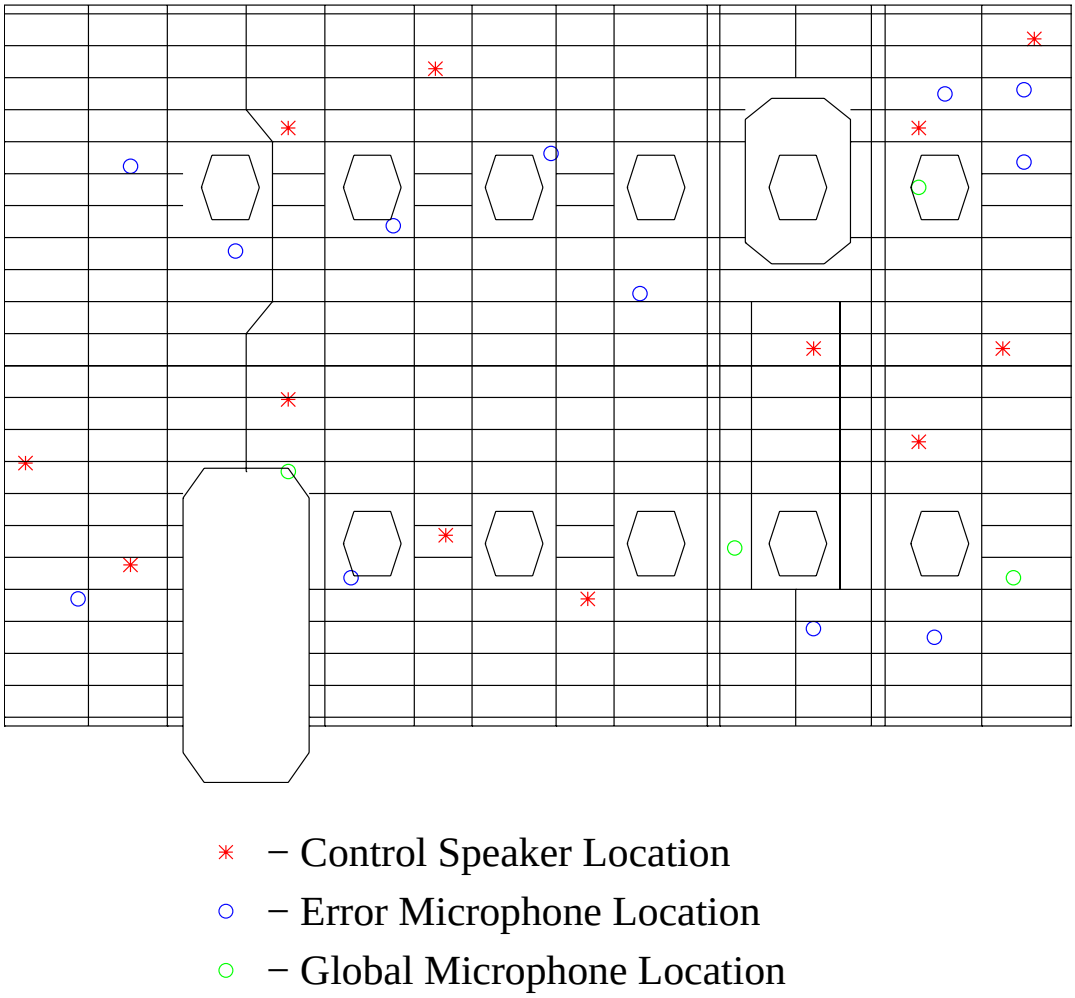

Figure 4.4 - Actuator and sensor locations for 125 Hz system identification tests

and is then locked. With the sinusoidal reference signal still driving the controller output, the disturbance shaker force is then removed, leaving an out-of-phase approximation of the disturbance noise field.

Figure 4.5 shows the cabin interior pressure response due to the secondary control actuators only. Figure 4.6 shows the structural vibration patterns caused by acoustic excitation via the active sources alone. More information about the ANC system performance is found in Figure 4.7, which shows sound level reductions for the 12 error sensors as well as the 4 additional reference microphones.

Several important results of the system identification experiment are immediately apparent in the above figures. A comparison of Figures 4.2 and 4.5 shows that the ANC system has very effectively approximated the gross shape of the disturbance pressure field. The sound level reductions in Figure 4.7 show an average sound pressure level reduction of 28 dB at the error sensors and global control on the order of 12 dB at the non-error reference microphones. Also, the similar peak magnitudes on the two pressure plots denote little if any control spillover in the acoustic space.

The fuselage vibrations induced by this approximated sound field, shown in Figure 4.6, are clearly seen to be much less complex in nature than the original disturbance vibration field shown in Figure 4.3. The measured velocity pattern shown in Figure 4.6 resembles a cylinder vibration mode of circumferential order 4, while the dominant response shape in Figure 4.3 is very unclear. Additionally, the differing plot scales in Figures 4.3 and 4.6 show that for identical sound levels in the aircraft cabin, the well coupled fuselage motions shown in Figure 4.6 are significantly lower in magnitude as compared to the total structural response composed of the sum of all vibrating modes.

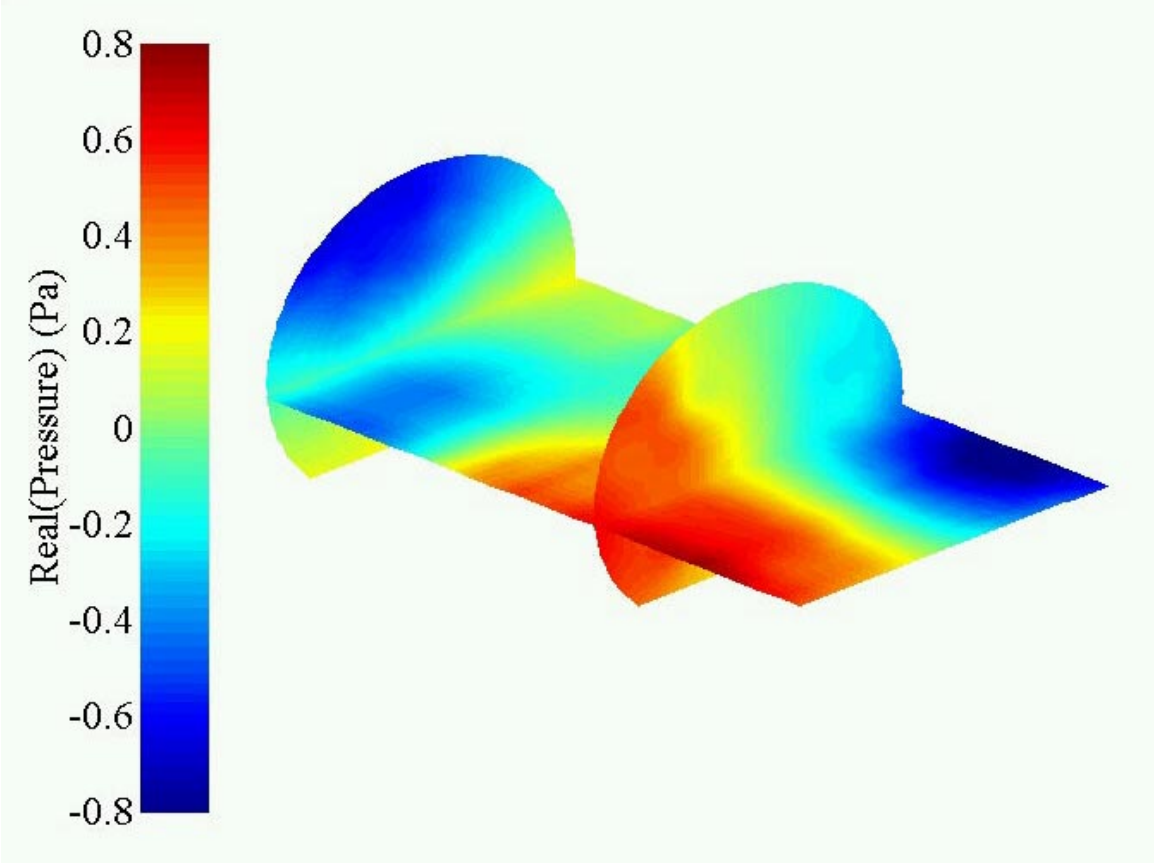

Figure 4.5 - Interior pressure field produced by control loudspeakers at 125 Hz

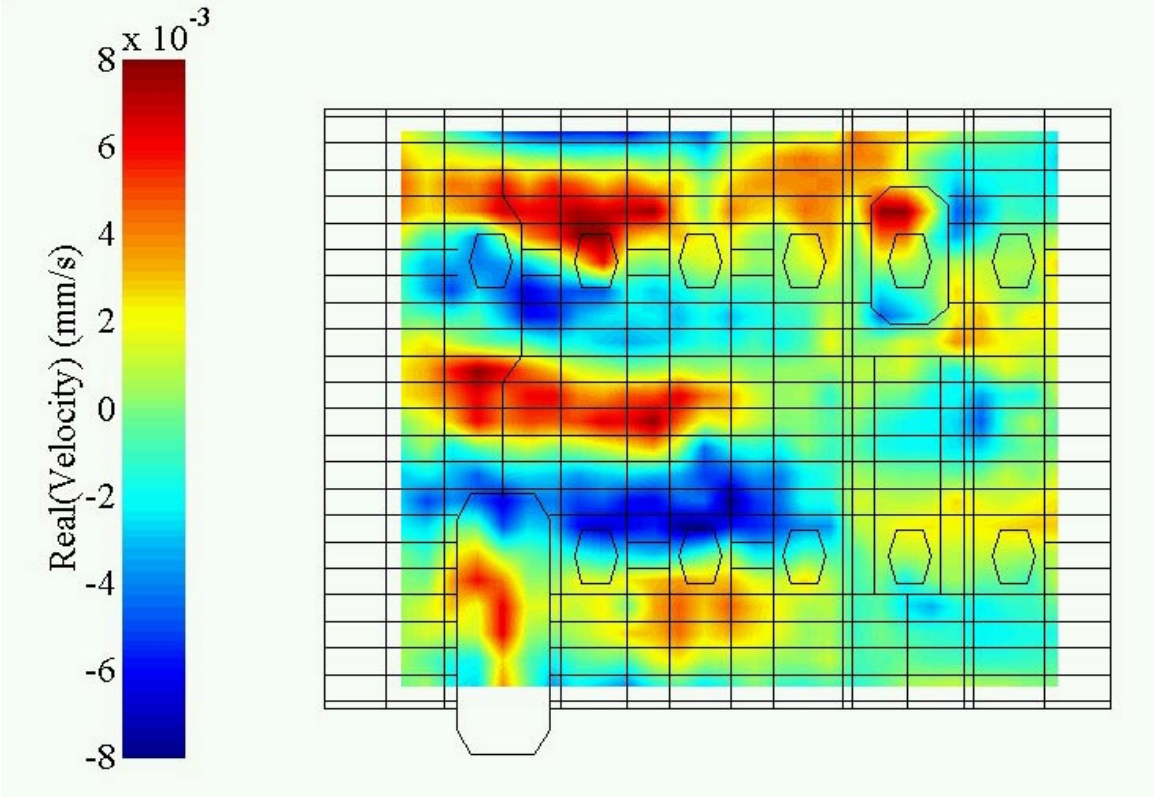

Figure 4.6 - Fuselage vibration field produced by control loudspeakers at 125 Hz

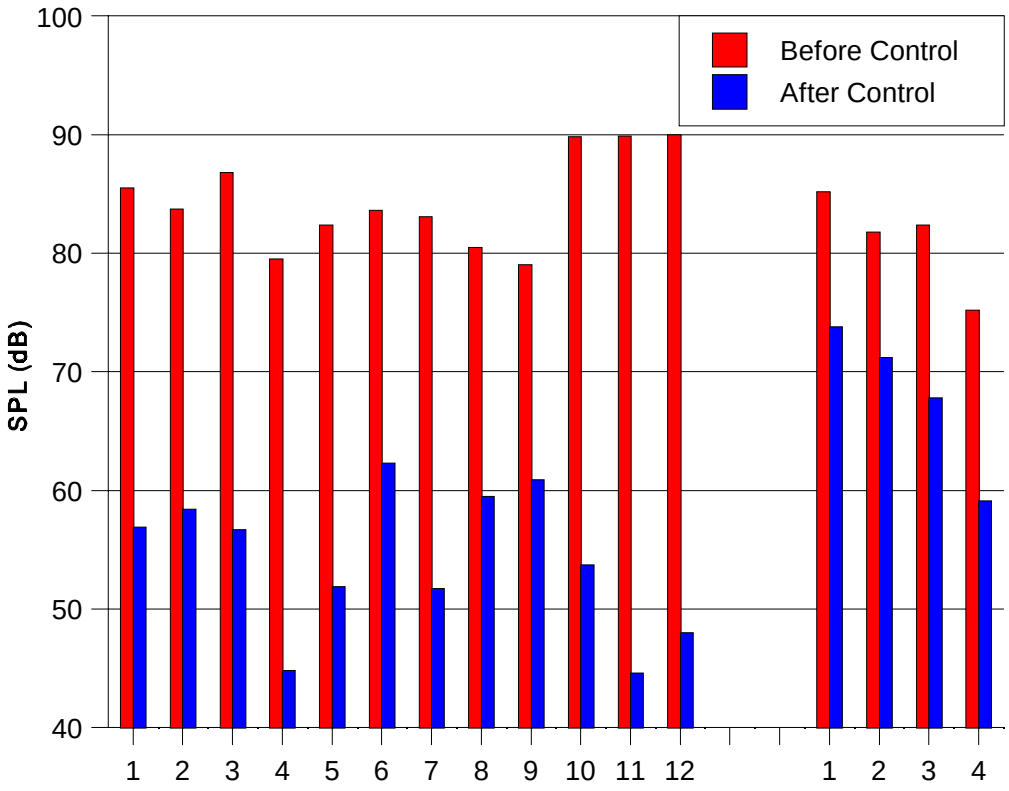

Figure 4.7 - Sound level reductions at error and global microphones for system identification experiments - 125 Hz test case

The singular value decomposition (section 2.2) provides additional insight into the performance of the system identification experiment. Table 4.1 shows a comparison of singular value magnitudes for the vibration fields caused by the primary force disturbance and the control source excitations. As the singular vectors resulting from the decomposition process are orthonormal and both excitation conditions took place with equivalent cabin sound levels, the table provides a direct comparison of vibration magnitudes among separate components. Note that the dominant vibration component in the acoustically-excited fuselage vibration field has a relative magnitude that is lower than the first three components in the decomposition of the primary disturbance field. Therefore, as expected, straightforward analysis of the original fuselage vibration without making use of the inverse excitation technique used in this work would face serious

Table 4.1 - Comparison of Velocity Field Singular Value Magnitudes for Primary Disturbance and Acoustic Excitation Cases at 125 Hz

Singular Value	Primary Excitation	Acoustic Excitation
1	0.1854	0.0807
2	0.1401	0.0356
3	0.0891	0.0277
4	0.0661	0.0200
5	0.0551	0.0166

difficulties in identifying the well-coupled motions that are important acoustically, as they might otherwise be obscured by other vibration components of larger magnitude. Additionally, the singular values in the acoustic excitation case can be seen to decrease far more quickly than in the structural disturbance case, again illustrating the effectiveness of the system identification technique in focusing on a simplified subset of a complex total system response.

The SVD also proves useful in selecting potential structurally-mounted actuator locations. By setting to zero all but a small number of singular values and reconstructing the vibration field, a very simplified pattern is produced. Figure 4.8 shows a reconstruction using only the first singular value, which clearly shows a modal pattern of circumferential order 4 with one axial node in the passenger cabin located near the wing attachment point. Adding only two more singular values yields the reconstruction shown in Figure 4.9, which shows that the well-coupled fuselage motions for this frequency case can be approximated with only three orthogonal components.

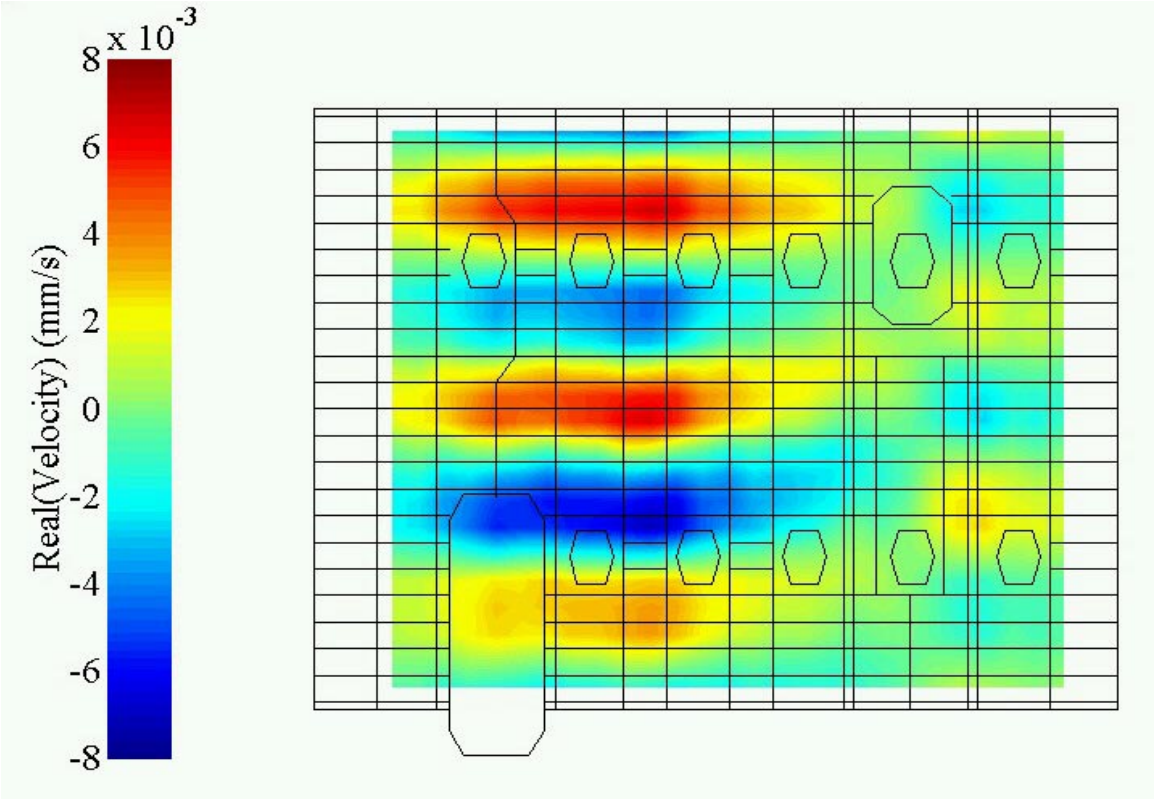

Figure 4.8 - Velocity field reconstruction from 1 singular value - 125 Hz case

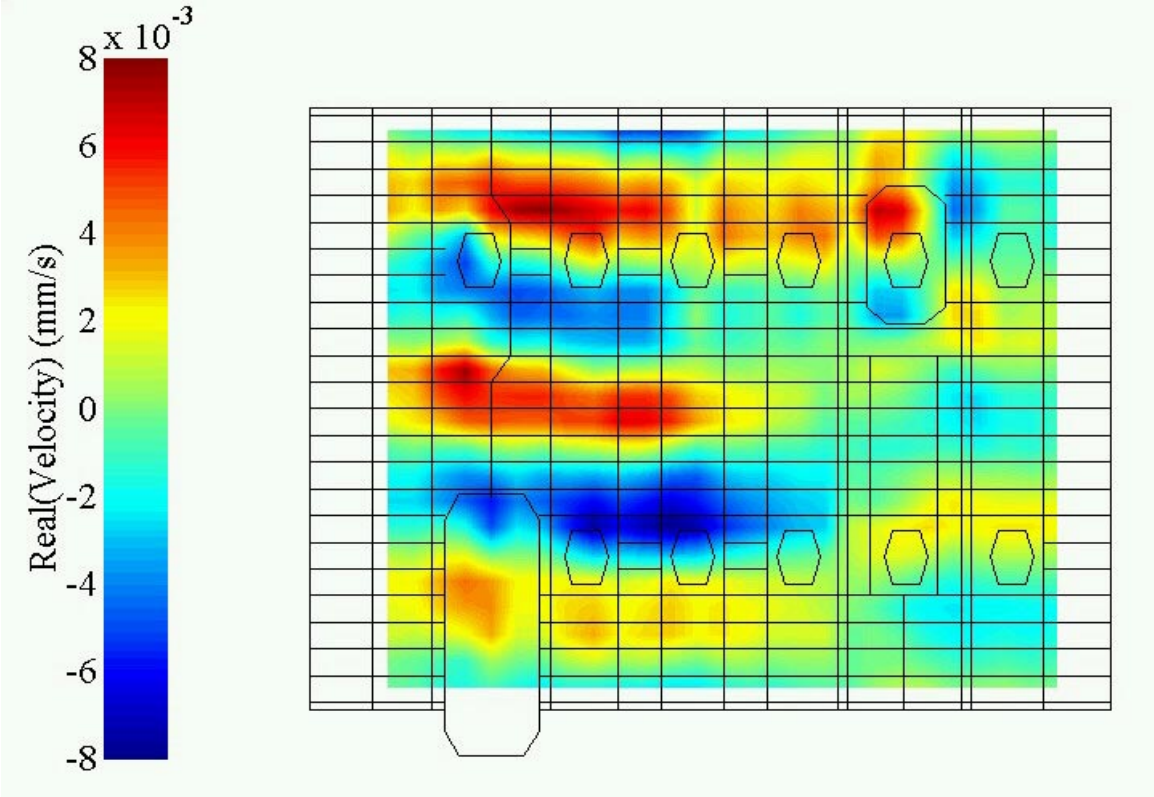

Figure 4.9 - Velocity field reconstruction from 3 singular values - 125 Hz case

4.2.2 System Identification Test Results: 170 Hz Case

The second test case examined is the off-resonance frequency of 170 Hz. Figures 4.10 and 4.11 show the uncontrolled acoustic and structural responses respectively, as produced by the shaker force disturbance at this frequency. The format and orientation of these plots has been previously described in section 4.2.1.

Following the procedure introduced in section 3.2, the 12 channel ANC system is positioned primarily examining the pressure anti-nodes from the response mapping shown in Figure 4.10. Figure 4.12 shows the chosen actuator and sensor locations on an unwrapped fuselage plot. After the components are positioned in this arrangement, the controller is initiated and allowed to converge. The controller is then locked, after which the disturbance force is removed, leaving the out-of-phase pressure field approximation. Figures 4.13 shows this cabin interior pressure field, and 4.14 shows the corresponding vibration field as induced by the acoustic drivers.

Comparison of the two interior pressure fields shows that the active control system is able to well approximate the shape of the disturbance sound field. Figure 4.15 details the sound level changes at the error and auxiliary microphones due to the ANC system. In this off-resonance situation, an average reduction of 13 dB was achieved at the error sensors, while a more modest 3 dB average was observed at the four additional global microphones. This decreased global performance is an effect of the off-resonance system behavior is this testing frequency, where the large number of contributing modes cannot all be effectively controlled by the ANC system.

As seen in Figures 4.11 and 4.14, the magnitude of the structural vibrations due to acoustic excitation is roughly half that produced by the shaker force disturbance.

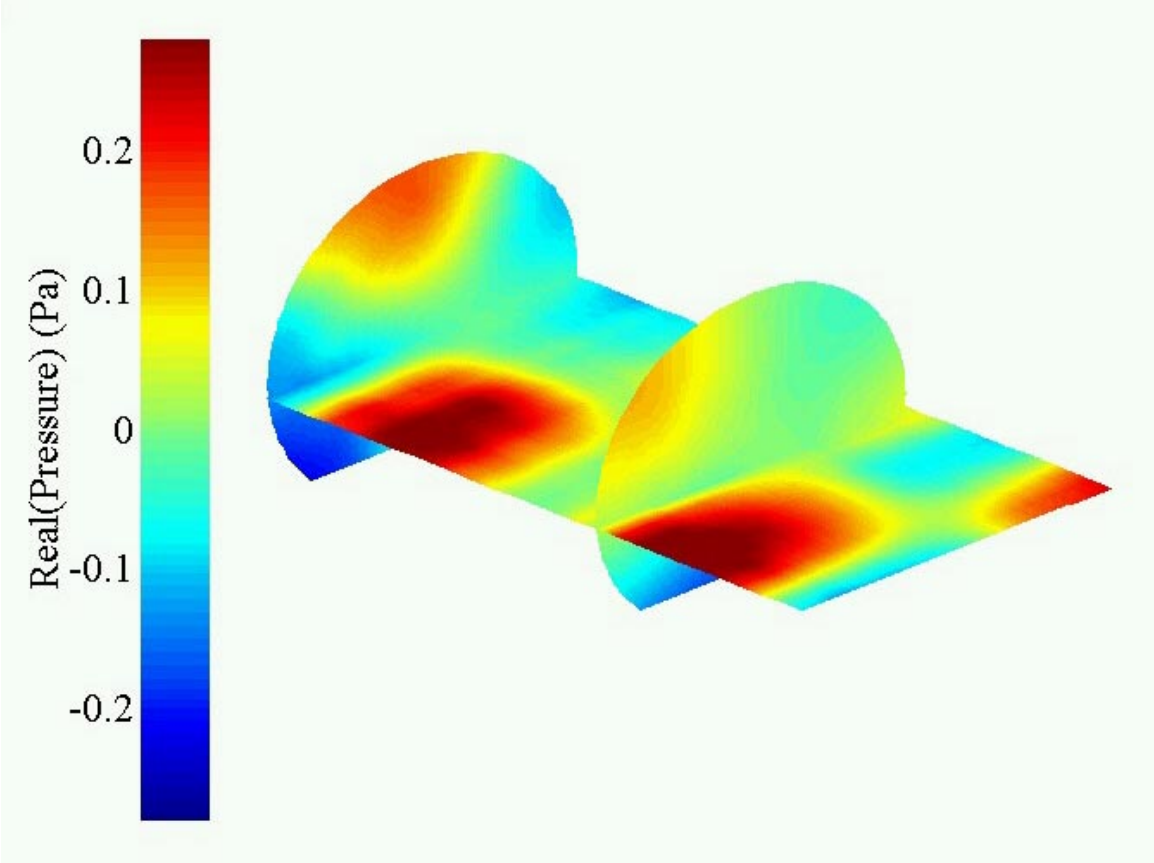

Figure 4.10 - Interior pressure field due to disturbance force at 170 Hz

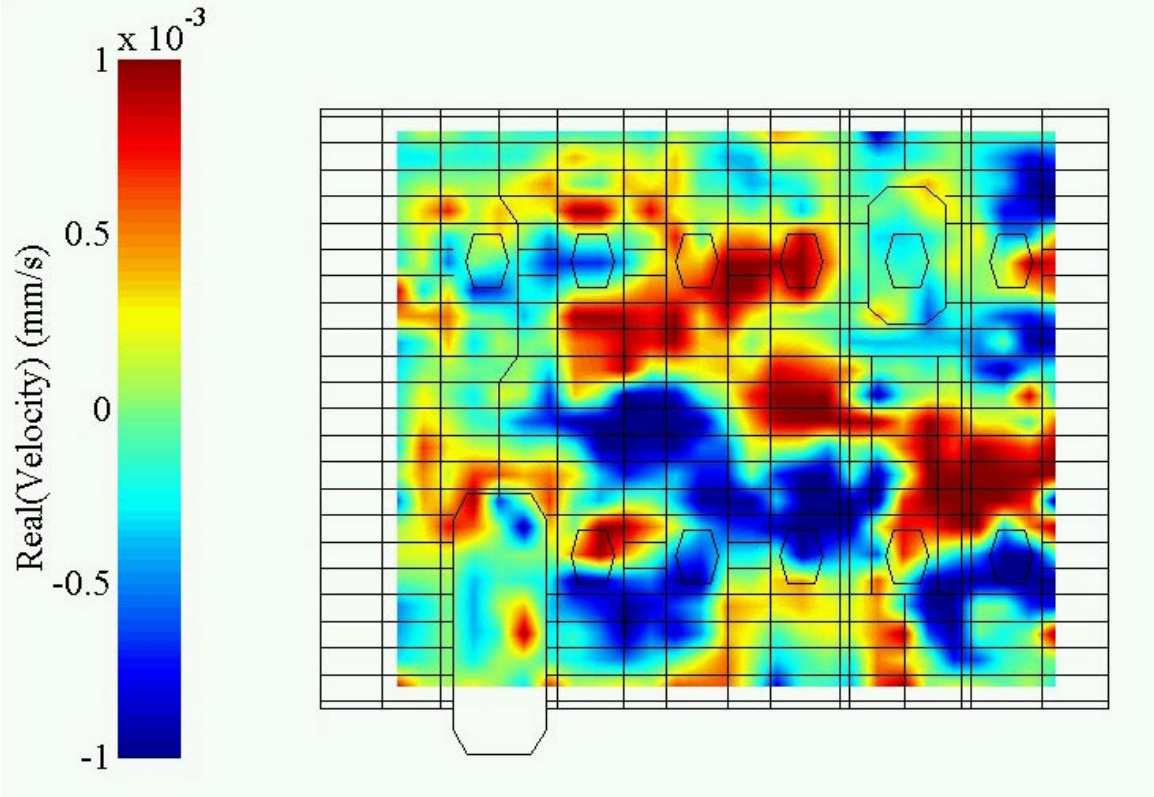

Figure 4.11 - Fuselage vibration field due to disturbance force at 170 Hz

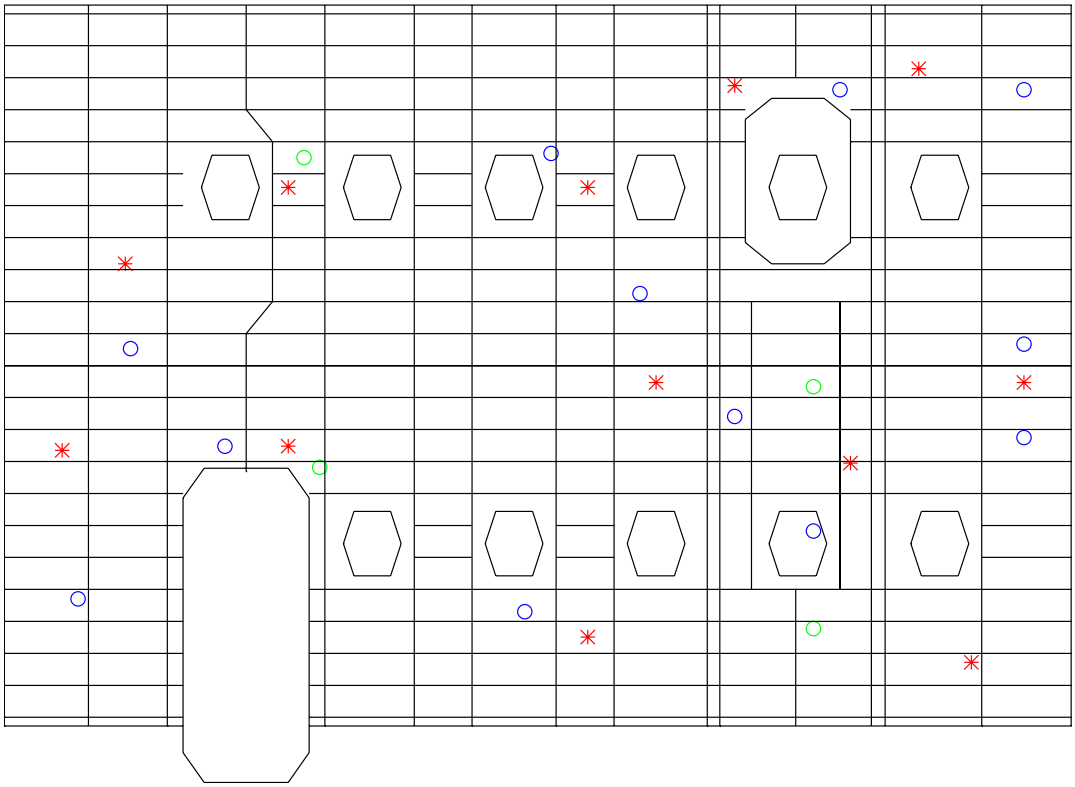

− Control Speaker Location

− Error Microphone Location

− Global Microphone Location

Figure 4.12 - Actuator and sensor locations for 170 Hz system identification tests

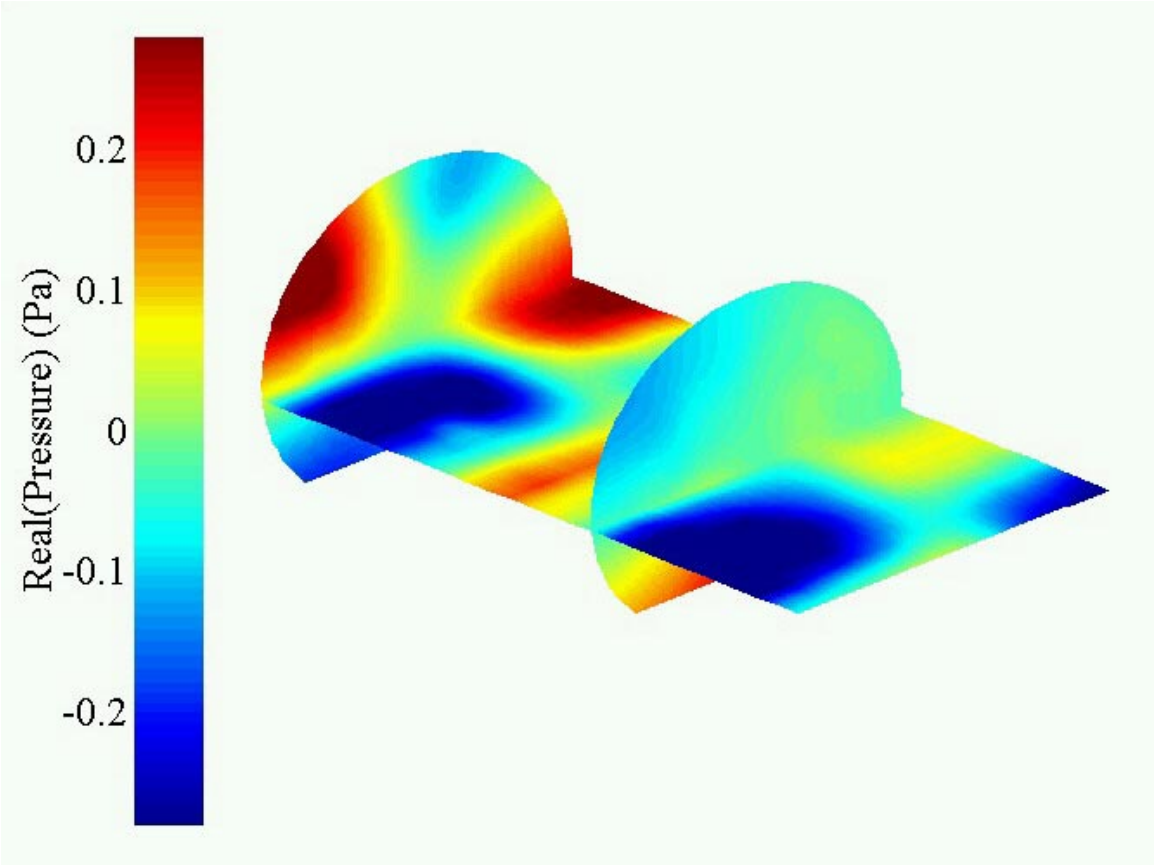

Figure 4.13 - Interior pressure field produced by control loudspeakers at 170 Hz

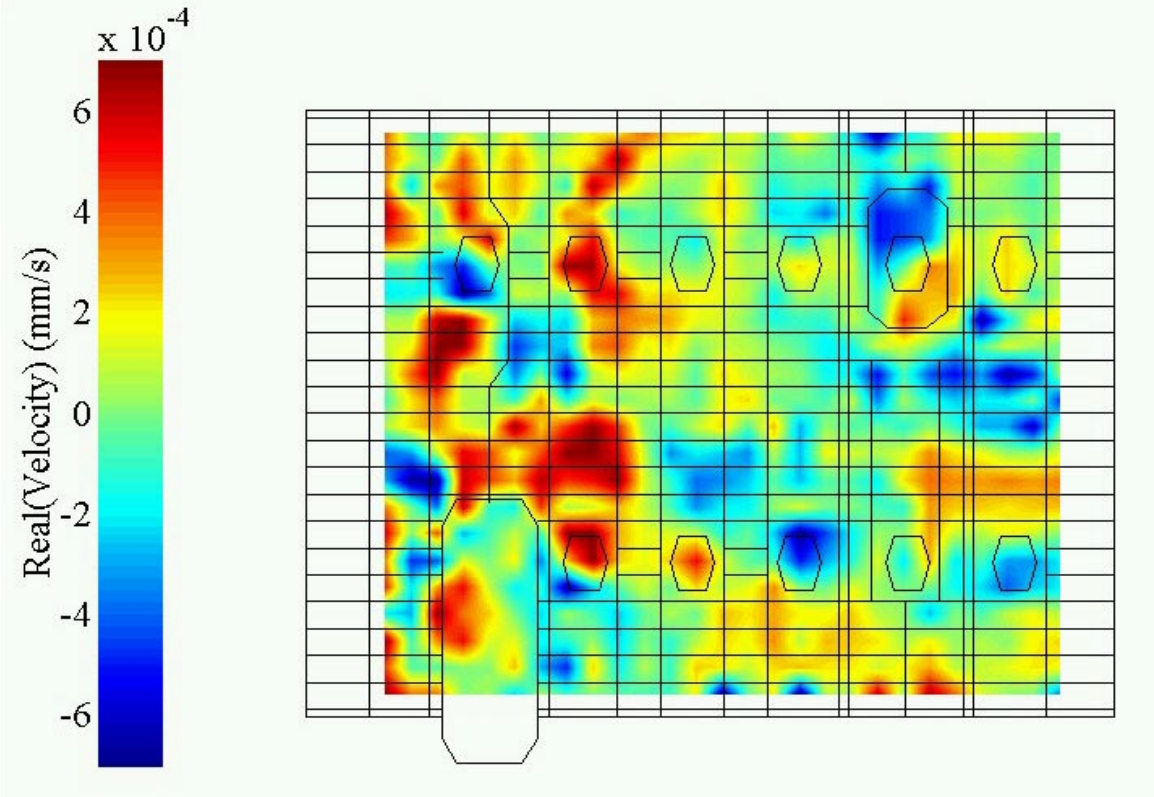

Figure 4.14 - Fuselage vibration field produced by control loudspeakers at 170 Hz

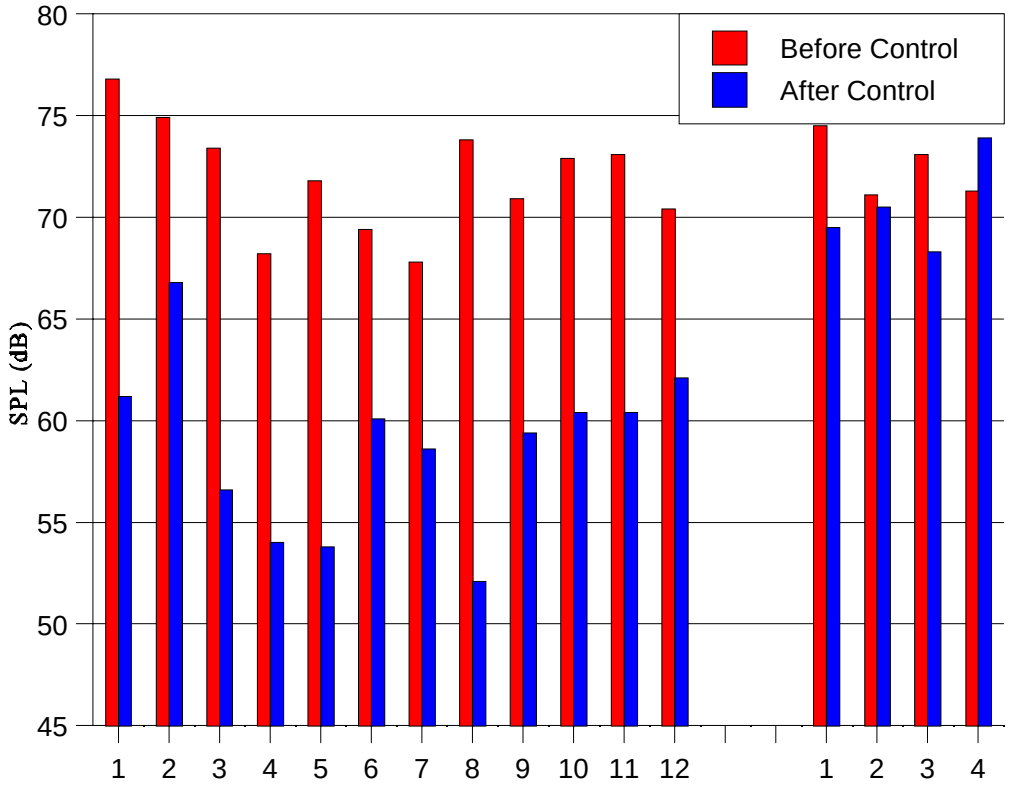

Figure 4.15 - Sound level reductions at error and global microphones for system identification experiments - 170 Hz test case

However, the vibration pattern measured during the system identification is not significantly simpler in form. As shown earlier in Figure 4.1, this test frequency corresponds to an off-resonance in both the acoustic and structural components of the total fuselage system, so significant contributions from many modes most likely cause this complex response behavior. Figure 4.16 shows a velocity reconstruction using one singular value. The plot in Figure 4.17 contains the sum of contributions from the first three singular values, showing an accurate reproduction of the gross shape of the measured velocity field. A dominant modal pattern is not apparent, though the regions of largest vibration magnitude can be observed to lie in the forward third of the cabin area.

Table 4.2 presents a comparison of singular values for the vibration fields measured in the 170 Hz test case. The singular values in the acoustic excitation column of the table are lower in magnitude than those in the force disturbance case, as expected from comparing the scales of the measured velocity fields. Note however that the proportions of values between the two column are quite similar, confirming the observation that the system identification results do not display a marked decrease in vibration complexity. In other words, the desired condition of one or very few orthogonal components completely describing the well coupled fuselage motions has not been met in at this off-resonance frequency case. This is because of the large number of fuselage structural modes, both well and poorly coupled to the interior acoustic space, that contribute to the total response at this frequency. A number of relatively modest contributions from several well coupled components can easily combine to produce a structural response of complex shape.

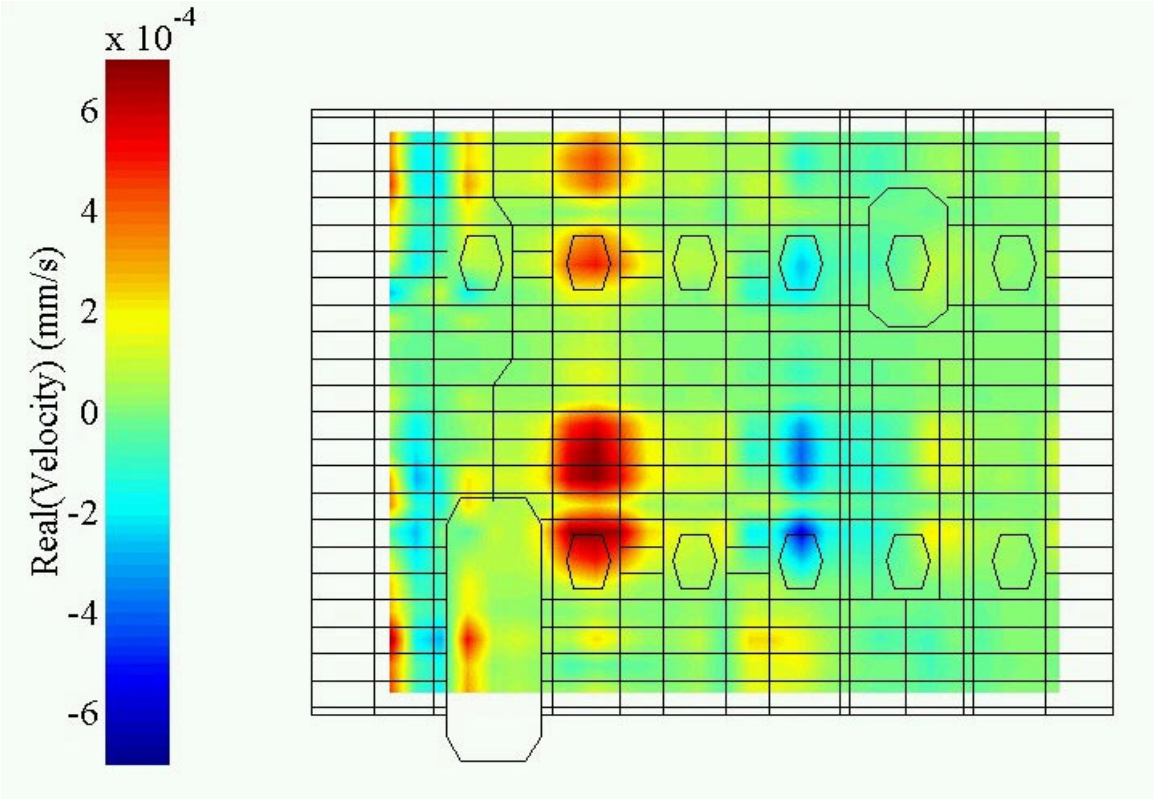

Figure 4.16 - Velocity field reconstruction from 1 singular value - 170 Hz case

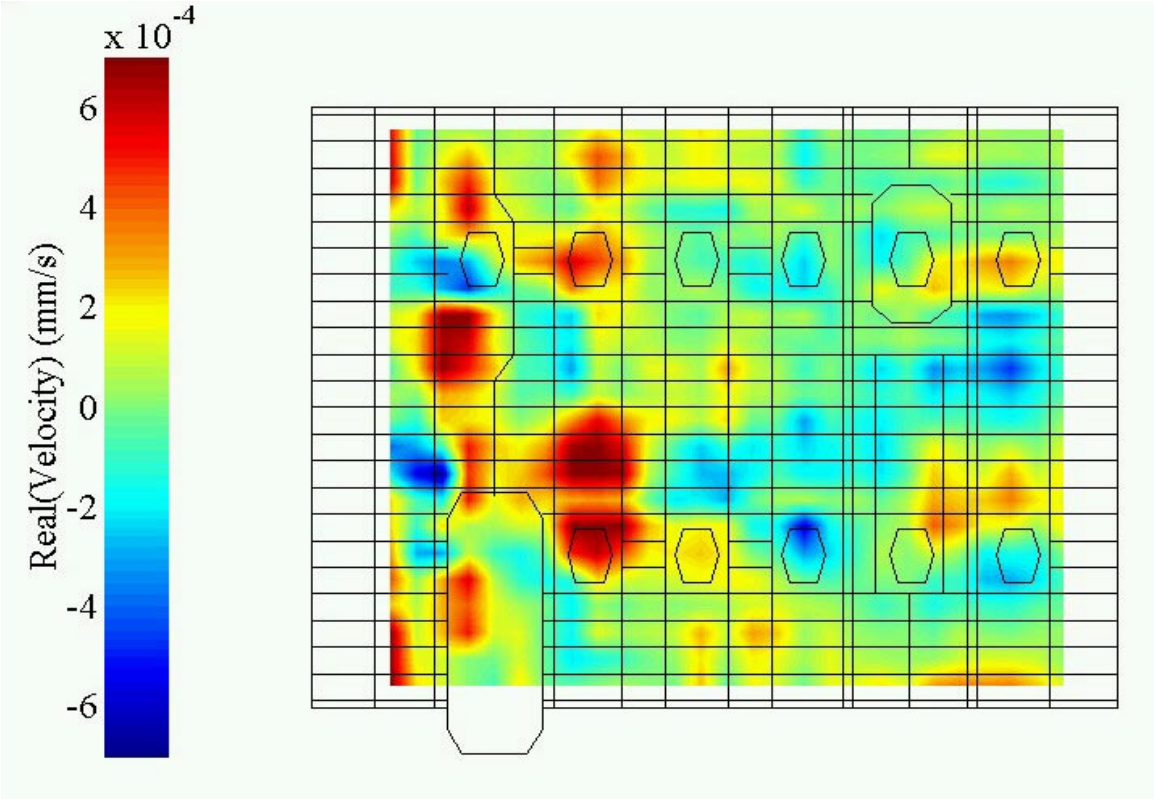

Figure 4.17 - Velocity field reconstruction from 3 singular values - 170 Hz case

Table 4.2 - Comparison of Velocity Field Singular Value Magnitudes for Primary Disturbance and Acoustic Excitation Cases at 170 Hz

Singular Value	Primary Excitation	Acoustic Excitation
1	0.0136	0.0055
2	0.0109	0.0044
3	0.0085	0.0038
4	0.0062	0.0034
5	0.0060	0.0030

4.2.3 System Identification Test Results: 225 Hz Case

This section presents system identification results for the third test case, the structural resonance frequency of 225 Hz. Figures 4.18 and 4.19 show the acoustic and structural responses due to the shaker force disturbance. The format and orientation of the plots has been previously described in section 4.2.1.

The selected positions of the actuators and sensors for the ANC system are detailed in Figure 4.20. After configuring the system as shown, the active controller is started and allowed to converge. The controller is then locked and the disturbance force removed, leaving the out-of-phase approximation of the disturbance pressure field. Figures 4.21 and 4.22 show the measured pressure and vibration fields produced by the acoustic excitation of the fuselage with the active control system.

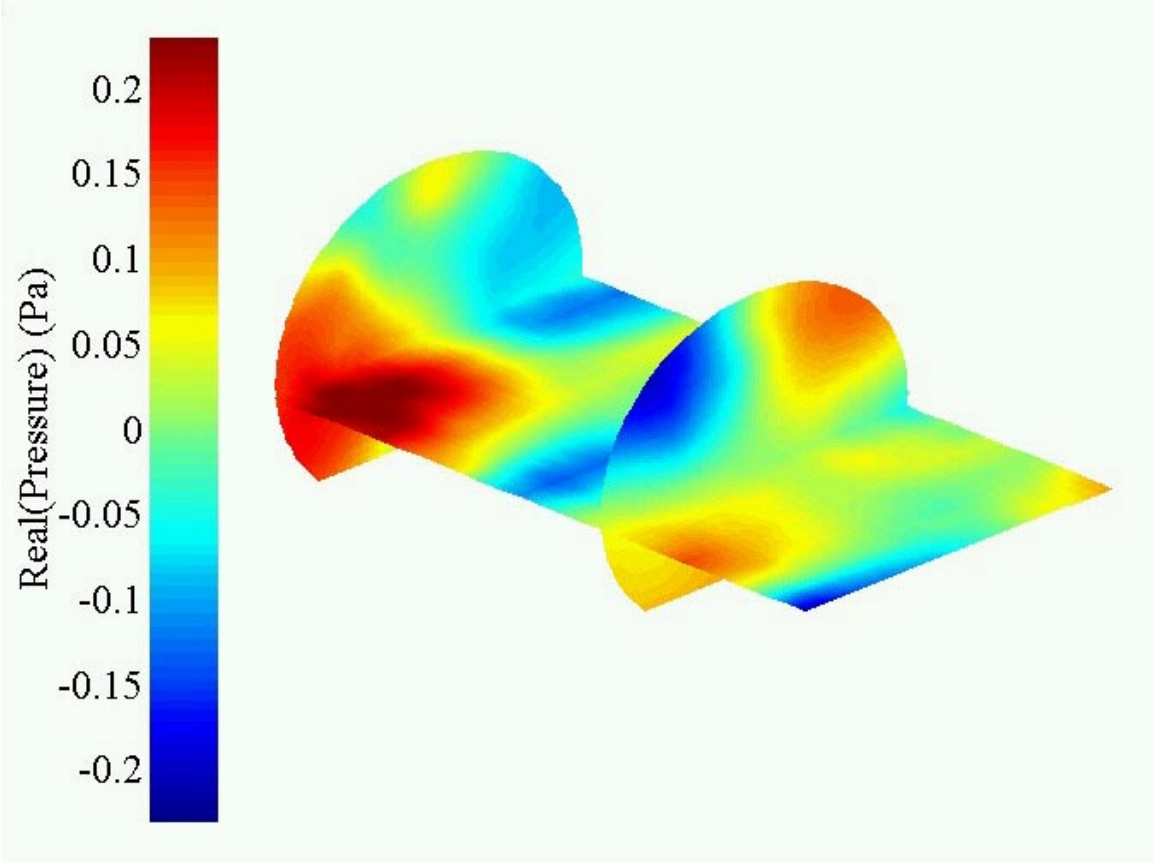

Figure 4.18 - Interior pressure field due to disturbance force at 225 Hz

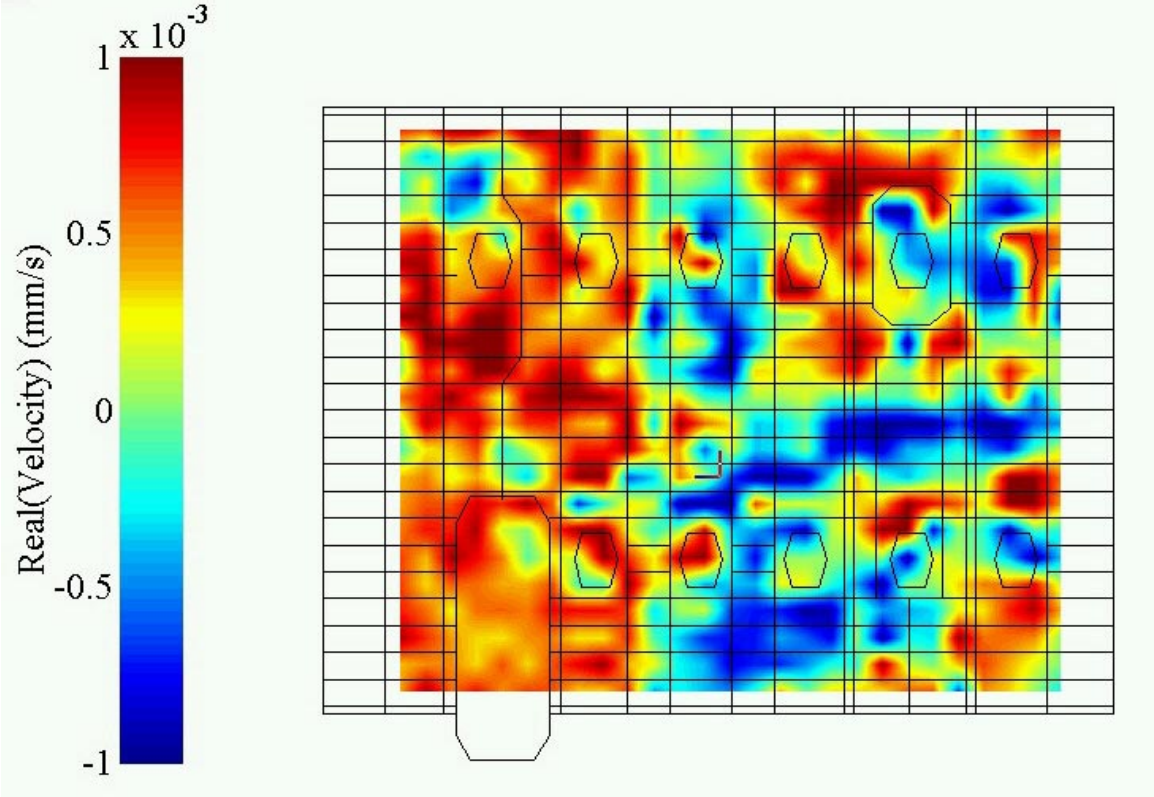

Figure 4.19 - Fuselage vibration field due to disturbance force at 225 Hz

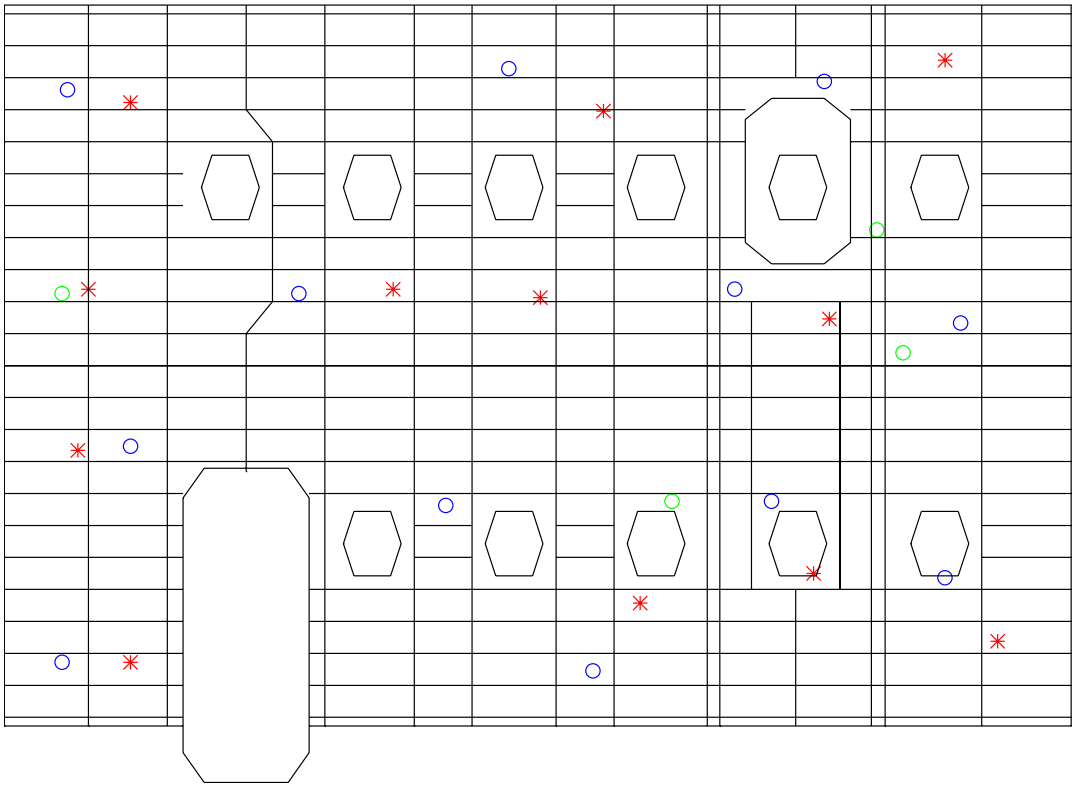

✳ − Control Speaker Location

○ − Error Microphone Location

○ − Global Microphone Location

Figure 4.20 - Actuator and sensor locations for 225 Hz system identification tests

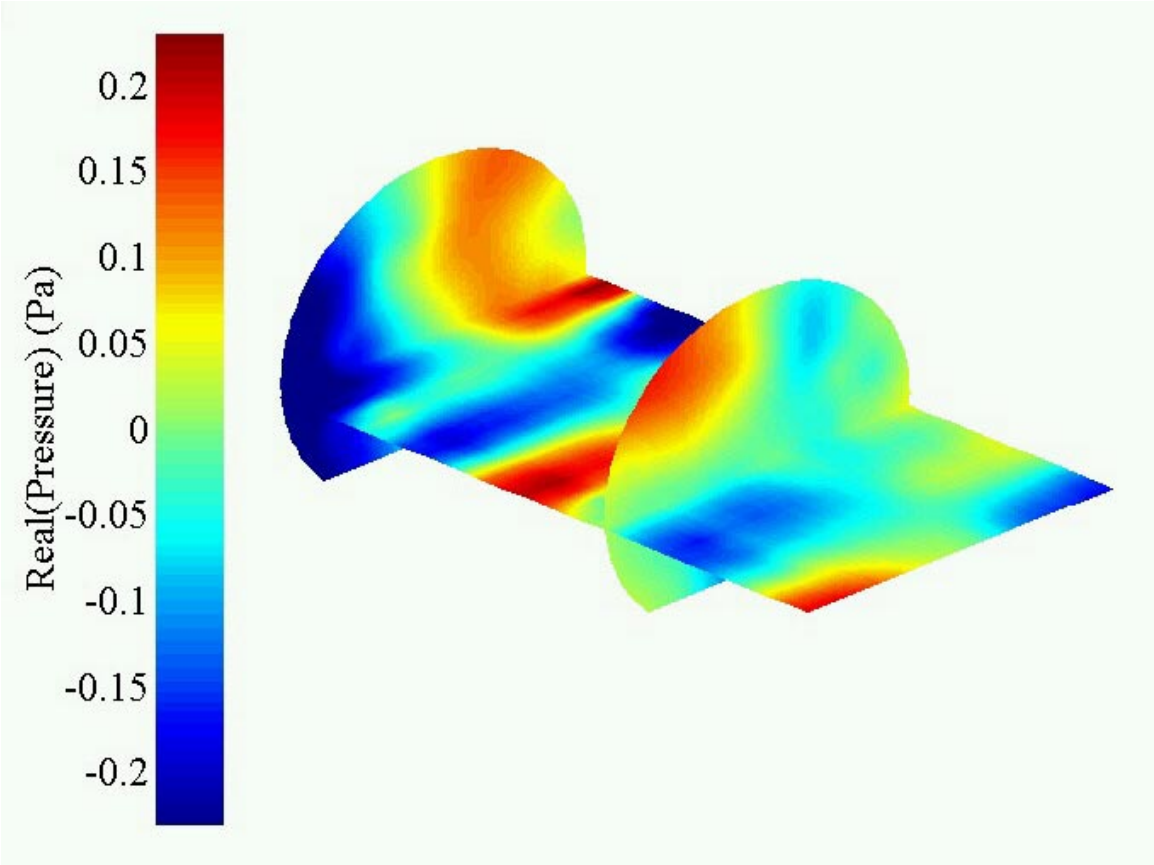

Figure 4.21 - Interior pressure field produced by control loudspeakers at 225 Hz

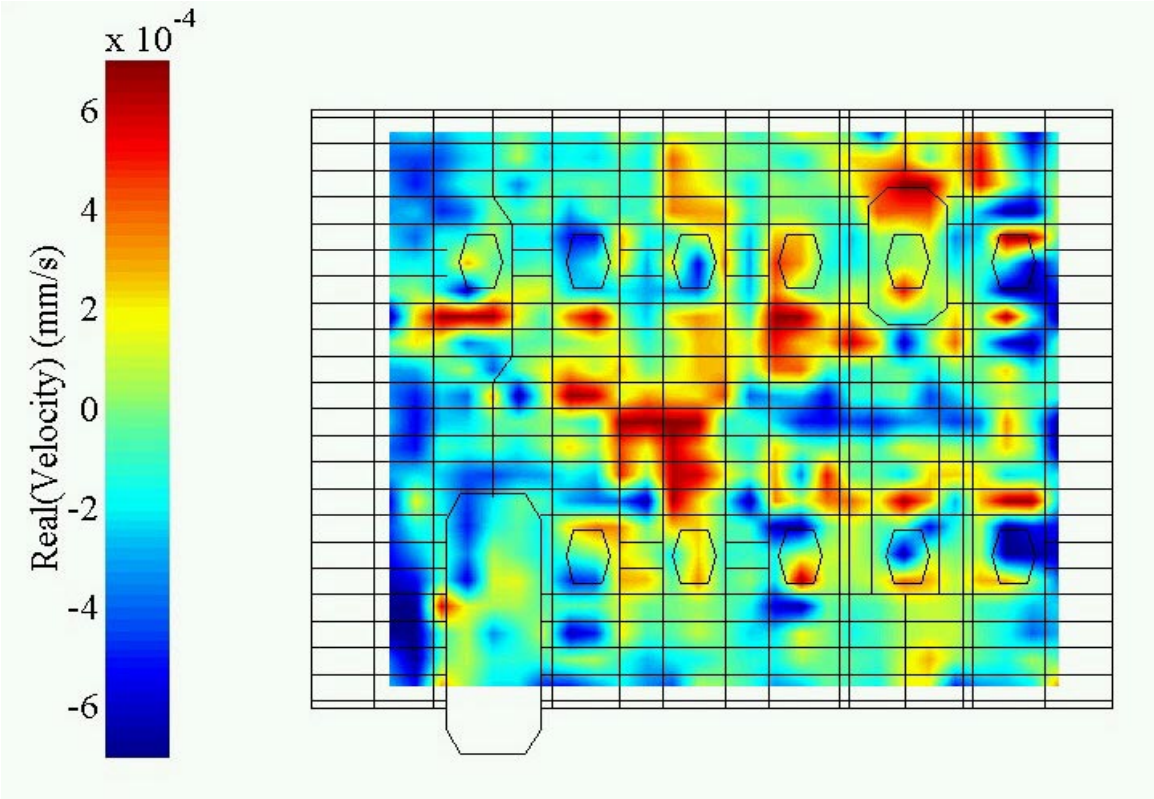

Figure 4.22 - Fuselage vibration field produced by control loudspeakers at 225 Hz

As in the earlier tests, the ANC system is seen to closely approximate an out-of-phase version of the disturbance pressure field. Figure 4.23 shows the sound level reductions at each microphone in the cabin area. At the 12 error microphones, an average sound level decrease of 10 dB was achieved. The remaining four microphones, placed away from the error sensors and used to evaluate global control levels in the cabin, measured an average reduction of 6 dB.

Comparison of the two vibration fields measured at this frequency shows a decrease in overall velocities in the acoustic excitation case. However, as seen in Figure 4.22 and in the SVD reconstructions plotted in Figures 4.24 and 4.25, the vibrations induced by the active control speakers alone are not apparently simpler in nature as compared to the force disturbance case. Instead of the clear axial modal behavior seen in Figure 4.19, the system identification results appear to contain a large number of localized regions of high-magnitude vibration. Table 4.3 shows a comparison of the singular values calculated from the responses in the two excitation cases, and reveals that despite lower magnitudes, a distinct simplification of vibration shapes is not revealed by the inverse system identification, most likely due to the structural resonance behavior at this test case.

Table 4.3 - Comparison of Velocity Field Singular Value Magnitudes for Primary Disturbance and Acoustic Excitation Cases at 225 Hz

Singular Value	Primary Excitation	Acoustic Excitation
1	0.0123	0.0078
2	0.0101	0.0044
3	0.0075	0.0039
4	0.0068	0.0037
5	0.0062	0.0031

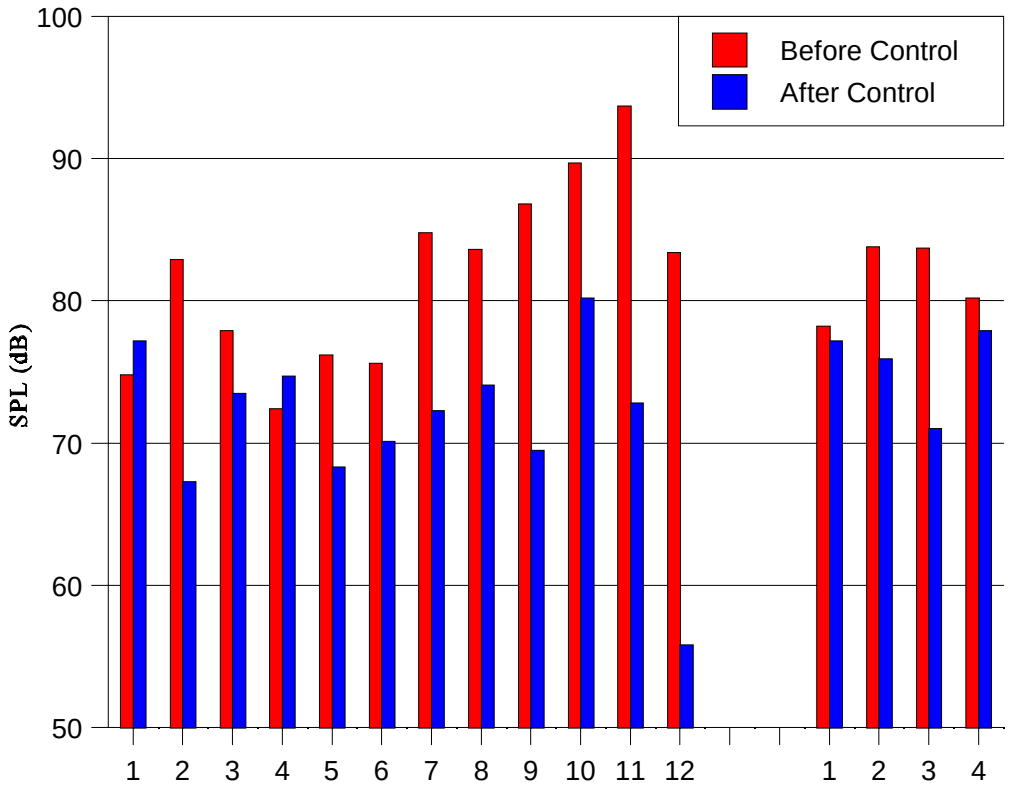

Figure 4.23 - Sound level reductions at error and global microphones for system identification experiments - 225 Hz test case

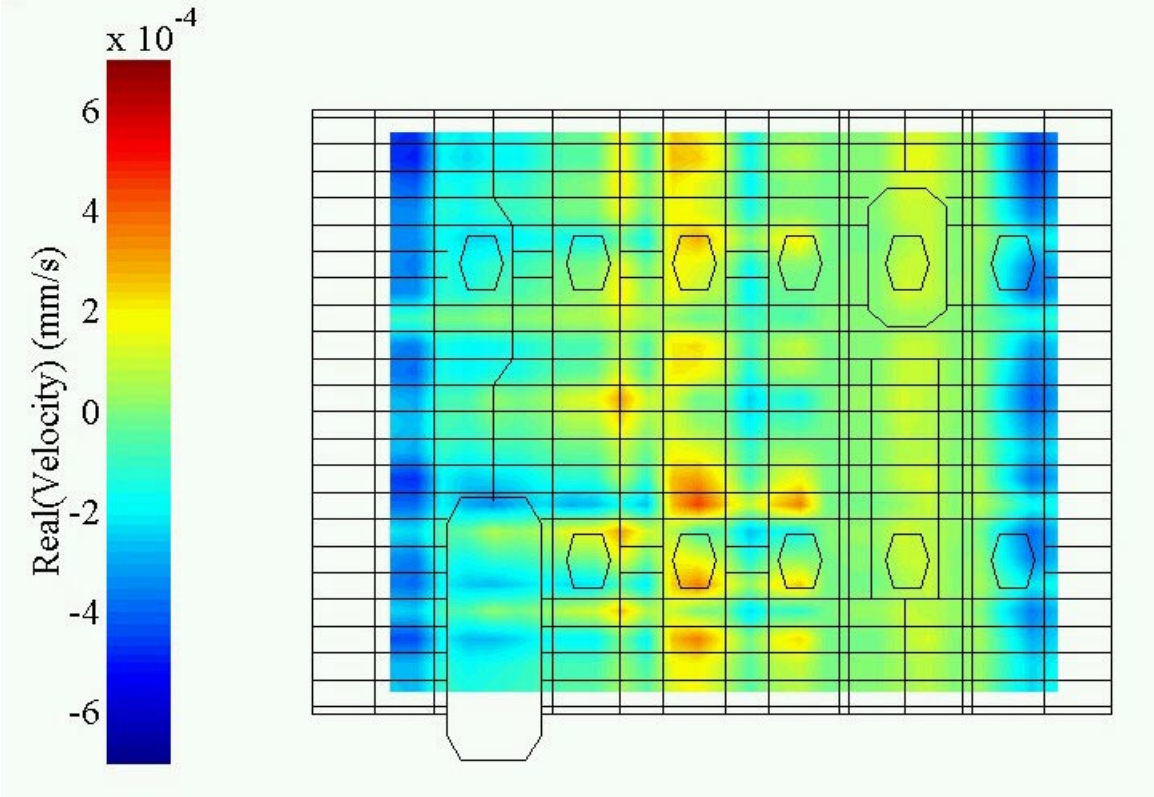

Figure 4.24 - Velocity field reconstruction from 1 singular value - 225 Hz case

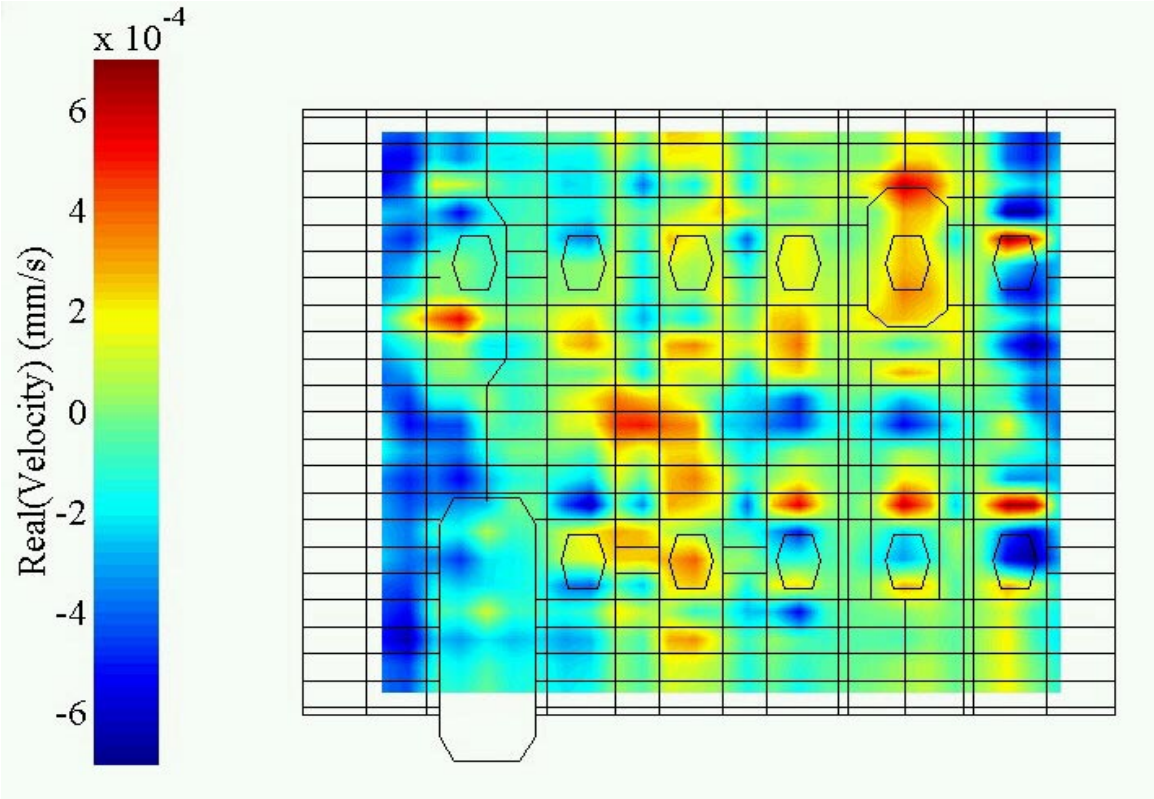

Figure 4.25 - Velocity field reconstruction from 3 singular values - 225 Hz case

4.2.4 System Identification Results Summary

A review of the system identification results for the three test cases acts to confirm many expectations about the fuselage system behavior. Clearly, the experiments at the acoustic resonance case (125 Hz) demonstrated the most successful control performance, both at error sensors and globally, which is expected due to the dominance of only one interior pressure mode. The accuracy of the pressure field reproduction in this case results in a high confidence that the measured vibration patterns indeed consist largely of the well-coupled fuselage motions that are key to the interior noise problem at this frequency.

The ANC performance at the off-resonance case (170 Hz), especially the global reduction levels of 3 dB, clearly shows the control system's inability to easily handle a large number of contributing acoustic modes. This behavior is to be expected in the more complex off-resonance situation. Despite the somewhat decreased performance, careful examination of the pressure scan results reveals that in the critical regions near the fuselage walls, excellent reproduction of the pressure field was achieved after several iterations of control system configuration. Thus, the measured system identification vibration pattern should still prove valuable in positioning the structural control actuators for this frequency case.

The results for the structural resonance case (225 Hz) show significant global sound reduction levels and another good approximation of the pressure response shape. Careful tuning of the ANC system configuration again resulted in best control results occurring over the area near the fuselage walls. However, despite high confidence in the pressure reproduction, no significant simplification of the measured vibration pattern was achieved

in this case. The measured vibration levels were lower however. This situation is likely due to the difficulty of applying the inverse excitation technique at a structural resonance frequency. In such a case, any acoustic excitation to the dominant mode or modes of vibration may result in significant structural response regardless of how well coupled those motions are in an acoustic sense.

4.3 Actuator Optimization

Following the procedure outlined in section 3.3, candidate piezoelectric actuator locations were determined by careful examination of the SVD velocity reconstructions presented above. Approximately 8 to 10 locations were chosen for each frequency test case, on areas of the fuselage shell exhibiting maximum vibration response during the system identification experiments. Nearly all of the chosen positions are located in the forward section of the fuselage, resulting in many repeated selections among the several test frequencies. This aspect is probably due to high structural stiffness at the wing mounts that acts to limit the vibrations in the rear of the cabin area. As a result of duplicated selections, a total of 16 distinct candidate locations were chosen, as shown in Figure 4.26.

The custom piezoelectric patches used in this project were bonded to the fuselage wall panels in the chosen candidate locations. Next, each actuator was excited individually at the frequencies of interest and transfer functions for a large number of structural measurement points of normal velocity were recorded at each test frequency. This data was used to compute fitness values for each possible set of 6 actuators via a series of enumerative search calculations. These results are used for comparison to the genetic

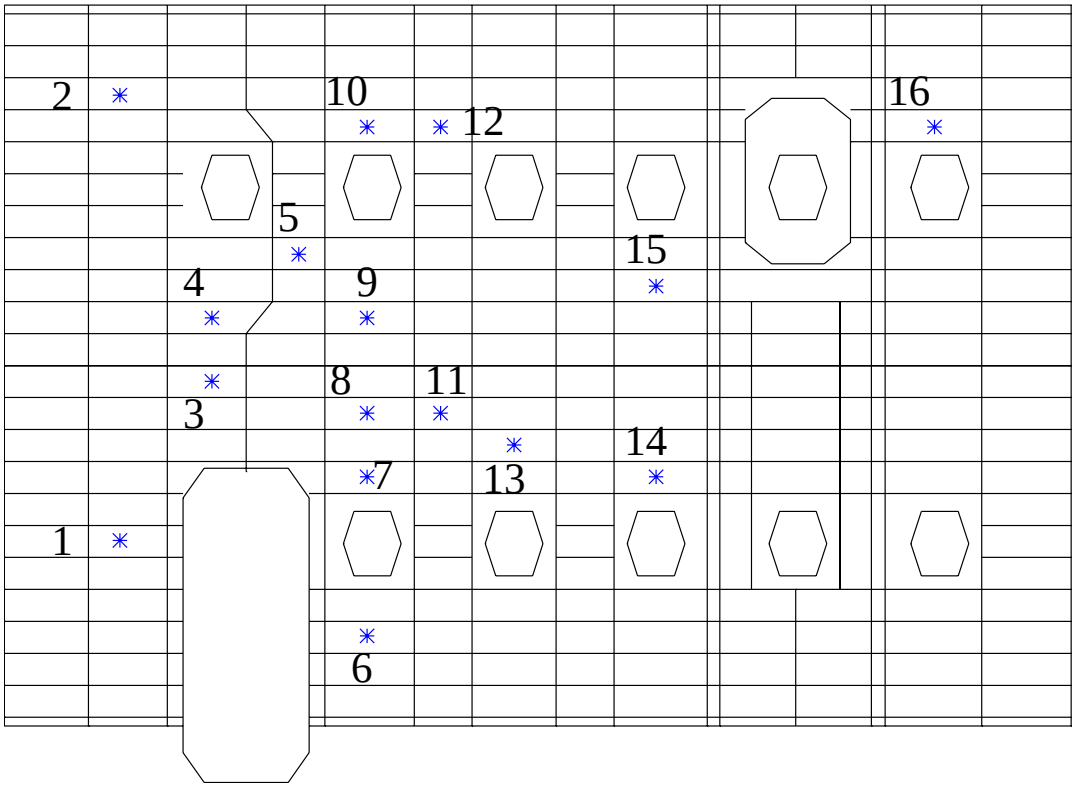

Figure 4.26 - Candidate PZT actuator positions on fuselage shell

algorithm results which follow. The fitness values were calculated as described in section 3.3.2, and for clarity the values presented in this analysis were then scaled to fall between 0 and 1000.

4.3.1 Actuator Optimization Test Results: 125 Hz Case

Examination of the enumerative search results reveals a very clear normal distribution of fitness values, centered on a mean of 432 for this frequency. Only 26 of 8008 possible actuator groupings have a fitness larger than 900, and merely 5 combinations rate above 950. The genetic algorithm optimization program was initialized with a population size of 50 strings per generation and a limit of 30 generations for the search. Several sets of crossover and mutation probabilities were examined, with a final selection of $P_c = 0.66$ and $P_m = 0.05$.

Figure 4.27 presents the results of the optimization search, showing the average and best case fitnesses for each search generation. Both of the plotted traces demonstrate that the GA rapidly converges towards the best solutions in the search space. In this case, the maximum achievable fitness of 1000 was first reached in the 13th generation, after approximately only 8% of the fitness calculations required by an enumerative search. This is followed by one of the several most fit combinations appearing as the best candidate in successive generations. It should be noted that these most fit groupings in later generations typically have all but one actuator in common with the best case group.

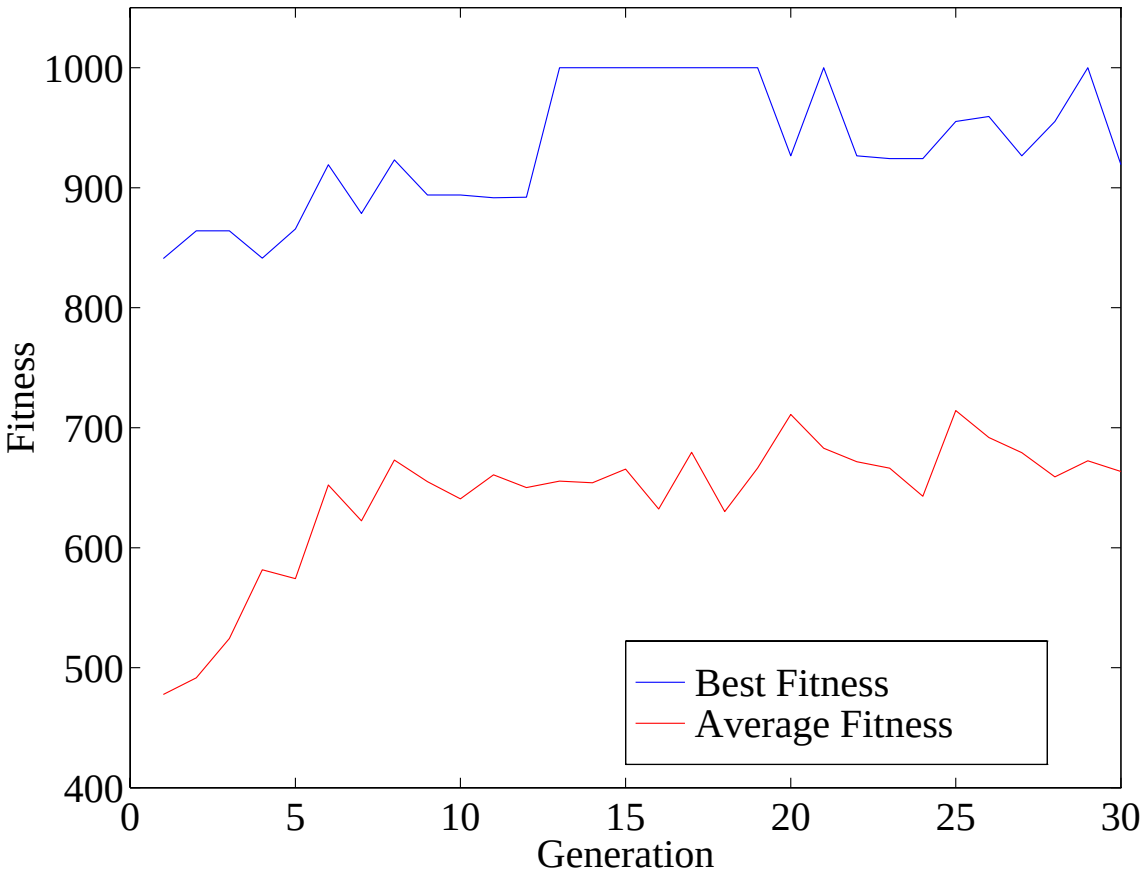

Figure 4.27 - GA optimization results for 125 Hz test case

4.3.2 Actuator Optimization Test Results: 170 Hz Case

The enumerative search results for this frequency shows a mean fitness of 448, with 29 groupings rating above 900 and only 7 combinations above a fitness of 950. The GA again used 30 generation of 50-string populations. In this case, the convergence parameters were set to $P_c = 0.7$ and $P_m = 0.05$.

Figure 4.28 presents the GA search results, showing the average and best case fitnesses for each generation. The GA is again seen to steadily converge towards the best actuator groupings. In this case, the maximum fitness of 1000 was first reached in the 13th generation, followed by search results alternating among several other high-fitness candidates. This again corresponds to approximately 8% of the calculations required in the enumerative search.

4.3.3 Actuator Optimization Test Results: 225 Hz Case

The normal distribution of fitness values for this frequency is centered around a mean of 437. In this case, 21 solutions have a fitness above 900 and only 4 rate above 950. The GA program was configured for the typical 50-string population size and a search lasting 30 generations. In this case, search probabilities of $P_c = 0.8$ and $P_m = 0.01$ were chosen.

Figure 4.29 presents the results of the GA optimization, showing the average and best case fitnesses for each search generation. The results again demonstrate steady convergence toward the best groupings, with the maximum fitness of 1000 first achieved in generation 14 in this case. This corresponds to approximately 9% of the search

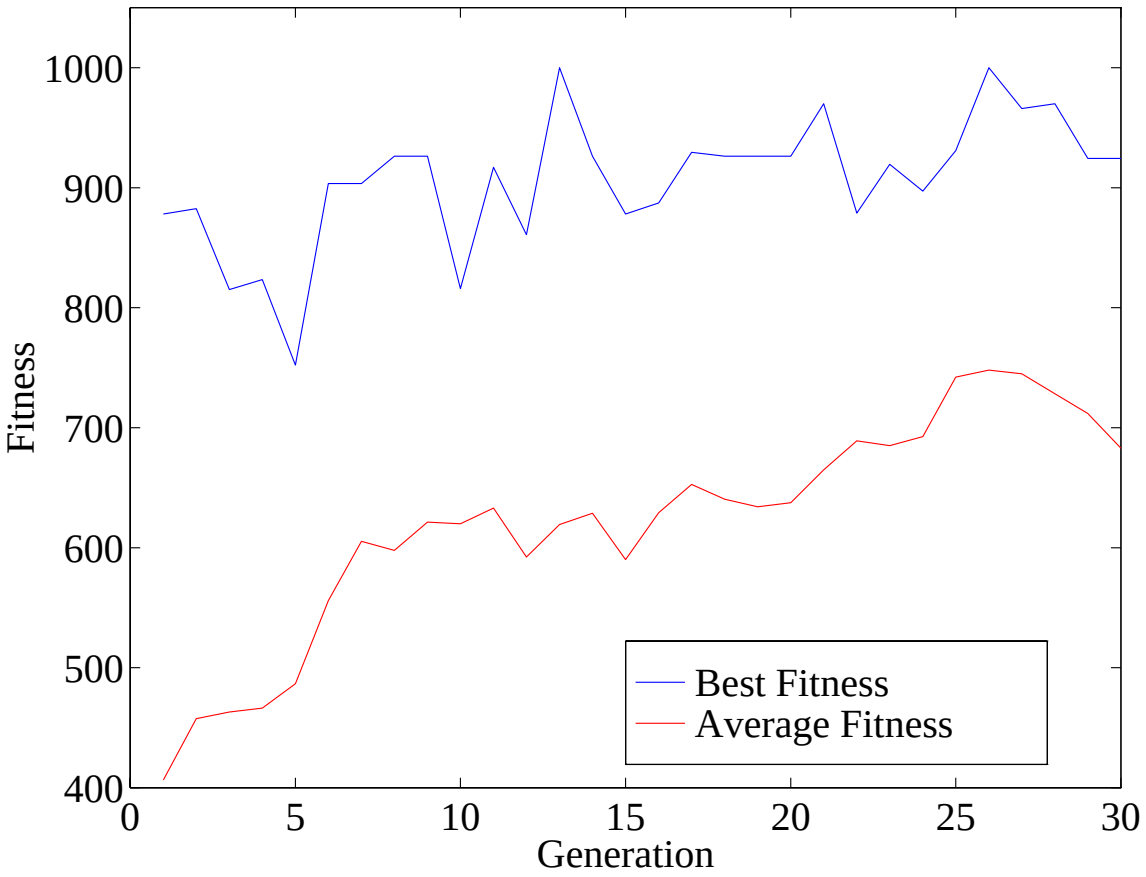

Figure 4.28 - GA optimization results for 170 Hz test case

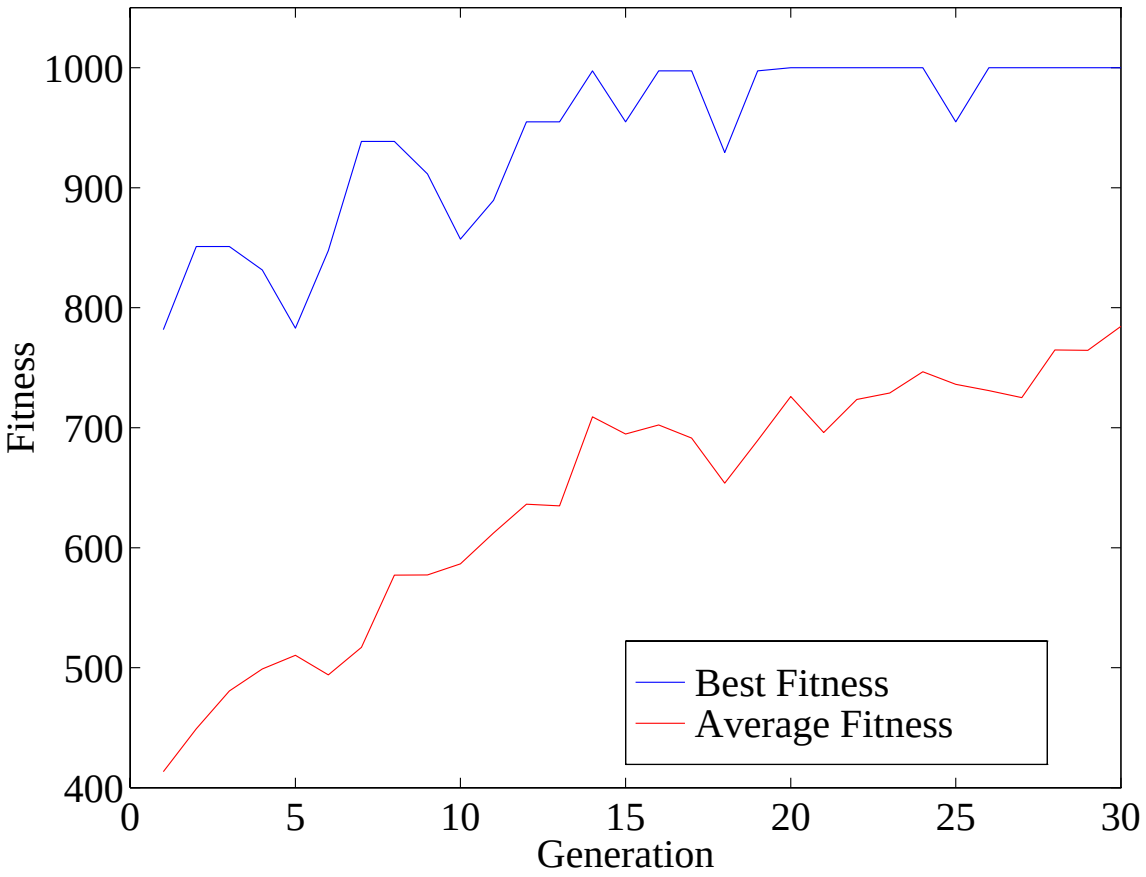

Figure 4.29 - GA optimization results for 225 Hz test case

duration required by the enumerative method. Again, the few successive generations with sub-1000 best fitnesses are typically populated with several alternate groupings containing all but one of the ideal actuators.

4.3.4 Actuator Optimization Results Summary

It is apparent that the GA optimization method used in this work was quite effective in determining an appropriate actuator grouping for ASAC testing. The results in all three cases show rapid convergence to the best candidate groups with a significant reduction in calculation time compared to an exhaustive search approach, less than 10% for each frequency. Even without the benefit of comparison with enumerative search results, much confidence can be placed in the GA results presented above because of the steadily increasing mean fitness for each generation. This trend signifies a slow narrowing of the search into the regions containing the best grouping combinations. It should be noted that the crossover and mutation probabilities were selected in an ad hoc manner for each test case. It is likely that a more rigorous criteria for selecting these parameters, as well as the addition of a fitness scaling procedure to the GA, could increase the speed of the optimization process even further. However, it is clear from these results that the GA method is quite simple to implement and performs very well on complex experimental data sets.

4.4 ASAC Results

For the ASAC validation tests, a 12 channel control system is assembled. For each test case, several control tests are performed. The best grouping of 6 PZT actuators, as determined by the optimization work detailed above, is used initially. In addition, a grouping with a fitness value near the mean for each frequency, as well as the worst-case actuator grouping are chosen for comparison purposes. The error microphones in all tests are positioned in their locations used in the system identification control work. For every test case, sound levels before and after control are recorded for the error and reference microphones. For the ASAC tests using the optimal actuator groupings, full fuselage measurement scans are performed with and without control applied, as well as in the locked-controller configuration used earlier in the system identification experiments.

4.4.1 ASAC Test Results: 125 Hz

The optimal PZT group selected for ASAC testing at 125 Hz contains the actuators numbered 3, 5, 7, 8, 11, and 12 (refer to Figure 4.26 for actuator numbering). Figure 4.30 shows the control system layout, detailing locations of the optimal actuator set as well as the error sensor and global microphone positions. Using this system configuration, ASAC was performed using the usual shaker force disturbance, and the controller was locked after convergence for scanning purposes. The control voltages to the piezoelectric patches ranged from 30 to 150 volts RMS.

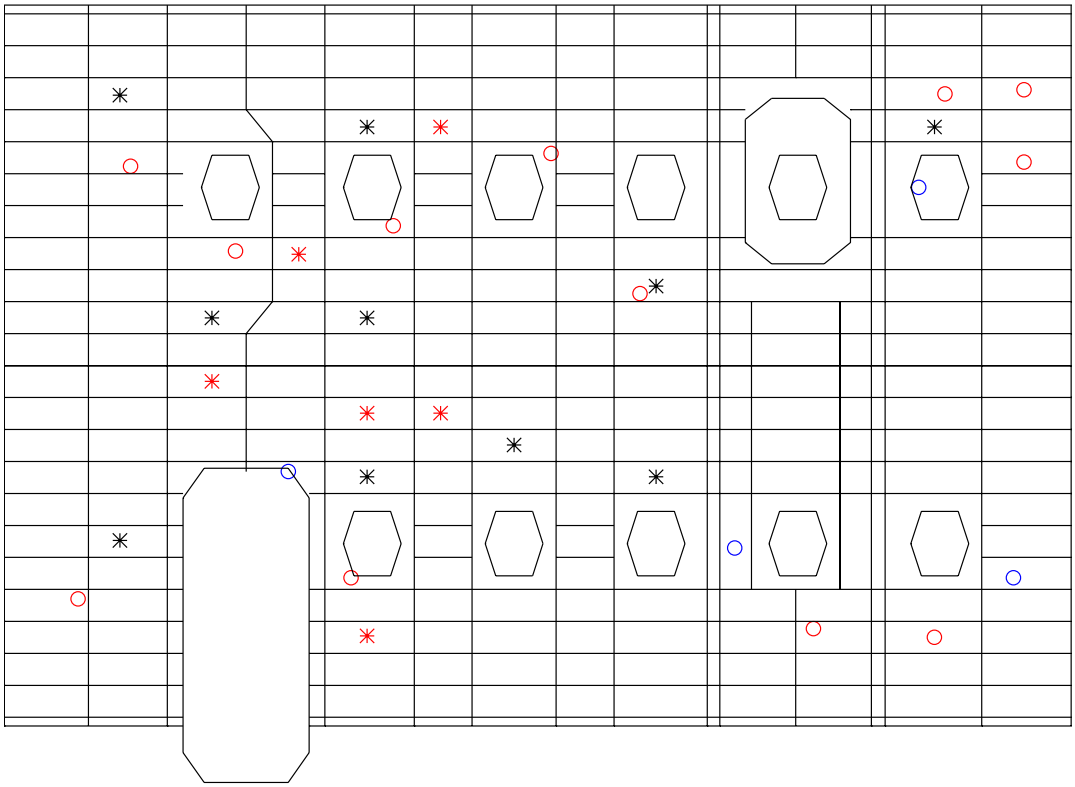

Figure 4.30 - Actuator and sensor locations for 125 Hz ASAC tests

Figure 4.31 presents the uncontrolled and controlled cabin sound levels measured at 16 microphones. An average sound reduction of 6 dB is observed at the 12 error sensors, while an average global reduction of 4 dB is recorded by the 4 additional microphones. An analysis of the roughly 1600 pressure measurements from the full fuselage scan shows an average reduction of approximately 2 dB. These global reductions are an improvement over previous ASAC work [35] with this test rig at an acoustic resonance case, which showed some notable spillover effects at the auxiliary microphones. Figure 4.32 shows the past ASAC results of Ref. 35 for an acoustic resonance, presenting sound reductions for 4 error microphones and 7 global reference microphones. In this previous work the actuators were located in a largely "ad-hoc" manner. Large attenuations are apparent at the error sensors, however the average sound level at the global microphones has significantly increased. Thus the benefit of optimally locating the actuators, as dicussed here, is apparent in that global reductions are then achieved.

Figure 4.33 shows the cabin interior pressure field in uncontrolled and controlled conditions. Comparison of the two views shows a generally uniform pressure reduction throughout the cabin, with no acoustic spillover apparent in the plotted regions. Figures 4.34 and 4.35 present the measured fuselage vibrations in the uncontrolled and controlled cases respectively. Note that while some areas of the response pattern were modified by the control system, overall vibration levels were raised markedly by the actuators, by a factor of 2 or more over much of the fuselage surface. Figure 4.36 shows the shell vibrations produced by the piezoelectric control actuators alone when the controller was locked and the disturbance removed. Notice that near the PZT patches, which are located predominantly in the forward cabin areas, these vibrations contain significant contributions from a high-wavenumber circumferential mode such that adjacent skin panels respond out-

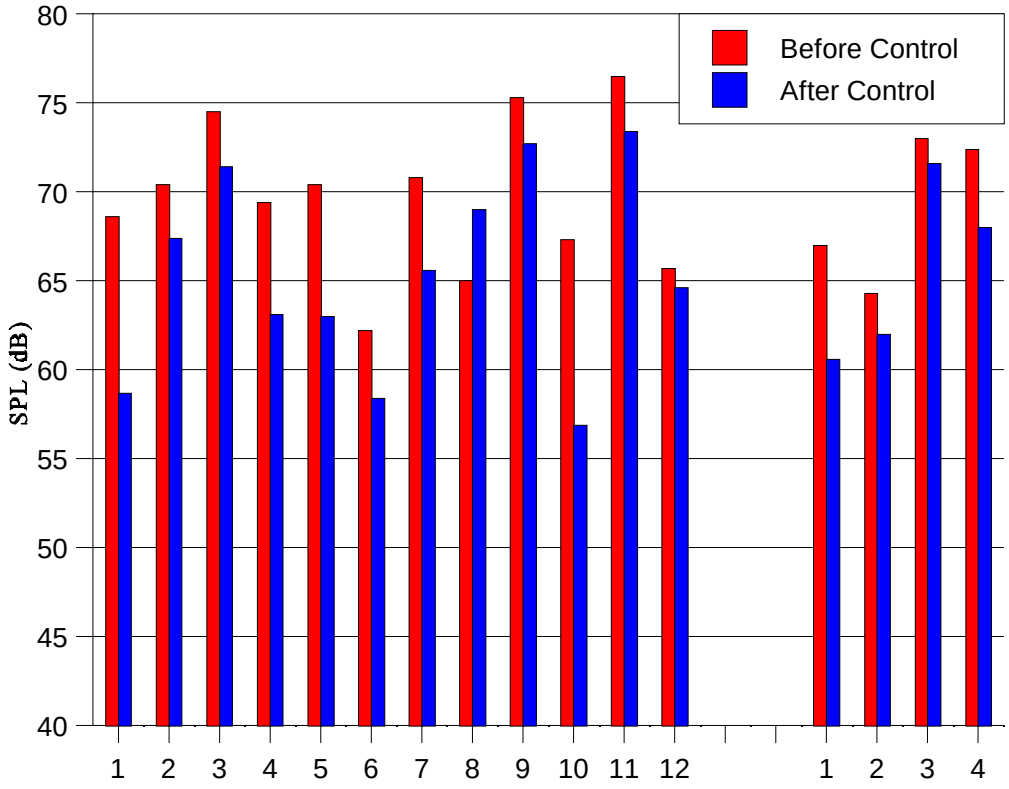

Figure 4.31 - Sound level reductions at error and global microphones during ASAC test - 125 Hz test case using optimal actuator group

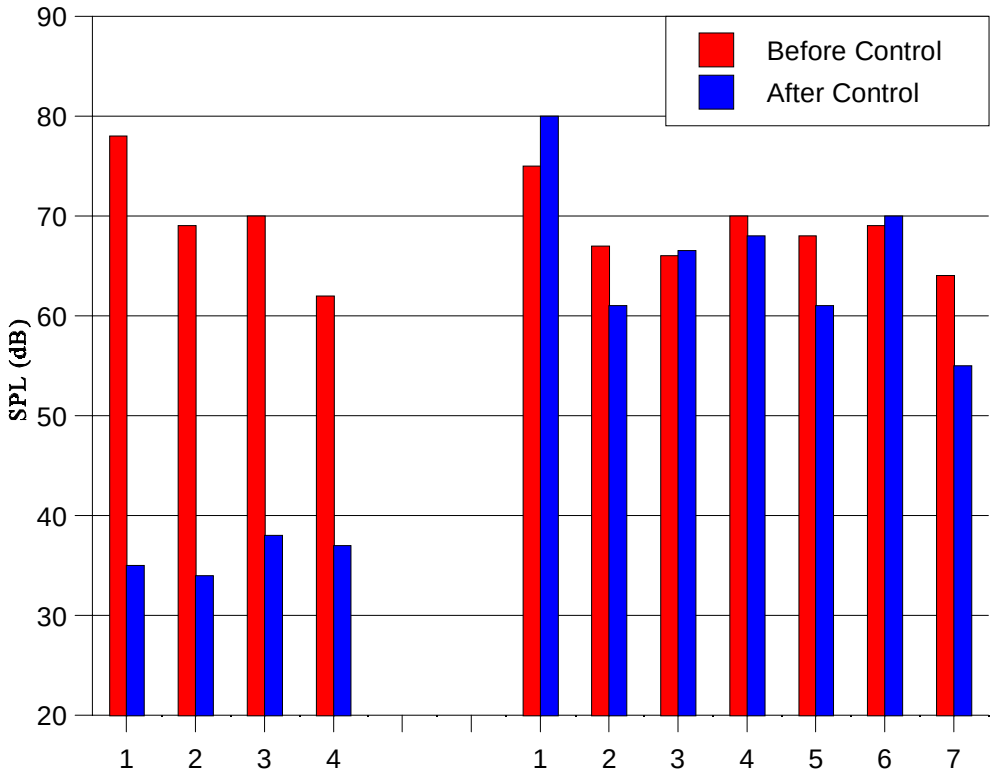

Figure 4.32 - Past ASAC results at error and global microphones for acoustic resonance test case

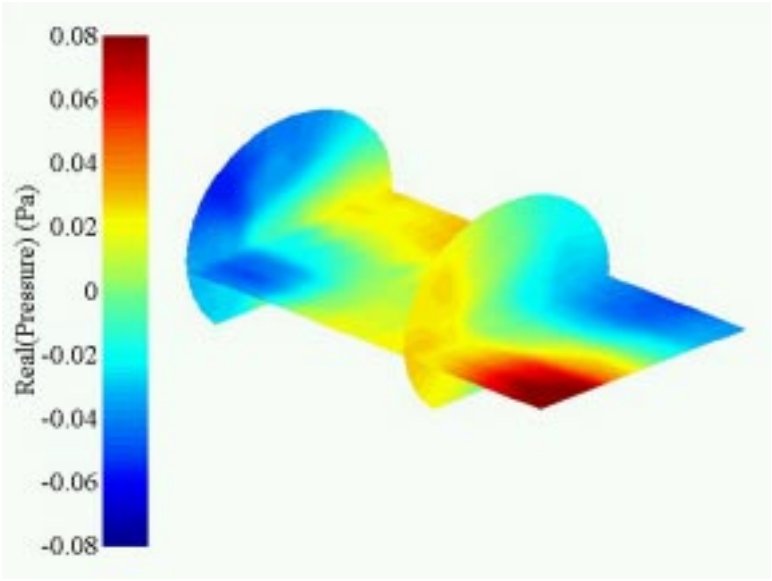

(a) Uncontrolled case

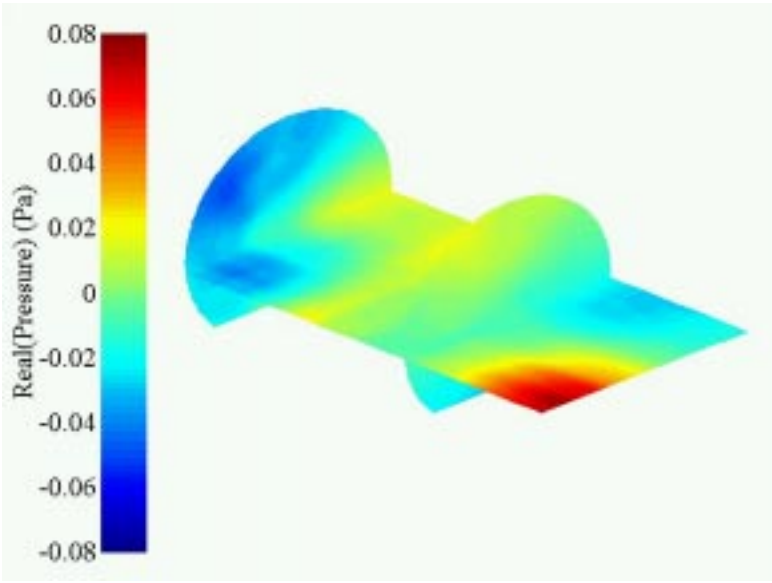

(b) Controlled case

Figure 4.33 - Comparison of uncontrolled and controlled interior pressure fields - 125 Hz case ASAC results

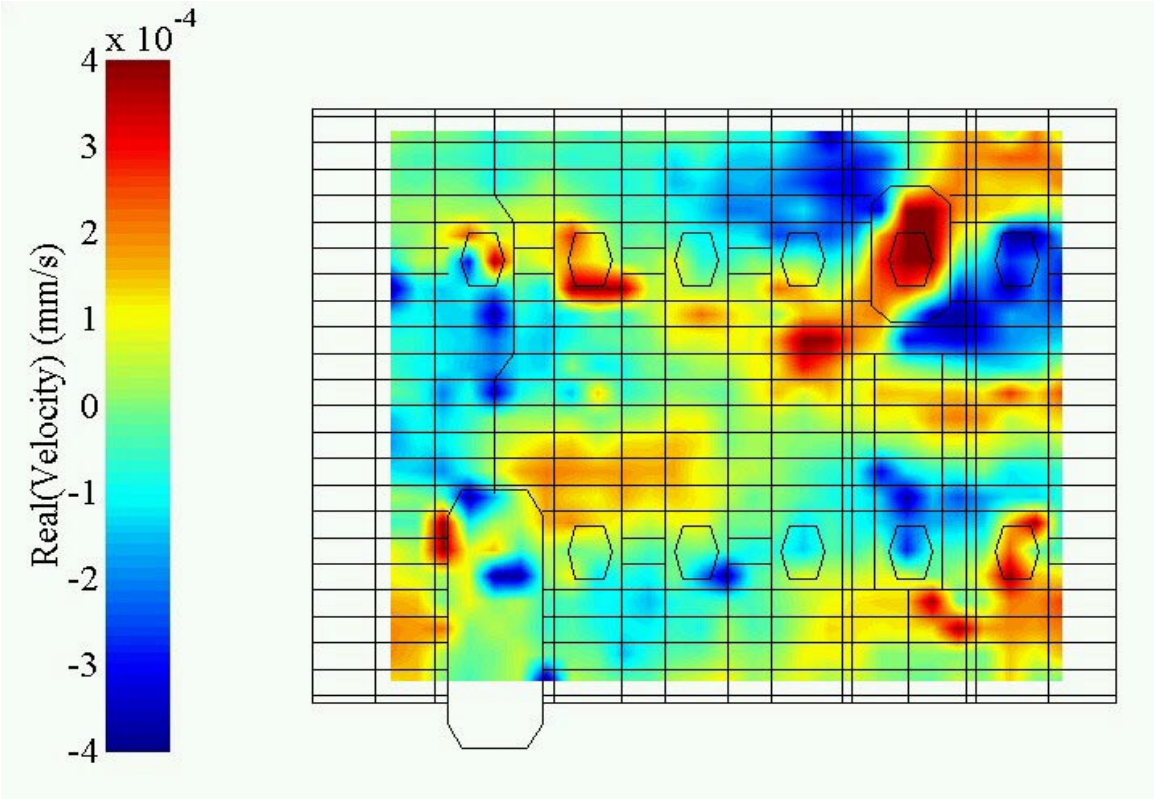

Figure 4.34 - Fuselage vibration field - uncontrolled case at 125 Hz

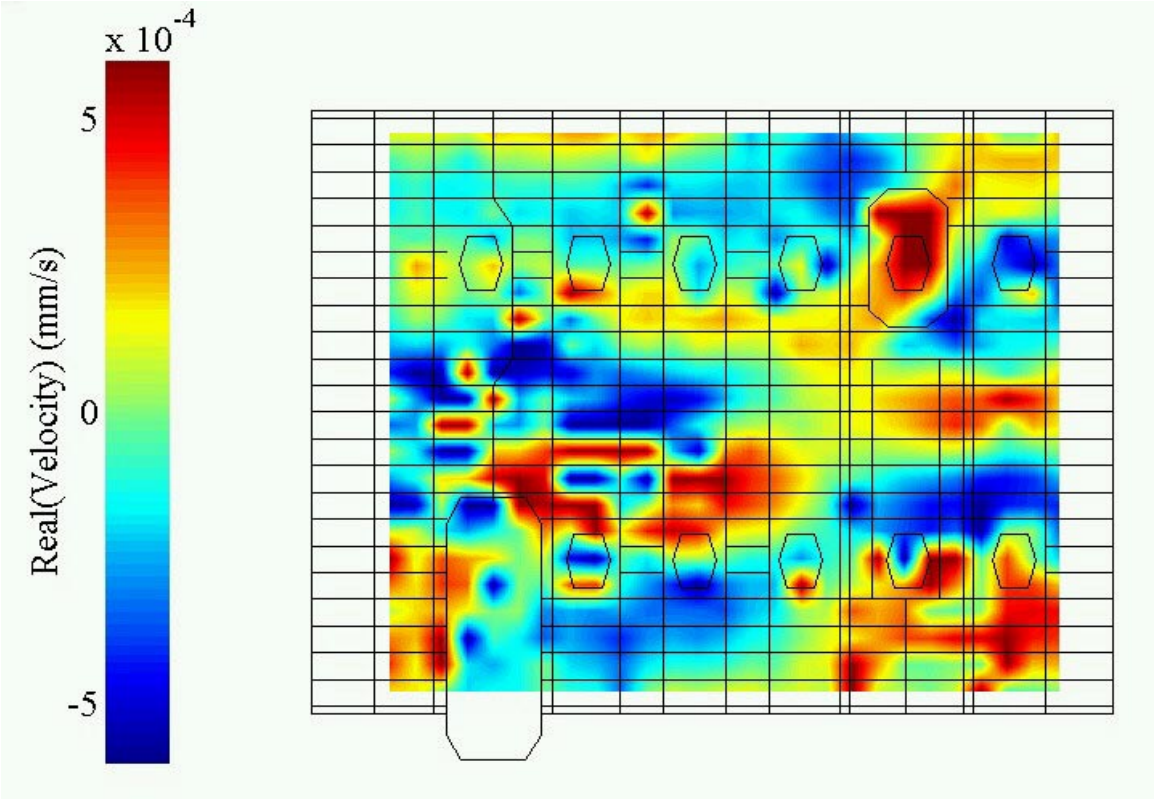

Figure 4.35 - Fuselage vibration field - controlled case at 125 Hz

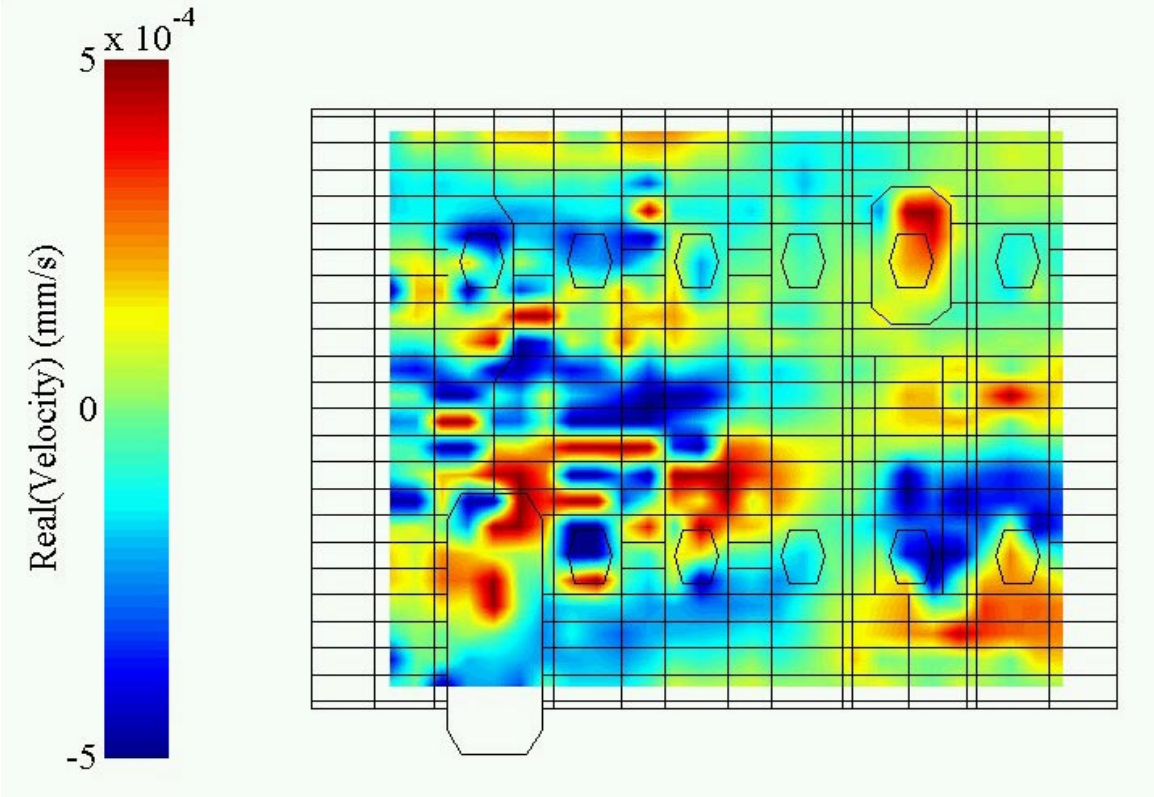

Figure 4.36 - Fuselage vibration field caused by ASAC actuators at 125 Hz

of-phase from each other. However, the overall features of the response field resemble the patterns measured during the system identification work for this frequency, shown earlier in Figure 4.6. It is therefore likely that modal suppression of the identified well-coupled fuselage motions is the dominant mechanism of control for this test case.

For comparison, additional ASAC tests were performed with alternate actuator groupings. The controller configuration was identical to the best-case testing setup and only the controller outputs were rerouted. Actuators 5, 10, 12, 13, 14, and 16 were selected as a representative mean-fitness group. Figure 4.37 presents the controlled and uncontrolled sound levels using this grouping. Average reductions of 4 dB at the error sensors and 2 dB at the auxiliary microphones are shown. Actuators 1, 2, 4, 6, 14, and 16 comprised the worst-case grouping for this frequency test case. Figure 4.38 presents the sound levels measured for this control system. Average sound level reductions of 4 dB at the error microphones and 1.5 dB at the global reference microphones were observed. As expected from the optimization process results, both the average-fitness and worst-case actuator grouping demonstrated reduced global performance as compared to the optimally-located actuator set.

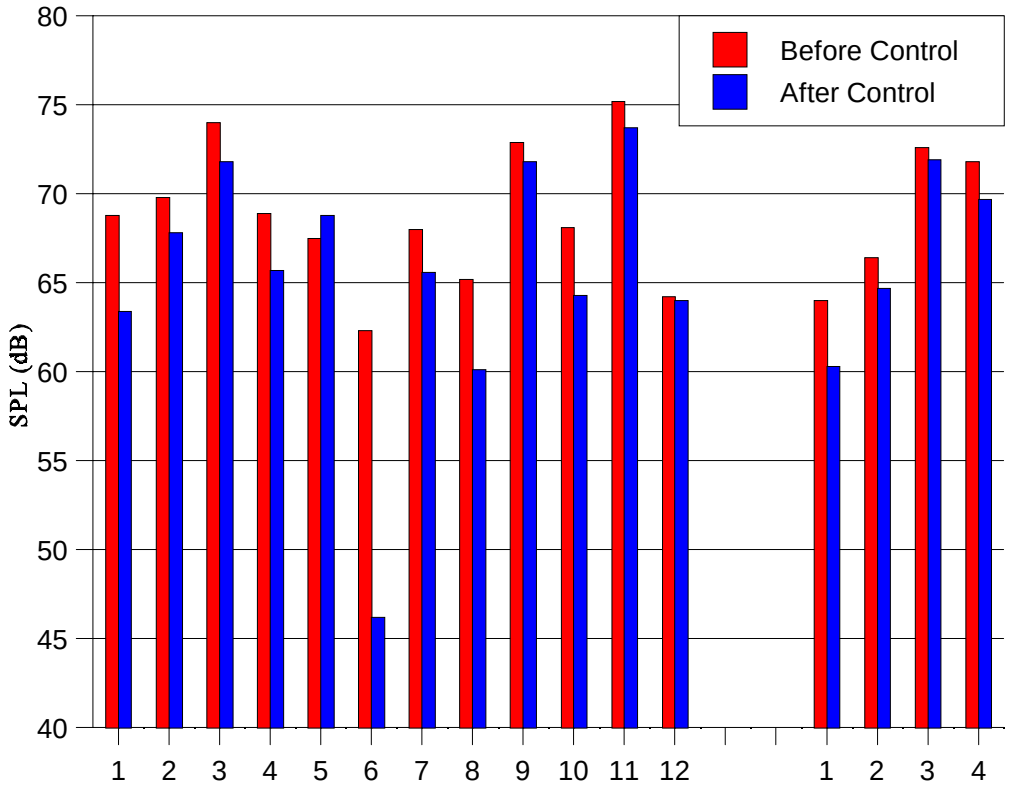

Figure 4.37 - Sound level reductions at error and global microphones during ASAC test - 125 Hz test case using average-fitness actuator group

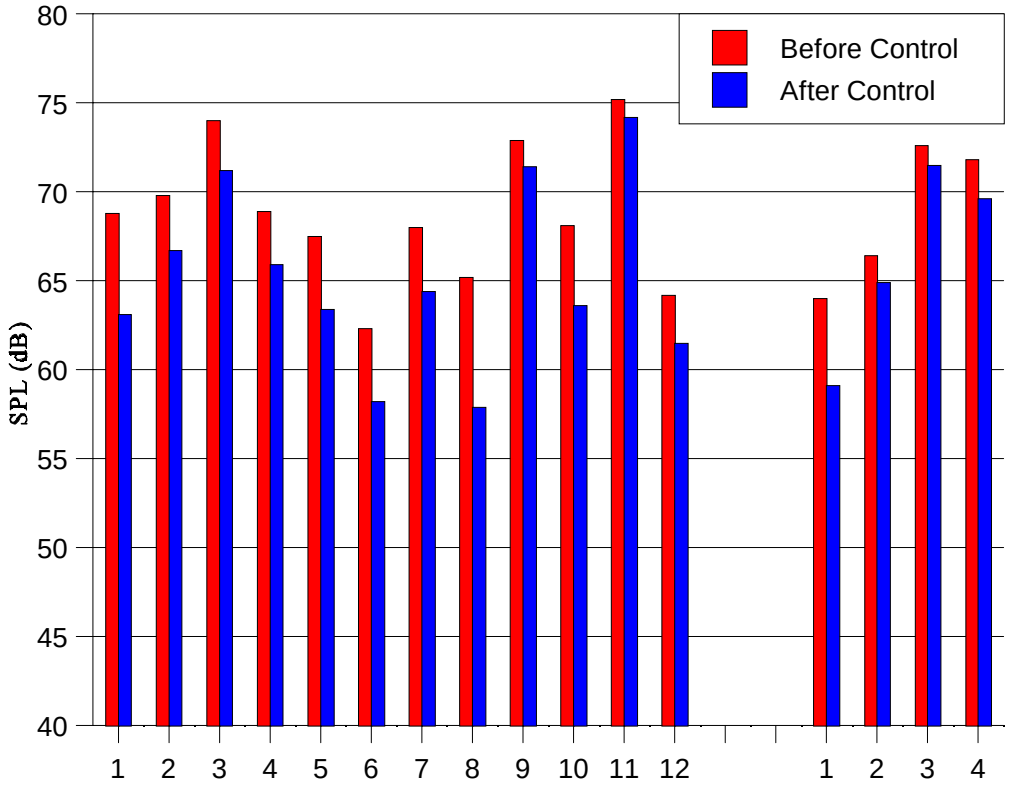

Figure 4.38 - Sound level reductions at error and global microphones during ASAC test - 125 Hz test case using worst-case actuator group

4.4.2 ASAC Test Results: 170 Hz

The optimal PZT group for the 170 Hz test case is composed of actuators 3, 9, 10, 11, 13, and 15 (Figure 4.26 contains actuator numbering information). Figure 4.39 presents the ASAC system layout for this test frequency, detailing the positions of the optimal structural actuators and the error and auxiliary microphone locations. Using this physical setup, ASAC tests were performed as described in section 3.4. For this test case, the controller output voltages to the actuators ranged from 15 to 130 volts RMS.

Figure 4.40 presents the uncontrolled and controlled pressure measurements from the 16 reference microphones. An average sound reduction of 3 dB was achieved at the 12 microphones used as error sensors. The 4 auxiliary microphones show an average global sound reduction of 1.5 dB. An average reduction of approximately 1 dB measured throughout the cabin by the traversing measurement array. It should be noted that relative to previous ASAC work with this test fuselage [35], the relatively modest reduction levels presented here represent a large increase in global control performance for an off-resonance frequency case. For comparison purposes, Figure 4.41 shows results of the previous ASAC tests at an off-resonance, reporting sound level changes for 4 error sensors and 7 global reference microphones. It can be seen that when ASAC was applied with the non-optimal actuator set, very large spillover effects were observed at every global reference microphone. This result again illustrates the importance of optimally configuring the actuators in that a reducation in spillover on the order of 10 dB has been achieved in this work.

Figure 4.42 shows the cabin interior pressure field in uncontrolled and controlled conditions. As expected from the microphone reduction levels discussed above, the global

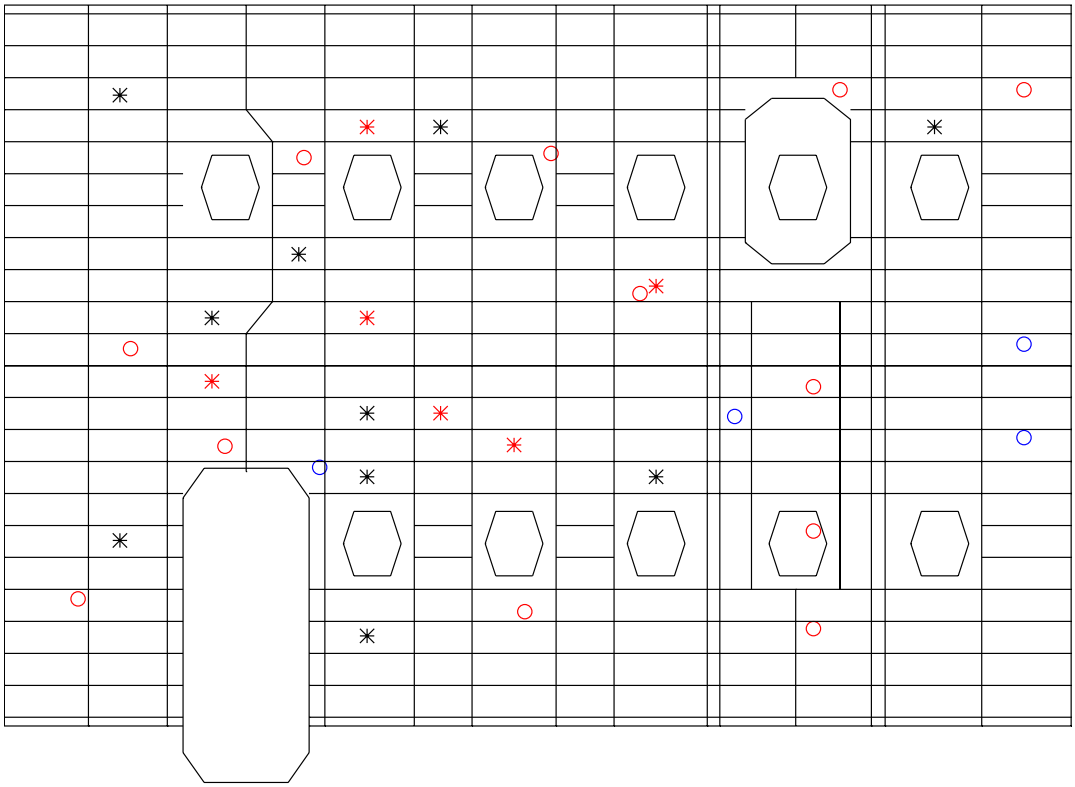

Figure 4.39 - Actuator and sensor locations for 170 Hz ASAC tests

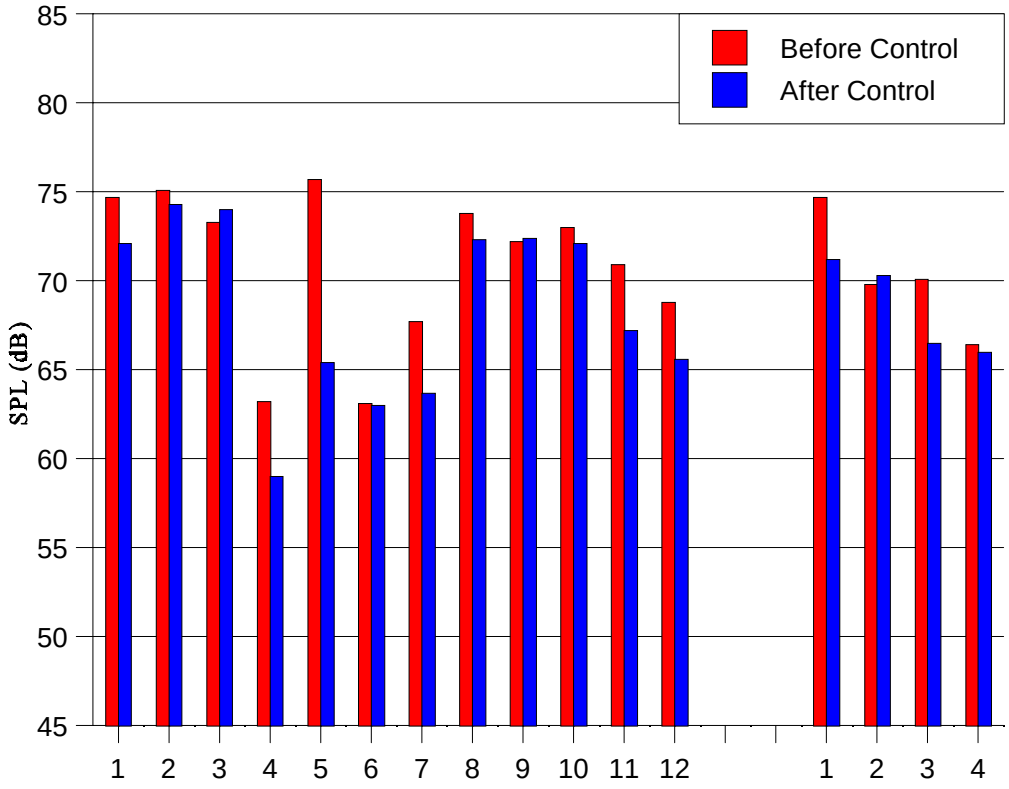

Figure 4.40 - Sound level reductions at error and global microphones during ASAC test - 170 Hz test case using optimal actuator group

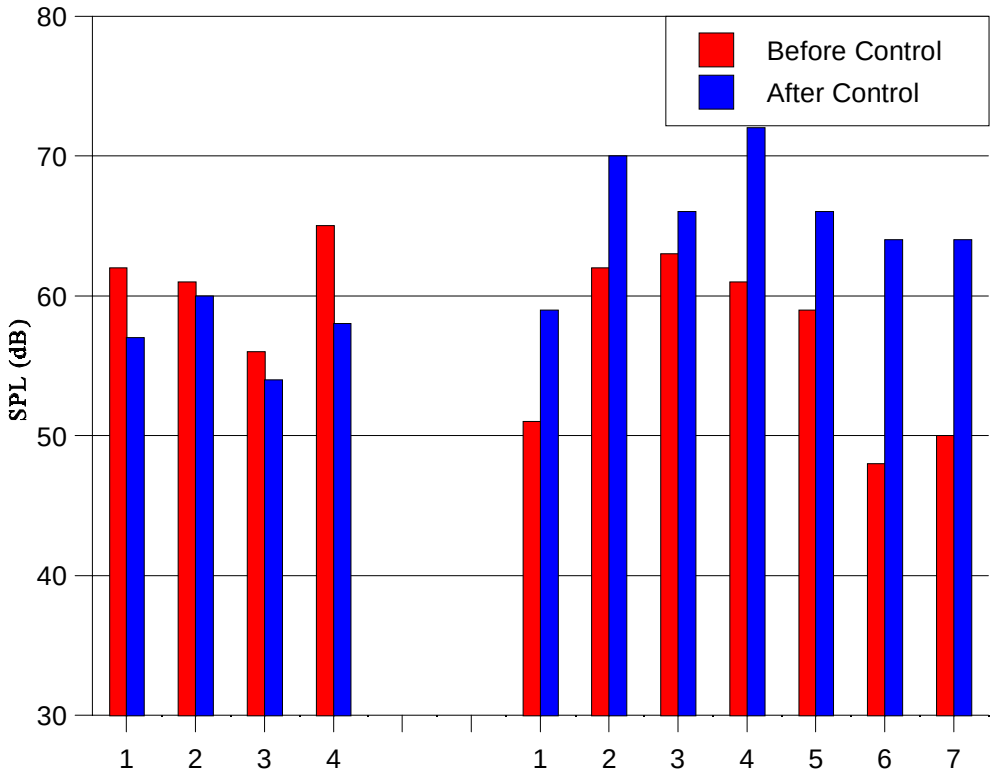

Figure 4.41 - Past ASAC results at error and global microphones for off-resonance test case

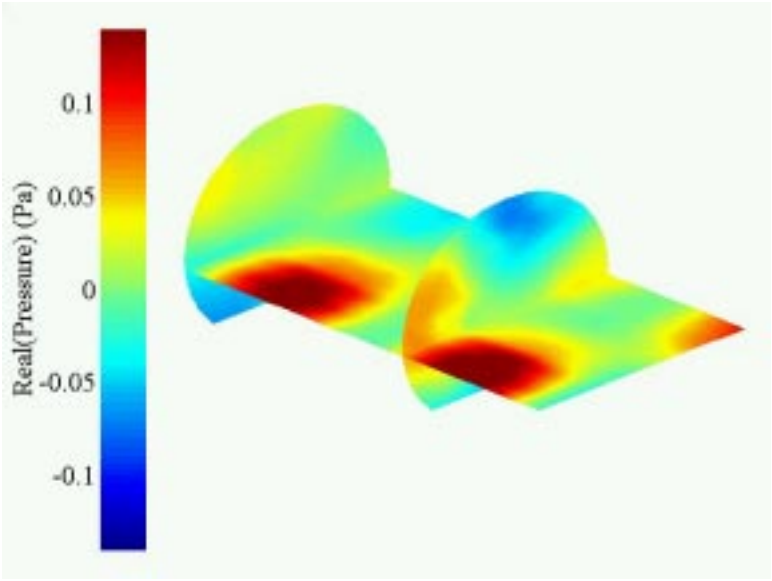

(a) Uncontrolled case

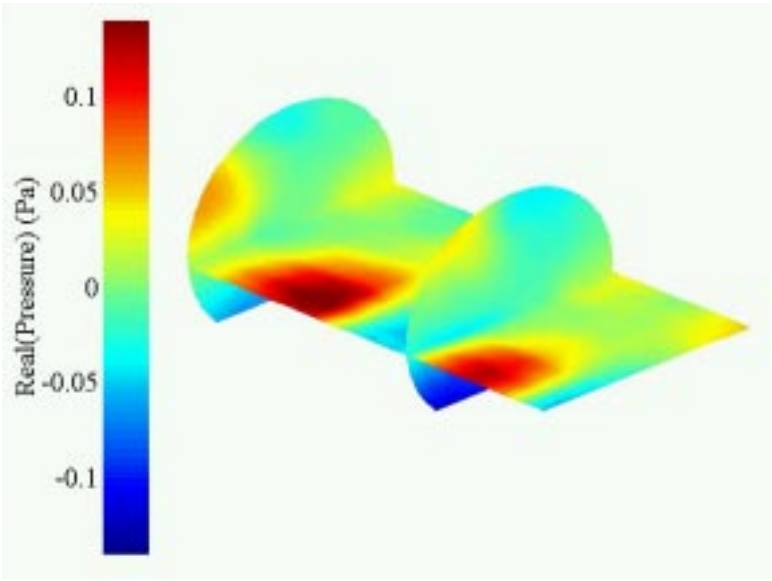

(b) Controlled case

Figure 4.42 - Comparison of uncontrolled and controlled interior pressure fields - 170 Hz case ASAC results

control levels in this case are modest, showing little or no spillover but also large regions in the cabin that were left relatively unaffected by the control system. This performance is noticeably less than in the acoustic resonance case presented earlier, most likely due to a large increase in the number of modes contributing to the acoustic disturbance. Therefore, increasing the number of control actuators may result in better ASAC performance at this frequency case. Figures 4.43 and 4.44 present the scanned fuselage vibrations in the uncontrolled and controlled cases respectively. These plots show that fuselage vibration levels were raised significantly by the ASAC system. Figure 4.45 shows the fuselage velocity field produced by the control actuators when the controller was locked and the disturbance removed. Note that a high-wavenumber circumferential response is again apparent in this test case. From the velocity field results presented here, it is not entirely clear what control mechanism is acting to reduce the interior sound in this case. However, the dominant high-order response induced by the actuators probably signifies some degree of modal restructuring of the fuselage vibrations into weakly-radiating modes.

Further ASAC tests were performed with alternative actuator groupings for comparison purposes. The controller configuration was identical to the best-case testing setup and only the controller outputs were changed. For a grouping with a predicted average performance, actuators 1, 3, 4, 5, 9, and 15 were selected. Figure 4.46 shows the sound level changes achieved with this grouping, with average reductions of 3 dB at the error sensors and a global average near 0 dB. The worst-case grouping for this frequency contains actuators 4, 5, 6, 7, 8, and 12. Figure 4.47 presents the reduction levels measured for this control setup, showing an average 3 dB sound level decrease at the error microphones and a global average reduction of only 1 dB observed at 4 additional microphones. Again, the non-optimal actuator groupings demonstrated poor global

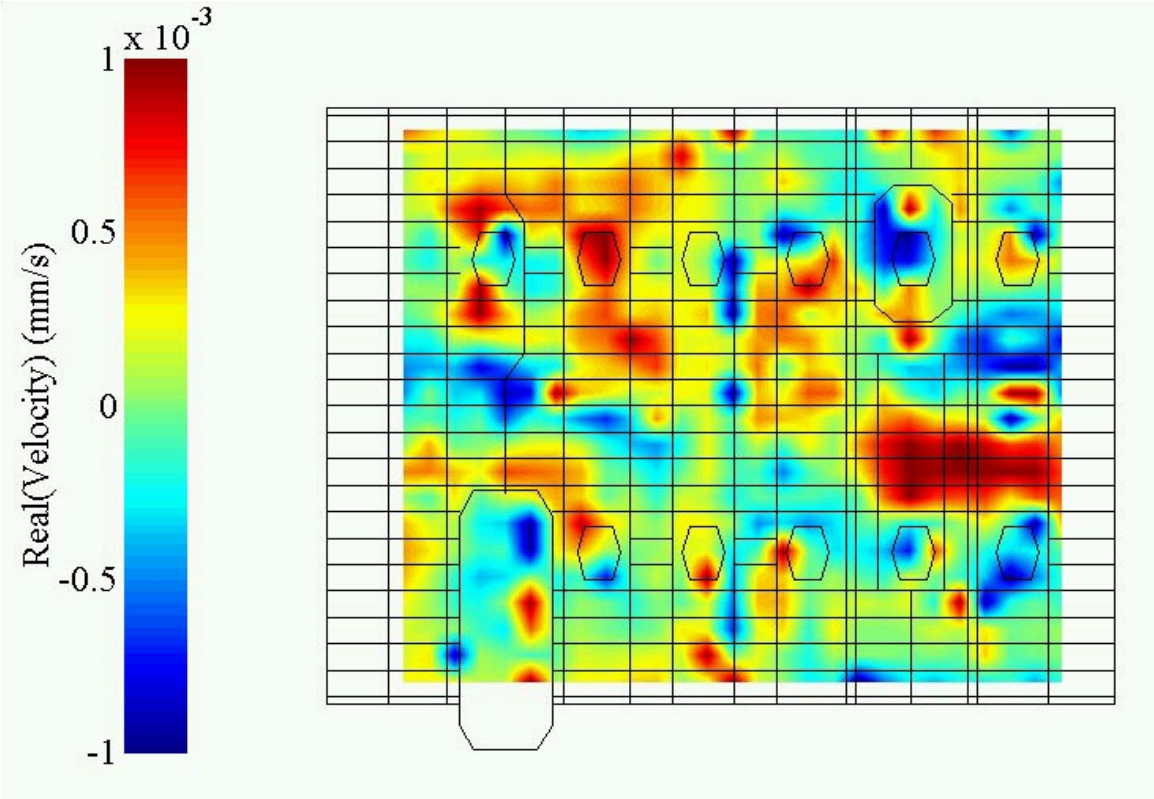

Figure 4.43 - Fuselage vibration field - uncontrolled case at 170 Hz

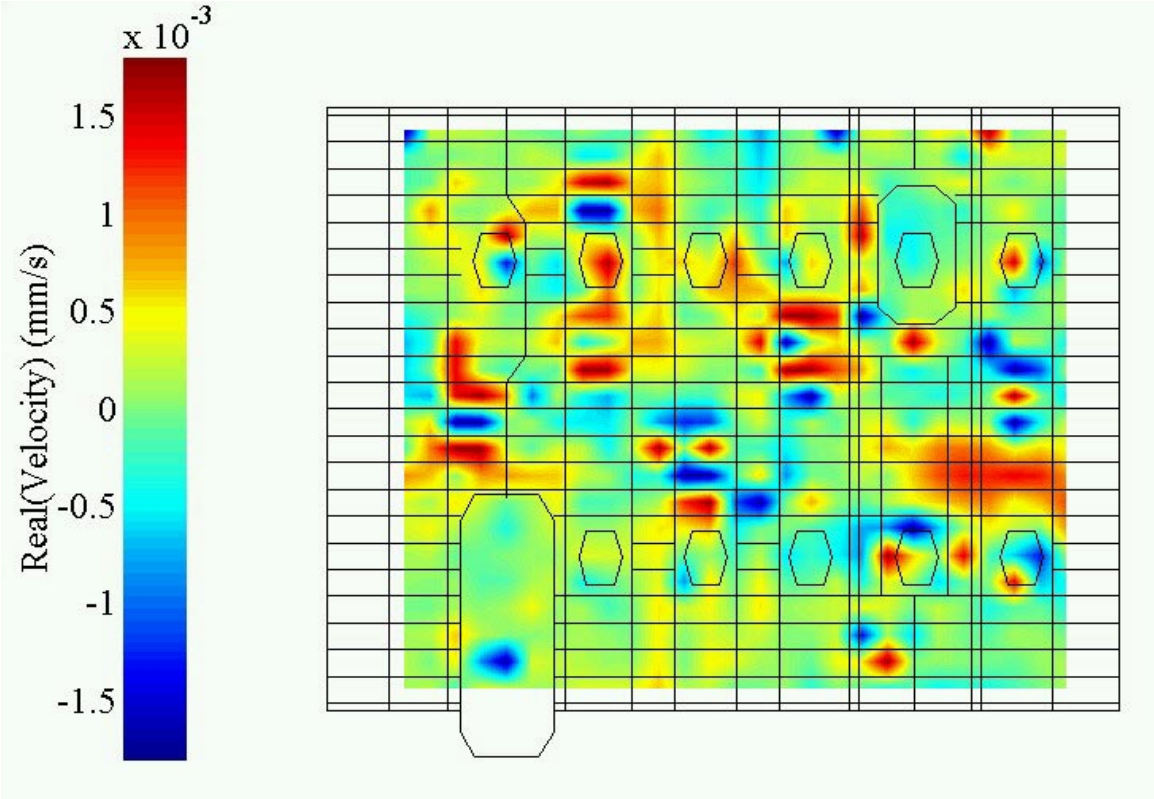

Figure 4.44 - Fuselage vibration field - controlled case at 170 Hz

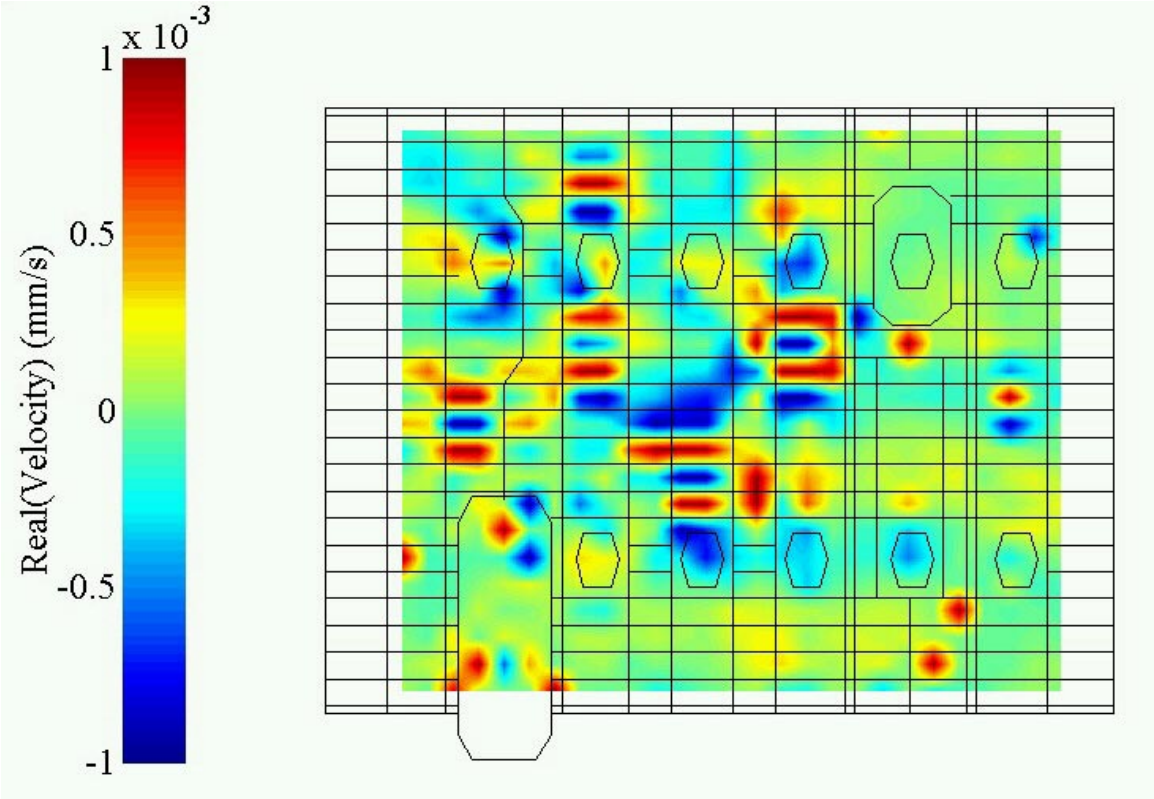

Figure 4.45 - Fuselage vibration field caused by ASAC actuators at 170 Hz

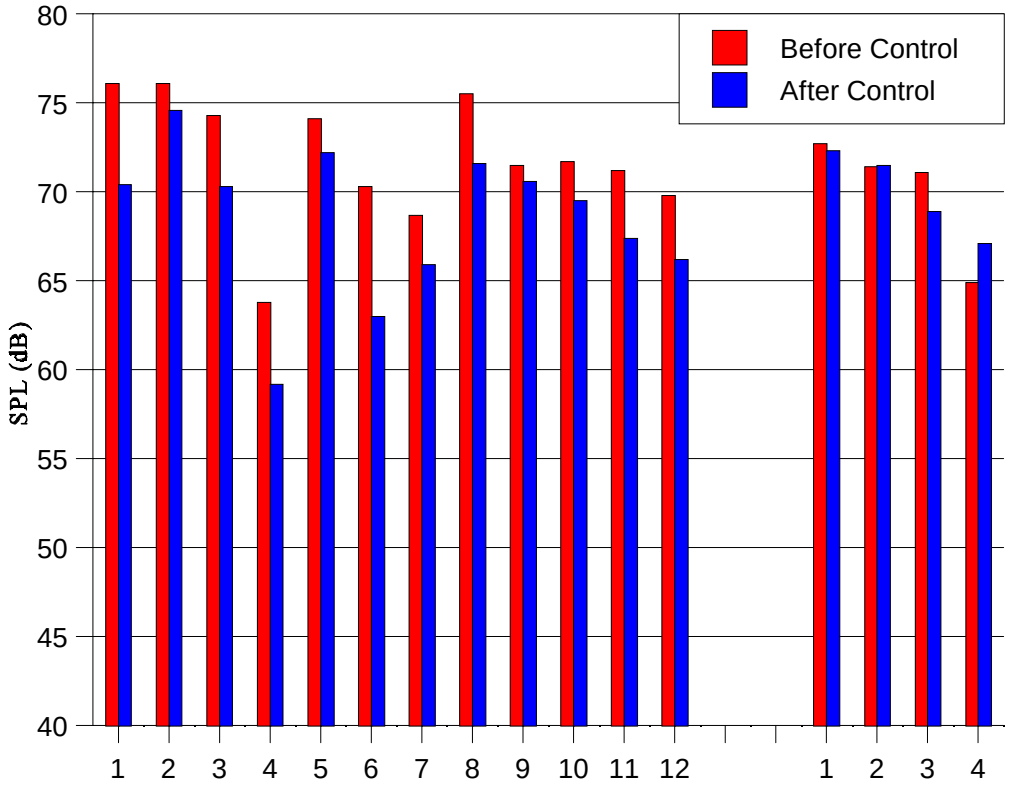

Figure 4.46 - Sound level reductions at error and global microphones during ASAC test - 170 Hz test case using average-fitness actuator group

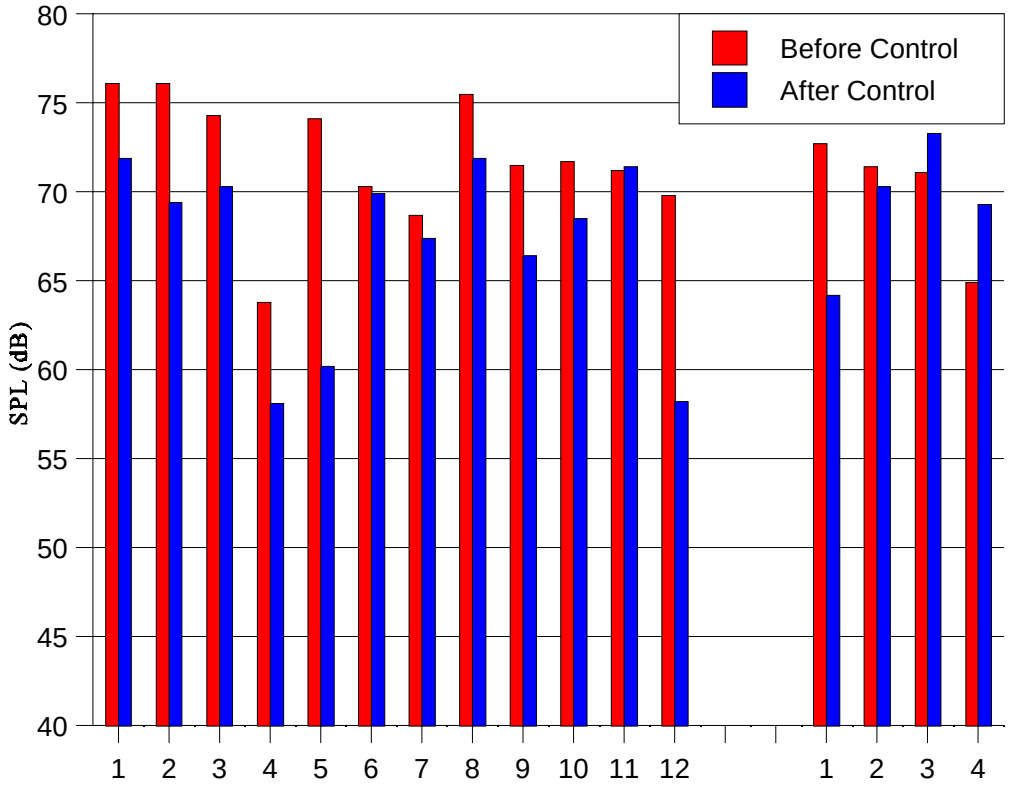

Figure 4.47 - Sound level reductions at error and global microphones during ASAC test - 170 Hz test case using worst-case actuator group

control effects, with the mean-fitness group in this case actually providing no net measured sound reductions away from the error sensors.

4.4.3 ASAC Test Results: 225 Hz

The optimal PZT group for the 225 Hz test case is composed of actuators 3, 4, 8, 10, 13, and 15 (Figure 4.26 shows actuator numbering information). Figure 4.48 shows the layout of the selected PZT actuator and microphone locations used for this test case. Using this physical configuration, ASAC tests were performed as described in section 3.4. For this case, the controller outputs to the actuators ranged from 10 to 160 volts RMS.

Figure 4.49 presents the uncontrolled and controlled pressure levels from 16 reference microphones. An average sound reduction of 4 dB was observed at the 12 error sensors. The 4 auxiliary reference microphones show an average global sound reduction of 3 dB. An average reduction throughout the cabin of approximately 2 dB was observed via the measurement array. Figure 4.50 shows the cabin interior pressure field in uncontrolled and controlled conditions. The plots reveal a uniform global reduction in sound levels with no spillover effects in the cabin area. Figures 4.51 and 4.52 present the measured fuselage vibrations in the uncontrolled and controlled cases respectively. These plots show that fuselage vibration levels were again raised significantly by the ASAC system. Figure 4.53 shows the fuselage velocity field produced by the control actuators acting alone. In this case, the response was dominated almost entirely by the high-wavenumber circumferential pattern observed in the earlier test cases. Modal restructuring of the fuselage vibrations into such high-order weakly-coupled patterns is the apparent control mechanism for this test frequency case.

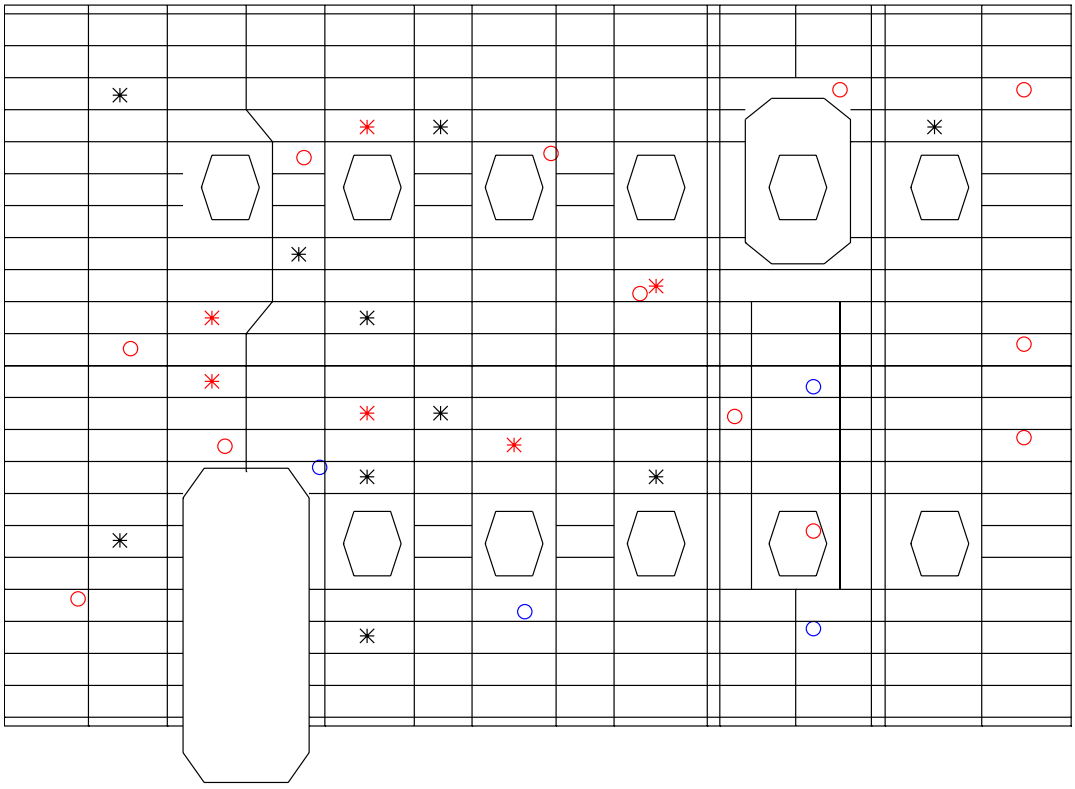

Figure 4.48 - Actuator and sensor locations for 225 Hz ASAC tests

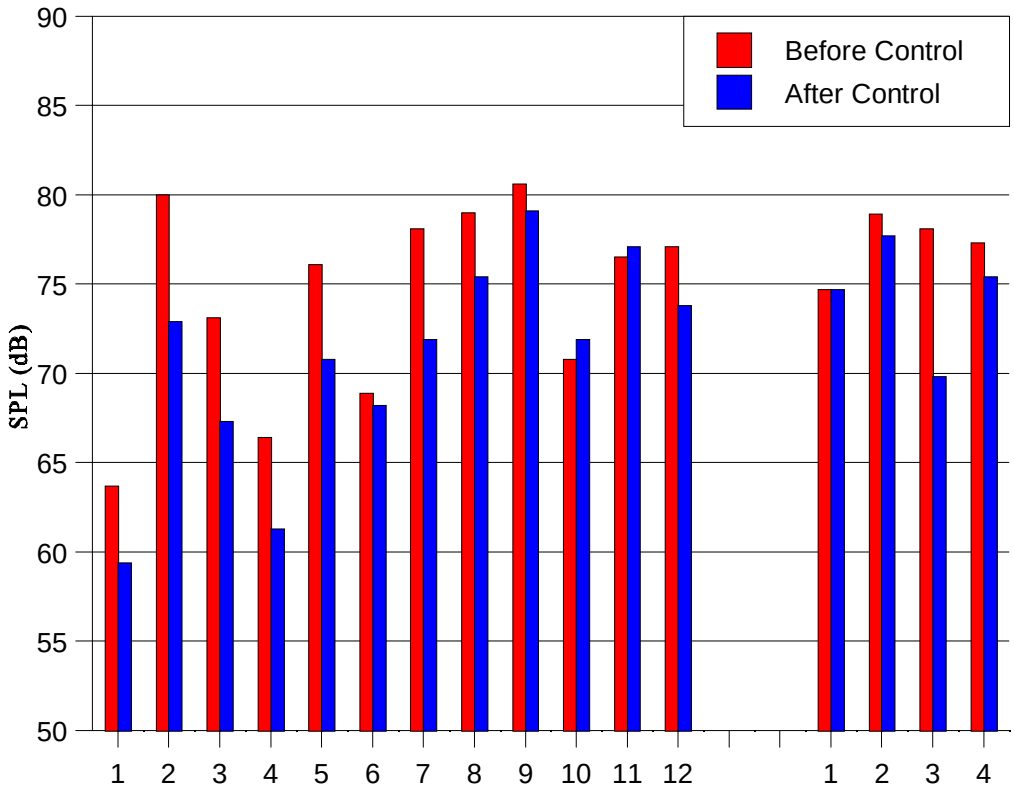

Figure 4.49 - Sound level reductions at error and global microphones during ASAC test - 225 Hz test case using optimal actuator group

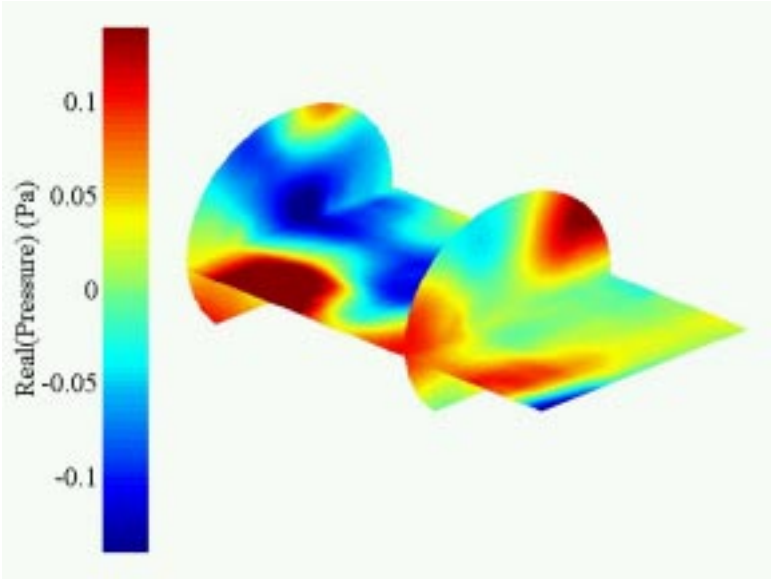

(a) Uncontrolled case

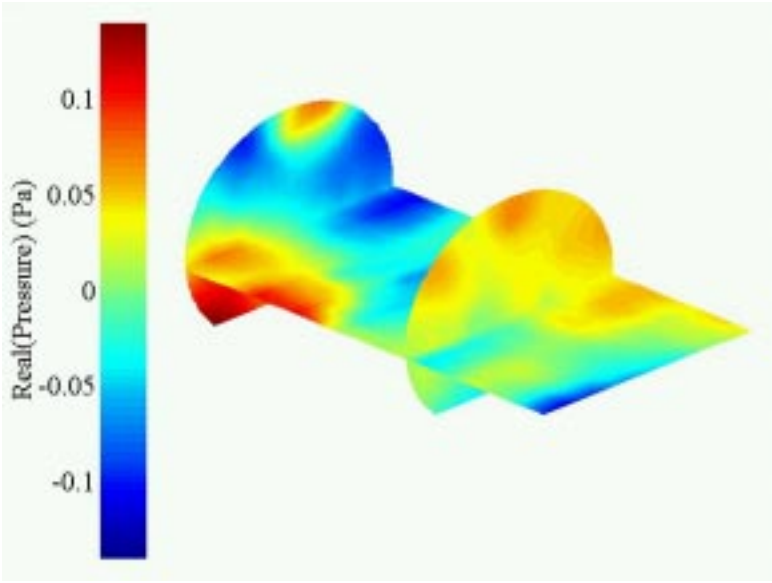

(b) Controlled case

Figure 4.50 - Comparison of uncontrolled and controlled interior pressure fields - 225 Hz case ASAC results

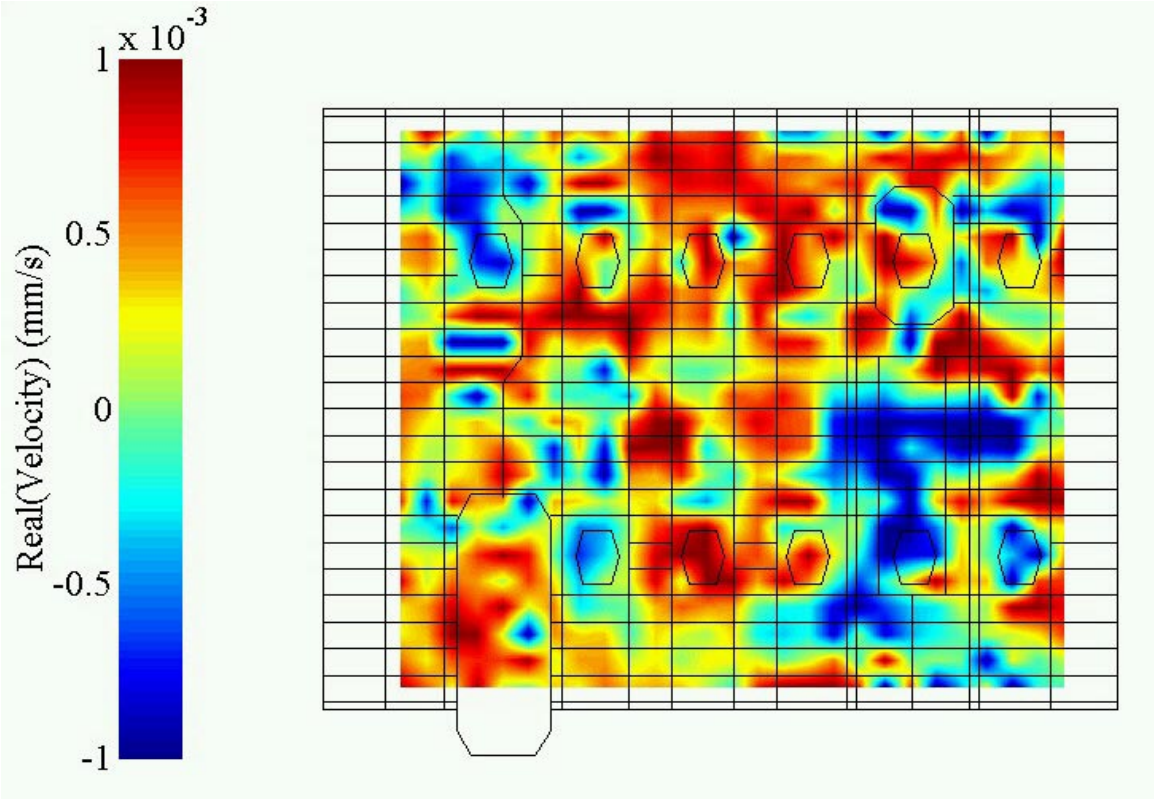

Figure 4.51 - Fuselage vibration field - uncontrolled case at 225 Hz

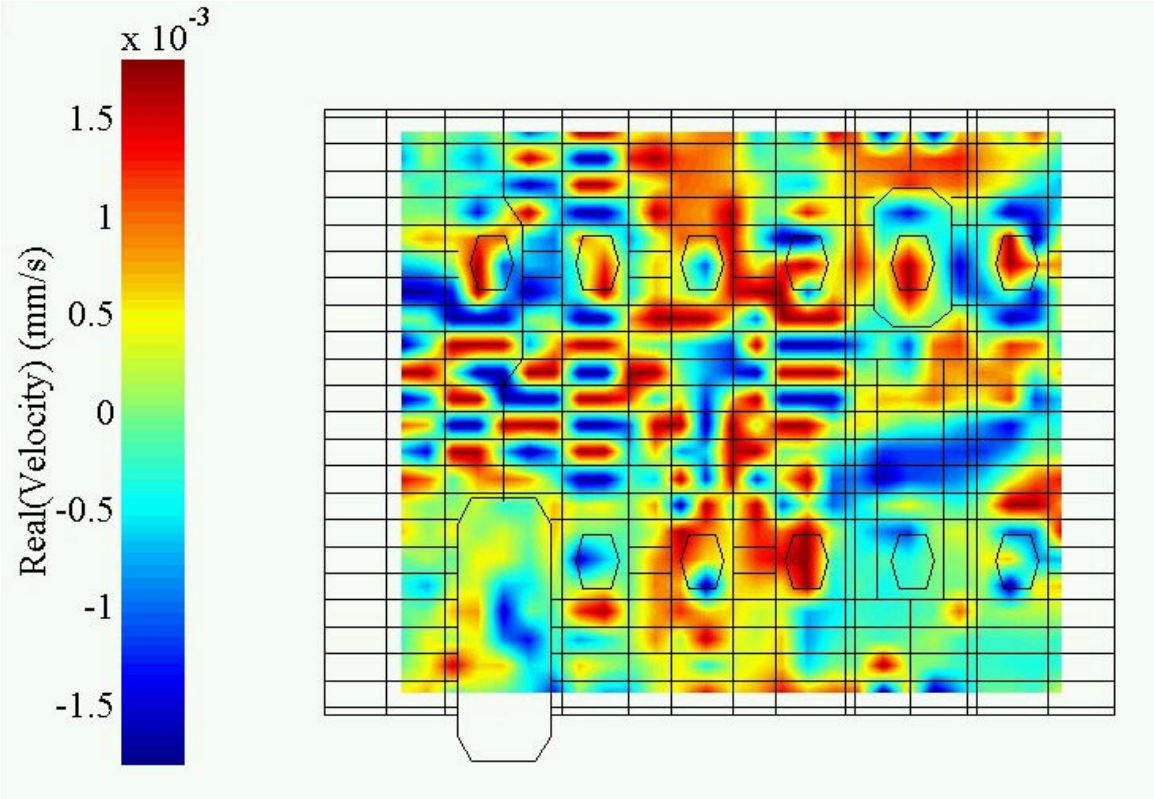

Figure 4.52 - Fuselage vibration field - controlled case at 225 Hz

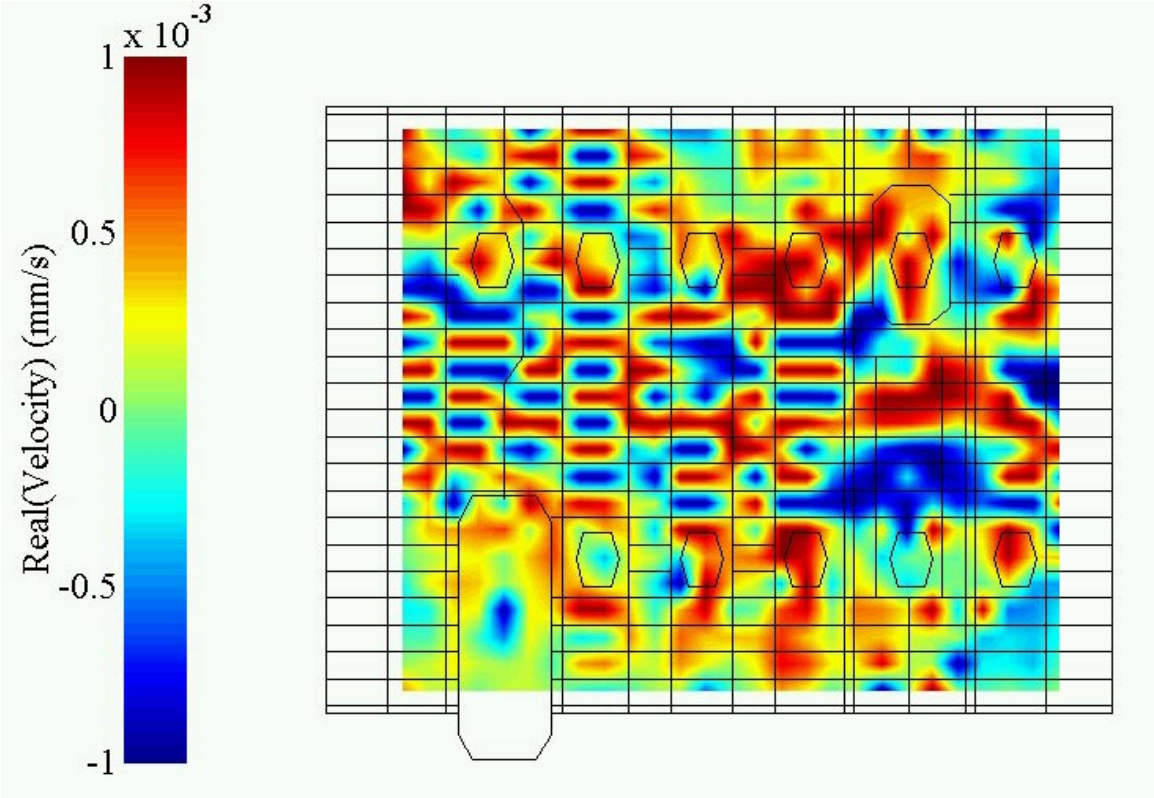

Figure 4.53 - Fuselage vibration field caused by ASAC actuators at 225 Hz

Further ASAC tests were performed with alternative actuator groupings for comparison purposes. The controller configuration was identical to the best-case testing setup and only the controller outputs were rerouted. For a grouping with a predicted average control performance, actuators 2, 4, 5, 9, 11, and 13 were selected. Figure 4.54 shows the sound level changes achieved with this grouping. Average reductions of 2 dB at the error sensors and 2 dB at the auxiliary microphones were observed. The worst-case grouping for this frequency was found to contain actuators 1, 2, 7, 8, 12, and 14. Figure 4.55 presents the reduction levels measured for this control setup. An average of a 1.5 dB sound level decrease was measured at the error microphones, while a global average reduction of approximately 1 dB was observed at the additional 4 microphones. As predicted, the alternate groupings both provided reduced global reductions away from the error sensors as compared to the optimal actuator set.

4.4.4 ASAC Test Results: 225 Hz with Rotating Imbalance Disturbance

The structural resonance frequency case of 225 Hz was selected for an additional ASAC test using a different disturbance input. To simulate a more realistic vibration source for another research project at VPI&SU, a rotating imbalance assembly was constructed in a typical engine casing. This engine rig was attached at the same rear mount position used for the shaker force input and provided realistic levels of disturbance force as well as realistic force vectors. Uncontrolled sound pressure levels in the cabin due to this alternate disturbance were on the order of 95-100 dB, which are significantly higher than the levels used in the earlier tests and are close to those observed in practice. Using the same optimal actuator set described above, and making use of an accelerometer

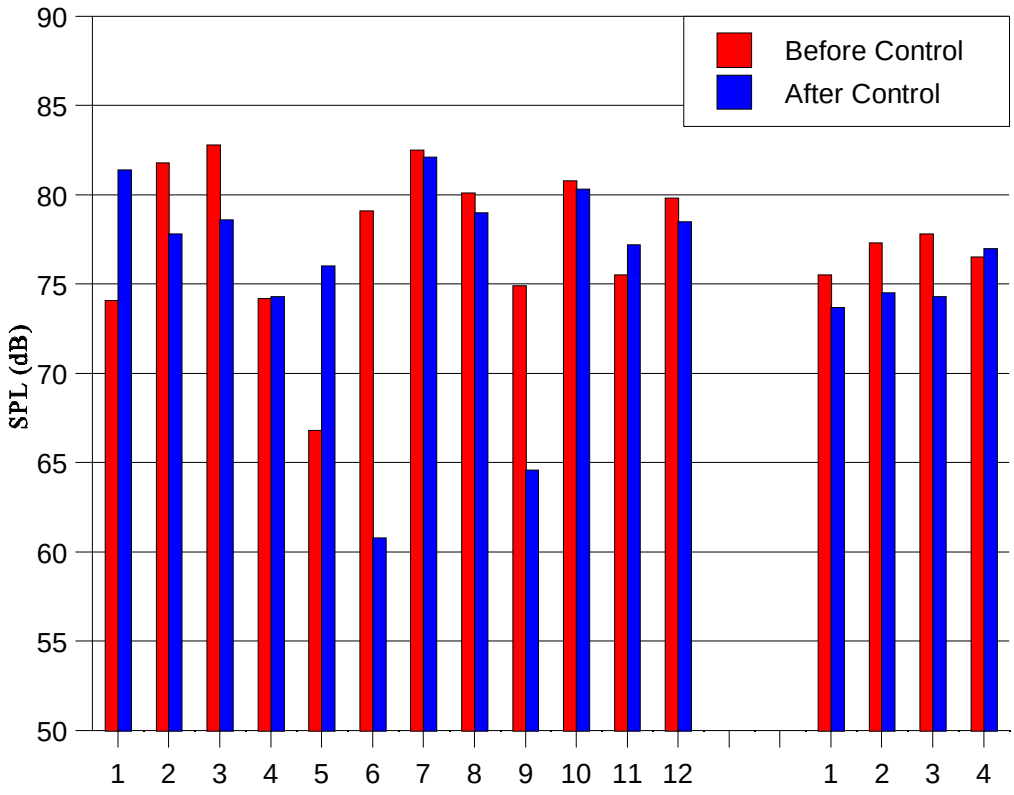

Figure 4.54 - Sound level reductions at error and global microphones during ASAC test - 225 Hz test case using average-fitness actuator group

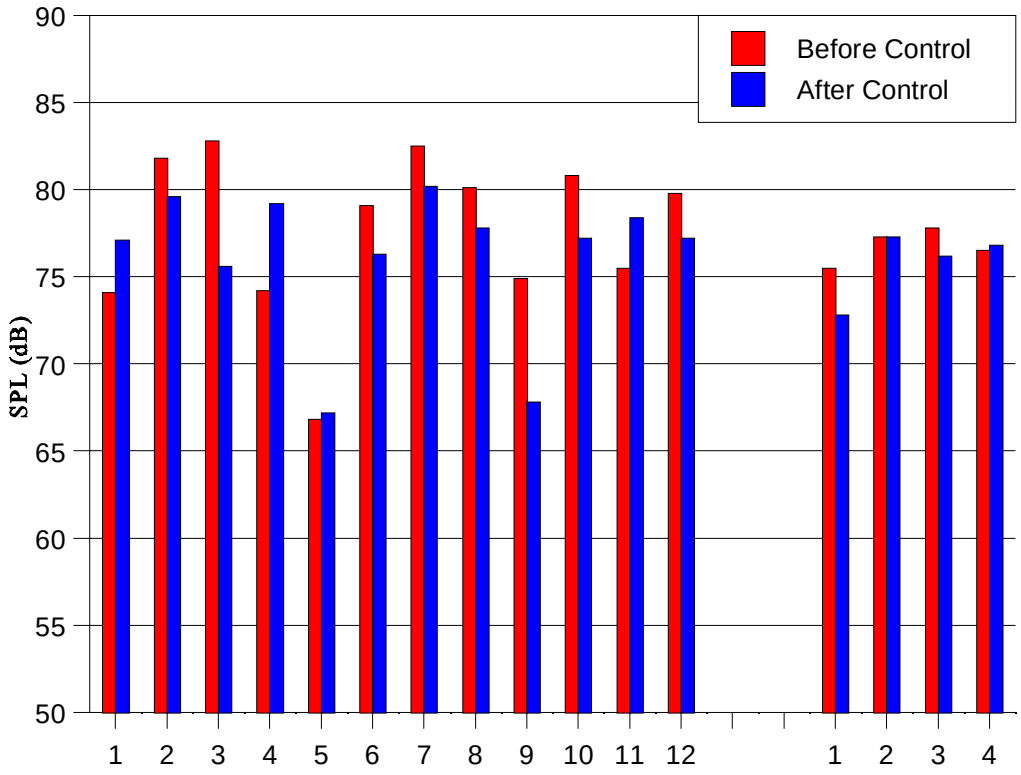

Figure 4.55 - Sound level reductions at error and global microphones during ASAC test - 225 Hz test case using worst-case actuator group

on the rotary imbalance apparatus for a controller reference signal, ASAC was performed with this alternate disturbance. After controller convergence, maximum control voltages to the piezoelectric actuators were observed to be on the order of 200 volts RMS or less. The error microphones recorded an average sound level reduction of approximately 2.5 dB. An average reduction of 1.5 dB was observed at the auxiliary microphones. Figure 4.56 details these control performance results. The results of this test demonstrate that the optimally-placed PZT actuators are capable of producing very high realistic sound levels while maintaining global control in the fuselage interior.

4.4.5 ASAC Results Summary

The ASAC tests detailed above show that the goal of reasonable global control of cabin noise was achieved for all three test cases. This is a significant improvement on previous ASAC work using the same test fuselage [35], which demonstrated some global control effects at an acoustic resonance case, but large acoustic spillover at every global sensor in an off-resonance situation.

The optimal actuator groupings as determined by the GA search process demonstrated better control performance than the other tested actuator groups at each frequency. While sound levels were reduced, significant structural control spillover occurred in each test, with vibration levels often increased by a factor of 2 or more in the vicinity of the control actuators. In addition, the piezoelectric actuators were shown to have sufficient control authority to reduce cabin noise due to a realistic disturbance.

Some additional general observations concerning control system performance were made during ASAC testing. It was found that environmental conditions often had a

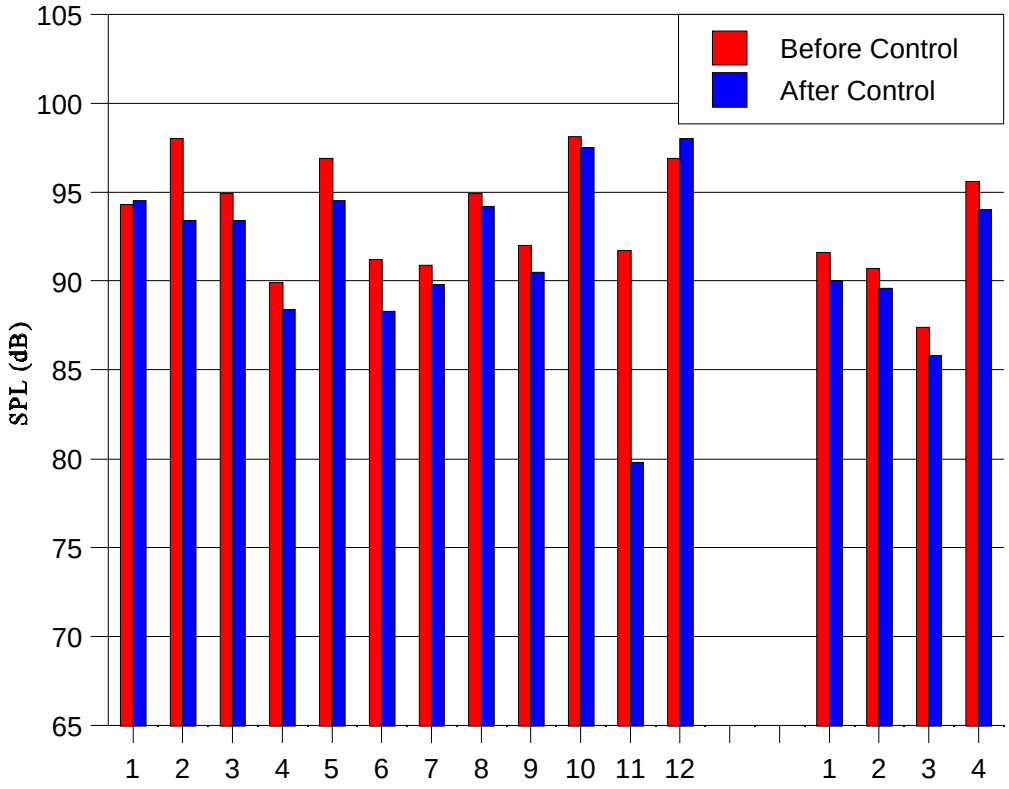

Figure 4.56 - Sound level reductions at error and global microphones during ASAC test - 225 Hz test case with rotating imbalance force disturbance

noticeable effect on the behavior of the coupled structural-acoustic fuselage system. In particular, the structural resonance frequency near 225 Hz shifted with temperature changes. In such circumstances, control performance at 225 Hz was reduced, as the test case approached an off-resonance condition. However, by adjusting the disturbance signal to match the new resonance frequency, control performance comparable to the results presented earlier were achieved. In all test cases, the optimized actuator sets provided similar control performance across a range of approximately 10 Hz when the disturbance input was varied in this manner. Thus some robustness of the design approach was demonstrated.

Chapter 5

Conclusions and Recommendations

The goals of this project, aimed at efficient application of active structural acoustic control to a complex aircraft fuselage system, can be divided into three main areas: (1) development of a new system identification technique, (2) position optimization of piezoelectric actuators, and (3) ASAC system validation tests. Promising results were achieved in all three areas of the development process, and in all three selected test cases. General conclusions drawn from this work are as follows:

1. The new system identification technique introduced and evaluated for this project was found to be effective at isolating important low-level fuselage vibrations from a complex response. The method uses an active control system to approximate a disturbance sound field and thus excite only the well-coupled fuselage motions. In essence, the control system acts in a filtering capacity, only concentrating on the gross response shape and ignoring the small details of the noise field. As a result, the most impressive system identification performance was observed at the acoustic resonance case, where the noise field approximation was excellent and simplification of the vibration field most extreme.

2. A genetic algorithm search method proved effective in quickly determining the best subset of a group of candidate piezoelectric actuators. The fitness calculations were based on the measured actuator-structure coupling behavior. In each test case, the GA succeeded in locating the optimal actuator grouping with less than 10% of the computation required for a full enumerative search.

3. The 12 input - 6 output ASAC systems assembled using the previously outlined system identification and actuator positioning information each proved capable of achieving global sound level reductions over the measured area of the passenger cabin. As the goal of the project was this global control effect, lesser reductions at error sensors were accepted in favor of increasing the regions of sound reduction and limiting any acoustic spillover.

4. In addition to the ASAC tests with the optimal actuator groupings, control experiments were performed with average and worst-case groups for each frequency. Each of these alternate groups provided markedly less global control effects, emphasizing the need for careful placement of control sources in a system as complex as an aircraft.

5. Structural control spillover in the form of greatly increased fuselage vibrations was observed in all test cases. The peak fuselage out-of-plane velocities were often raised by a factor of two or more in the vicinity of the control actuators after control was applied. At each frequency, a high-order circumferential response was induced by the PZTs.

6. Overall, the tests for the acoustic resonance case (125 Hz) demonstrated the best results. The system identification provided the clearest simplification of vibration data in this case, resulting in a pattern of well-coupled motions dominated by a single cylinder mode shape. The ASAC results using the optimal actuator set for this test case showed global reductions averaging 4 dB throughout the cabin, with an average of a 6 dB decrease at the error microphones.

7. The tests at the structural resonance case (225 Hz) also provided promising results. The system identification technique used in this work will probably yield its most uncertain results in such a resonance case, but careful tuning of the control system resulted in excellent sound field approximation in the critical region near the fuselage walls. The measured vibration again consisted of a set of low-level well-coupled fuselage motions which were used to position ASAC actuators. The resultant optimal ASAC system provided a global average reduction of 3 dB, with a 4 dB average at the error microphones.

8. The off-resonance test case (170 Hz) provided the greatest challenges in seeking an effective control system. Once again, careful tuning of the ANC system in the system identification experiments provided a simplified set of important vibrations. The optimal ASAC configuration for this frequency achieved an average global reduction of 1.5 dB and an average error sensor reduction of 3 dB. It should be noted that even these modest global control levels are an extreme improvement over previous ASAC work on the same fuselage test rig, where ad hoc actuator placement resulted in significant acoustic spillover effects throughout the passenger cabin.

9. Additional experiments at the structural resonance frequency (225 Hz) demonstrated the ability of the ASAC system to reduce very large sound levels due to a realistic disturbance. A rotating imbalance test rig was used to simulate an engine disturbance with realistic loads in these tests, resulting in uncontrolled noise levels approaching 100 dB SPL. The piezoelectric actuators were capable of providing sufficient output to control the resulting cabin noise, resulting in noise reductions comparable to the shaker disturbance test cases.

Several recommendations for future development work on this project are as follows:

1. Expand the set of candidate locations in the actuator optimization process. In the work presented here, the number of candidates was kept sufficiently small to allow for comparison between the results of the enumerative search and genetic algorithm search methods. The GA performance was seen to be excellent, and the selected actuator groups were all composed of members expected to perform well at each frequency. Therefore, an increase in the number of candidate actuators and reliance on a GA technique for efficient optimization calculations could lead to better-performing ASAC systems.

2. Examine the effects of controller dimensionality on global control performance, during both the ANC (system identification) and ASAC portions of the testing procedure. Because one of the primary goals of this work was to maximize the global effects of ASAC system performance, a 12 input - 6 output over-determined control setup was used for the ASAC tests. However, increased numbers of control actuators would increase total control authority and therefore the maximum potential sound reductions. An analysis

of the tradeoff between controller order and actuator numbers for this fuselage could result in further optimization of the ASAC approach.

3. Hierarchical grouping schemes that combine multiple actuators into one logical control output may prove useful in increasing control performance. A conceptually attractive solution for the fuselage system would be to combine a number of PZT actuators into distributed systems designed to drive a specific structural response pattern, such as that measured by the system identification process. Alternatively, several controller outputs could be assigned to different orthogonal components of a desired vibration response pattern, with each output signal shifted in magnitude and phase for a large number of component actuators.

4. Along with alternate actuator groupings, alternate controller schemes could be explored in the context of the cabin noise problem. By the nature of the new system identification technique, the transfer functions between structural force input at the engine mount and acoustically well-coupled response at many points on the fuselage walls are known. Therefore, it is possible to construct a simplified non-adaptive control system with a number of PZT actuators to directly drive the fuselage motions that are known to cause the cabin noise problem.

5. With sufficient computational power, a broadband test of the system identification and ASAC procedures could be performed. The experimental techniques developed for this work only assume that the fuselage system is linear, so the inverse excitation measurement technique and actuator optimization can all be generalized to broadband use.

6. To achieve larger sound reductions in important areas of the cabin, an ASAC system designed using the methods presented here could be focused towards limited regions by using alternate error sensor locations. The error microphones in this work were scattered throughout the cabin interior in an attempt to achieve uniform global sound reductions. However, preferentially placing sensors near seated passenger locations or in a head-level plane throughout the cabin could increase the apparent effects of the noise reduction system while still restricting control spillover to less important cabin areas.

7. As structural fatigue issues are important in aerospace applications, additions to the control system that limit vibration increases may prove useful. Using accelerometers or other more distributed structural sensors as one or more controller error sensors could limit structural spillover. Additional control actuators may limit the spillover problem as well, allowing lower force levels per actuator while acting to cancel some of the high-order response so prevalent in the after-control vibration fields.

References

[1]. Warnaka, G.E., "Active attenuation of noise - The state of the art," Noise Control Engineering, Vol. 18, No. 3, 1982, pp.100-110.

[2]. Elliott, S.J., and Nelson, P.A., "The active control of sound," Electronics and Communication Engineering Journal, Aug, 1990, pp. 127-136.

[3]. Nelson, P.A., and Elliott, S.J. *Active Control of Sound.* New York: Academic Press, 1992.

[4]. Fuller, C.R., Elliott, S.J., and Nelson, P.A. *Active Control of Vibration.* New York: Academic Press, 1996.

[5]. Lueg, P. "Process of silencing sound oscillations," 1936, US Patent No. 2,043,416.

[6]. Olson, H.L., and May, E.G. "Electronic sound absorber," Journal of the Acoustical Society of America, Vol. 25, No. 6, 1953, pp. 1130-1136.

[7]. Conover, W.B., "Recent contributions to transformer audible noise control," AIEE Transactions, Applications and Industry, Vol. 74, Part D, 1955, pp. 77-86.

[8]. Fuller, C.R., "Mechanisms of transmission and control of low-frequency sound in aircraft interiors," SAE Technical Paper 850879, April, 1985.

[9]. Fuller, C.R., "Structural influence of the cabin floor on sound transmission into aircraft - Analytical investigations," Journal of Aircraft, Vol. 24, No. 10, Oct, 1987, pp. 731-736.

[10]. Lester, H.C., and Fuller, C.R., "Active control of propeller-induced noise fields inside a flexible cylinder," AIAA Journal, Vol. 28, No. 8, 1990, pp. 1374-1380.

[11]. Abler, S.B., and Silcox, R.J., "Experimental evaluation of active noise control in a thin-walled cylinder," Proceedings of Noise-Con 87, 1987, pp. 341-346.

[12]. Bullmore, A.J., Nelson, P.A., and Elliott, S.J., "Theoretical studies of the active control of propeller-induced cabin noise," Journal of Sound and Vibration, Vol. 140, No. 2, 1990, pp. 191-217.

[13]. Nelson, P.A., Curtis, A.R.D., Elliott, S.J., and Bullmore, A.J., "The active minimization of harmonic enclosed sound fields, Part I: Theory," Journal of Sound and Vibration, Vol. 117, No. 1, 1987, pp. 1-13.

[14]. Bullmore, A.J., Nelson, P.A., Curtis, A.R.D., and Elliott, S.J., "The active minimization of harmonic enclosed sound fields, Part II: Computer simulation," Journal of Sound and Vibration, Vol. 117, No. 1, 1987, pp. 15-33.

[15]. Elliott, S.J., Curtis, A.R.D., Bullmore, A.J., and Nelson, P.A., "The active minimization of harmonic enclosed sound fields, Part III: Experimental verifications," Journal of Sound and Vibration, Vol. 117, No. 1, 1987, pp. 35-58.

[16]. Bullmore, A.J., Nelson, P.A., Elliott, S.J., Evers, J.F., and Chidley, B., "Models for evaluating the performance of propeller aircraft active noise control systems," AIAA-87-2704, Proceedings of the AIAA 11th Aeroacoustics Conference, 1987.

[17]. Dorling, C.M., Eatwell, G.P., Hutchins, S.M., Ross, C.F., and Sutcliff, S.G.C., "A demonstration of active noise reduction in an aircraft cabin," Journal of Sound and Vibration, Vol. 128, No. 2, 1989, pp. 358-360.

[18]. Elliott, S.J., Nelson, P.A., Stothers, I.M., and Boucher, C.C., "In-flight experiments on the active control of propeller-induced cabin noise," Journal of Sound and Vibration, Vol. 140, No. 2, 1990, pp. 219-238.

[19]. Salikuddin, M., and Ahuja, K.K., "Application of localized active control to reduce propeller noise transmitted through fuselage surface," Journal of Sound and Vibration, Vol. 133, No. 3, 1989, pp. 467-481.

[20]. Warner, J.V., and Bernhard, R.J., "Digital control of local sound fields in an aircraft passenger compartment," AIAA Journal, Vol. 28, No. 2, 1990, pp. 284-289.

[21]. Carme, Ch., Delemotte, V., and Montassier, A., "ANR (Active noise reduction) in turbo-prop aircraft," Proceedings of Active 95, 1995, pp. 607-618.

[22]. Fuller, C.R., "Apparatus and method for global noise reduction," 1987, U.S. Patent No. 4,715,599.

[23]. Fuller, C.R., and Jones, J.D., "Experiments on reduction of propeller induced interior noise by active control of cylinder vibration," Journal of Sound and Vibration, Vol. 112, No. 2, 1987, pp. 389-395.

[24]. Jones, J.D., and Fuller, C.R., "Active control of sound fields in elastic cylinders by vibrational inputs," Proceedings of Noise-Con 87, 1987, pp. 413-418.

[25]. Jones, J.D., and Fuller, C.R., "Active control of structurally-coupled sound fields in elastic cylinders by vibrational force inputs," International Journal of Analytical and Experimental Modal Analysis, Vol. 5, No. 3, 1990, pp. 123-140.

[26]. Silcox, R.J., Fuller, C.R., and Lester, H.C., "Mechanism of active control in cylindrical fuselage structures," AIAA Journal, Vol. 28, No. 8, 1990, pp. 1397-1403.

[27]. Rossetti, D.J., and Norris, M.A., "A comparison of actuation and sensing techniques for aircraft cabin noise control," Noise Control Engineering Journal, Vol. 44, No. 1, 1996, pp. 53-58.

[28]. Simpson, M.A., Luong, T.M., Fuller, C.R., and Jones, J.D., "Full-scale demonstration tests of cabin noise reduction using active vibration control," Journal of Aircraft, Vol. 28, No. 3, 1991, pp. 208-215.

[29]. Houston, B.H., Marcus, M.H., and Bucaro, J.A., "Mechanism based control of aircraft interior noise," Proceedings of Active 95, 1995, pp. 583-594.

[30]. Clark, R.L., Fuller, C.R., and Wicks, A., "Characterization of multiple piezoelectric actuators for structural excitation," Journal of the Acoustical Society of America, Vol. 90, No. 1, 1991, pp. 346-357.

[31]. Clark, R.L., and Fuller, C.R., "Experiments on active control of structurally radiated sound using multiple piezoelectric actuators," Journal of the Acoustical Society of America, Vol. 91, No. 6, 1991, pp. 3313-3320.

[32]. Fuller, C.R., Snyder, S.D., Hansen, C.H., and Silcox, R.J., "Active control of interior noise in model aircraft fuselages using piezoceramic actuators," AIAA Journal, Vol. 30, No. 11, 1992, pp. 2613-2617.

[33]. Silcox, R.J., Lefebvre, S., Metcalf, V.L., Beyer, T.B., and Fuller, C.R., "Evaluation of piezoceramic actuators for control of aircraft interior noise," Proceedings of the DGLR/AIAA 14th Aeroacoustics Conference, 1992, pp. 542-551.

[34]. Lefebvre, S., "Active control of interior noise using piezoelectric actuators in a large-scale composite fuselage model," M.S. Thesis, Virginia Tech, 1991.

[35]. Fuller, C.R., and Gibbs, G.P., "Active control of interior noise in a business jet using piezoceramic actuators," Proceedings of Noise-Con 94, 1994, pp. 389-394.

[36]. Clark, R.L., and Fuller, C.R., "Optimal placement of piezoelectric actuators and polyvinylidene fluoride error sensors in active structural acoustic control approaches," Journal of the Acoustical Society of America, Vol. 92, No. 3, 1992, pp. 1521-1533.

[37]. Wang, B., Burdisso, R.A., and Fuller, C.R., "Optimal placement of piezoelectric actuators for active structural acoustic control," Journal of Intelligent Material Systems and Structures, Vol. 5, Jan., 1994, pp. 67-77.

[38]. Burdisso, R.A., and Fuller, C.R., "Design of active structural acoustic control systems by eigenproperty assignment," Journal of the Acoustical Society of America, Vol. 96, No. 3, 1994, pp. 1582-1591.

[39]. Yang,D., and Fuller, C.R., "Numerical simulation of active control of interior noise in a business jet with point force actuators - optimization of transducers," Proceedings of Inter-noise 95, 1995.

[40]. Cabell, R.H., Smith, G.C., and Fuller, C.R., "Experimental investigation of actuator grouping for active structural acoustic control," Proceedings of Active 95, 1995, pp. 347-358.

[41]. Cabell, R.H., Lester, H.C., Mathur, G.P., and Tran, B.N., "Optimization of actuator arrays for aircraft interior noise control," AIAA Paper No. 93-4447, Presented at 15th AIAA Aeroacoustics Conference, 1993.

[42]. Golub, G.H., and Van Loan, C.F., *Matrix Computations*, Baltimore: Johns Hopkins University Press, 2nd Ed., 1989.

[43]. Goldberg, D.E. *Genetic algorithms in search, optimization, and machine learning.* Reading, MA: Addison-Wesley, 1989.

[44]. Holland, J.H. *Adaptation in natural and artificial systems.* Ann Arbor: The University of Michigan Press, 1975.

[45]. Bäck, T., and Schwefel, H. "An overview of evolutionary algorithms for parameter optimization," Evolutionary Computation, Vol. 1, No. 1, 1993, pp. 1-23.

[46]. Bäck, T. *Evolutionary algorithms in theory and practice.* Oxford: Oxford University Press, 1996.

[47]. Zimmerman, D.C., "A Darwinian approach to the actuator number and placement problem with non-negligible actuator mass," Mechanical System and Signal Processing, Vol. 7, No. 4, 1993, pp. 363-374.

[48]. Yao, L, Sethares, W.A., and Kammer, D.C., "Sensor placement for on-orbit modal identification via a genetic algorithm," AIAA Journal, Vol. 31, No. 10, 1993, pp. 1922-1927.

[49]. Rao, S.S., Pan, T., and Venkayya, V.B., "Optimal placement of actuators in actively controlled structures using genetic algorithms," AIAA Journal, Vol. 29, No. 6, 1991, pp. 942-943.

[50]. Simpson, M.T., and Hansen, C.H., "Use of genetic algorithms to optimize vibration actuator placement for active control of harmonic interior noise in a cylinder with floor structure," Noise Control Engineering Journal, Vol. 44, No. 4, 1996, pp. 169-184.

[51]. Tsahalis, D.T., Katsikas, S.K, and Manolas, D.A., "A genetic algorithm for optimal positioning of actuators in active noise control: results from the ASANCA project," INTER-NOISE 93 Proceedings, edited by Pierre Chapelle and Gerrit Vemier (Noise Control Foundation, Poughkeepsie, New York, 1993), pp. 83-88.

[52]. Gibbs, G.P., Mahnken, B., and Fuller, C.R., “System identification and preliminary active control of the interior acoustic field of a Cessna Citation III fuselage: Year One Annual Report,” VAL Technical Report VAL-9401, Aug. 1994.

[53]. Widrow, B., and Stearns, S.D. *Adaptive Signal Processing*. Englewood Cliffs, New Jersey: Prentice Hall, 1985.

[54]. Timoshenko, S. *Theory of Plates and Shells*. New York, NY: McGraw-Hill Book Company, Inc., 1940.

Appendix A - Genetic Algorithm Code Listing

This Appendix contains the C++ code developed for the genetic algorithm optimization process used in this project.

```
/* GENOPT.CPP
   Genetic Algorithm Optimization Project - Main program module
   October 1996
   by Scott Paxton */

#include <stdio.h>
#include <stdlib.h>
#include "genopt.h"
#include "gene.h"

Gene BestList[MAXGEN];  // best group from each generation
float AverageFitness[MAXGEN];
int CurrentGen=0;  // counter


// A note on fitness: because an enumerative search was already
// performed for each test case, coding of a complex-valued SVD
// and pseudoinverse routines was avoided by using a look-up
// table containing the fitness results as computed in matlab.

// The following are look-up tables for fitness evaluation
int IndexLUT[6][16]={{0,3003,2002,1287,792,462, 252, 126, 56, 21, 6},
                     {0, 1001, 715, 495, 330, 210, 126, 70, 35, 15, 5},
                     {0, 286, 220, 165, 120, 84, 56, 35, 20, 10, 4},
                     {0, 66, 55, 45, 36, 28, 21, 15, 10, 6, 3},
                     {0, 11, 10, 9, 8, 7, 6, 5, 4, 3, 2},
                     {0, 1, 1, 1, 1, 1, 1, 1, 1, 1, 1}};
float FitnessLUT[8008];

int main(int argc, char * argv)
{
  int i,j;
  int *tempgene;
  Population pop1(50);
  Population pop2;
  Population *popcurrent, *popnext, *popswap;
  popcurrent=&pop1;
  popnext=&pop2;
```

```
  LoadFitnessValues(FitnessLUT);
  while(CurrentGen<StopGen) {
      popnext->NextGen(*popcurrent);
      CurrentGen++;
      popswap=popcurrent;
      popcurrent=popnext;
      popnext=popswap;
    }

  for(i=0;i<CurrentGen;i++) {
      tempgene=BestList[i].getSortedGeneString();
      printf("Gen: %2d  Best Fit: %8.3f  Ave. Fit: %8.3f  Group:
        %2d,%2d,%2d,%2d,%2d,%2d\n", i+1,
BestList[i].getFitness(),AverageFitness[i],tempgene[0],
              tempgene[1],tempgene[2],tempgene[3],tempgene[4],
              tempgene[5]);
    }
};

/*********************************************/
float RND(void)  // return a normalized floating point random value
  {
    return (((float)rand())/((float)RAND_MAX));
  }
/*********************************************/
void LoadFitnessValues(float FitnessLUT[])
{
  FILE *fileptr;
  int i;
  float temp;

  fileptr=fopen("fitness.dat","r");
  for(i=0;i<8008;i++) {
      fscanf(fileptr,"%f", &temp);
      FitnessLUT[i]=temp;
    }
  fclose(fileptr);
}
/*********************************************/




/* GENOPT.H
   Genetic Algorithm Optimization Project - Main include file
   October 1996
   by Scott Paxton */

#ifndef GENOPT_H_
#define GENOPT_H_

#define MAXLOCATIONS 16  // number of candidate locations to choose from
#define MAXLENGTH 6  // max number of actuators that can be turned on at
                     // once (i.e. string length)
#define MAXMEMBERS 100  // max number of members in a population
#define MAXGEN 50 // max number of generations to iterate
```

```
#define NumberofActuators 6
#define NumberofCandidates 16
#define Pc 0.8       // crossover probability
#define Pm 0.01      // mutation probability
#define StopGen 30   // maximum generations to iterate

// Best Case Parameters:
// 125 Hz - Pc 0.66  Pm 0.05
// 170 Hz - Pc 0.7  Pm 0.05
// 225 Hz - Pc 0.8  Pm 0.01

float RND(void);                  // function prototypes
void LoadFitnessValues(float *);
#endif

/*****************************************************/



/* GENE.H
   Genetic Algorithm Optimization Project - Gene class definition
   October 1996
   by Scott Paxton */

#ifndef GENE_H_
#define GENE_H_

#include "genopt.h"
#include <stdio.h>
#include <stdlib.h>

class Gene;  // forward reference

extern Gene BestList[MAXGEN];
extern float AverageFitness[MAXGEN];
extern int CurrentGen;
extern int IndexLUT[6][16];
extern float FitnessLUT[8008];
/*****************************************************/
class Gene {
private:
  int genestring [MAXLENGTH];
  int genelength;
  float fitness;
  int i, j, k, notunique;
  int temp [MAXLENGTH];

public:
  Gene() { };

  void setGene(int * setstring, int stringlength)
    {
      genelength=stringlength;  // number of digits in gene
      for(i=0;i<genelength;i++)
        genestring[i]=setstring[i];  // element by element string copy
    }
```

```
int * getGeneString()  { return genestring; }

void SortString()
  {
    for(i=0;i<genelength;i++)
      temp[i]=genestring[i]+1;  // copy string

    for(i=0;i<NumberofActuators;i++) {    // sort
        for(j=0;j<NumberofActuators-i-1;j++) {
            if(temp[j]>temp[j+1]) {
                k=temp[j];
                temp[j]=temp[j+1];
                temp[j+1]=k;
              }
          }
      }
  }

int * getSortedGeneString()
  {
    SortString();
    return temp;
  }

float getFitness() { return fitness; }

friend Gene Crossover (Gene a, Gene b)
  {
    Gene c; // resulting string
    int i,j,notunique;

    c.genelength=a.genelength;  // copy length info
    for(i=0;i<c.genelength;i++) {
        if(RND()<0.5)      // randomly pick which parent to copy from
          c.genestring[i]=a.genestring[i];
        else
          c.genestring[i]=b.genestring[i];
        for(j=0;j<i;j++)  // test for all unique elements
          if(c.genestring[i]==c.genestring[j]) {
              notunique=1;
              while(notunique) {
                  notunique=0;
                  c.genestring[i]=
                       (int)((float)NumberofCandidates*RND());
                  for(j=0;j<i;j++)  // test for all unique elements
                    if(c.genestring[i]==c.genestring[j])
                      notunique=1;
                }
            }
      }
    return c;
  }

void Mutate()
  {
    int mutelement=(int)(RND()*genelength);
    notunique=1;
```

```
      while(notunique) {
          notunique=0;
          genestring[mutelement]=(int)((float)NumberofCandidates*RND());
          for(i=0;i<genelength;i++)  // test for all unique elements
            if((genestring[mutelement]==
                genestring[i])&&(!(i==mutelement)))
              notunique=1;
        }
    }

  void EvalFitness()
    {
      int tableindex=0;

      SortString();
      for (i=0;i<=temp[0];i++) {
          tableindex+=IndexLUT[0][i];
        }
      for (i=1;i<NumberofActuators;i++) {
          if((temp[i]-temp[i-1]) > 1)
            for(j=temp[i-1]-i+2;j<=temp[i]-i;j++)
              tableindex+=IndexLUT[i][j];
        }
      fitness=FitnessLUT[tableindex];
    };
};
/*****************************************************/
class Population {
private:
  Gene list[MAXMEMBERS];
  int nummembers;
  float sumfitness;
  int i,j,k,notunique;

public:
  Population() { }

  Population(int nummem)  // constructor for starting population
    {
      nummembers=nummem;
      int newstring[MAXLENGTH];
      // fill a starting population with random values
      for(i=0;i<nummembers;i++) {
          for(j=0;j<NumberofActuators;j++) {
              notunique=1;
              while(notunique) {
                  notunique=0;
                  newstring[j]=(int)((float)NumberofCandidates*RND());
                  for(k=0;k<j;k++)
                    if(newstring[k]==newstring[j])
                      notunique=1;
                }
            }
          list[i].setGene(newstring, NumberofActuators);
        }
    }
```

```
  int Select(Population pop)
    {
      float partialsum=0.0;
      int member=-1;
      float selectvalue=RND()*pop.sumfitness;
      do {  // weighted roulette wheel selection
          member++;
          partialsum+=pop.list[member].getFitness();
        } while((partialsum<selectvalue)&&(member<nummembers));
      return member;
    }

  void NextGen(Population parentpop)
    {
      int parent1, parent2;
      Gene offspring1, offspring2;
      float highfit=0.0;
      int highfitindex=0;

      nummembers=parentpop.nummembers;
      parentpop.sumfitness=0.0;
      for(i=0;i<nummembers;i++) {
          parentpop.list[i].EvalFitness();
          parentpop.sumfitness+=parentpop.list[i].getFitness();
          if(highfit<parentpop.list[i].getFitness()) {
              highfit=parentpop.list[i].getFitness();
              highfitindex=i;
            }
        }

      for(i=0;i<nummembers;i+=2) {
          parent1=Select(parentpop); // select 2 genes from parent pop
          parent2=Select(parentpop);
          if(RND()<Pc) {            // if crossover
              offspring1=Crossover(parentpop.list[parent1],
            parentpop.list[parent2]);
              offspring2=Crossover(parentpop.list[parent1],
            parentpop.list[parent2]);
            } else {
              offspring1=parentpop.list[parent1];
              offspring2=parentpop.list[parent2];
              offspring1.Mutate();  // force mutation if direct copies
              offspring2.Mutate();
            }
          if(RND()<Pm) offspring1.Mutate();
          if(RND()<Pm) offspring2.Mutate();
          list[i]=offspring1;
          list[i+1]=offspring2;
        }
      BestList[CurrentGen]=parentpop.list[highfitindex];
      AverageFitness[CurrentGen]=parentpop.sumfitness/nummembers;
    }
};
#endif
```

Vita

Scott Paxton

Scott Paxton was born on March 16, 1972 in Pompton Plains, New Jersey. Upon graduation from high school in 1990, he enrolled at the Massachusetts Institute of Technology. While there, he took part in an internship program and worked at the research center of The Timken Company. He graduated with a Bachelor of Science degree in Mechanical Engineering in May, 1994. Then he began graduate studies at the Virginia Polytechnic Institute and State University in August 1994, earning a Masters of Science degree in July, 1997.